Modelling accreting white dwarf populations in galaxies

Hailiang Chen

München 2016

Modelling accreting white dwarf populations in galaxies

Hailiang Chen

Dissertation
an der Fakultät fuï Physik
der Ludwig–Maximilians–Universität
München

vorgelegt von
Hailiang Chen
aus Hubei, China

München, den 24. Juni 2016

Erstgutachter: Prof. Dr. Rashid Sunyaev
Zweitgutachter: Prof. Dr. Gerhard Börner
Tag der mündlichen Prüfung: 9. August 2016

Contents

List of Figures

List of Tables

Zusammenfassung

Diese Arbeit beschäftigt sich mit der Modellierung von Binärsystemen akkretierender weißer Zwerge in Galaxien. Wir verwenden einen hybriden Binärpopulation-Synthese Ansatz um die Entstehung und Entwicklung von akkretierenden weißen Zwergen zu untersuchen. Mit den Ergebnissen des Models machen wir Vorhersagen über die Emission der Populationen im optischen, UV und weichen Röntgenband und die Eigenschaften der Nova Populationen in Galaxien mit unterschiedlicher Sternentstehungsgeschichte und vergleichen unsere Vorhersagen mit Beobachtungen.

In akkretierenden Binärsystemen weißer Zwerge akkretieren die weißen Zwerge Material von nicht entarteten Spendern. Abhängig von der Masse und der Akkretionsrate des weißen Zwergs brennt das wasserstoffreiche Material auf der Oberfläche stabil oder instabil. Wenn das akkretierte Material stabil brennt, strahlt der akkretierende weiße Zwerg hauptsächlich im weichen Röntgenstrahlen- oder EUV-Band. Die Emission dieser weißen Zwerge ist imstande, das interstellare Medium zu ionisieren, was eine Reihe von charakteristischen Rekombinations Linien erzeugt, wie die von He II 4686Å und verbotene Linien von Metallen. Frühere Arbeiten haben die Beobachtungsresultate der Emission von akkreditierenden weißen Zwergen benutzt um das Vorgänger Modell von Supernovae vom Typ Ia im einfach entarteten Szenario einzugrenzen. Diese Beobachtungen sollten auch gut geeignet sein, um die Population von akkretierenden weißen Zwergen insgesamt einzugrenzen. Wenn das akkreditierende Material instabil brennt, führt das zu Nova Explosionen. Mehrere frühere beobachtende Studien haben sich auf die Eigenschaften von Nova Populationen in Galaxien von verschiedenen Hubble Typen spezialisiert. Der Vergleich von Beobachtungen mit den Vorhersagen von Populations- Synthese -Modellen ist ein mächtiges Werkzeug um die grundlegenden Annahmen der Populations - Synthese Rechnungen zu testen und zu verifizieren.

In dieser Arbeit modellieren wir die Entstehung und Entwicklung der Population akkreditierender weißer Zwerge mit einem hybriden Binärpopulations-Synthese Ansatz mit Hilfe der Codes BSE (Binary Star Evolution) und MESA (Modules for Experiments in Stellar Astrophysics). Zunächst benutzen wir den schnellen Binärpopulations-Synthese Code um eine Population von weißen Zwergen mit nicht entarteten Begleitern zu berechnen, welche sich an der Grenze zur Füllung ihres Roche Lobe befinden. Dann folgen wir ihrer Entwicklung mit dem detaillierten Sternentwicklungscode MESA. Wir untersuchen die Entwicklung der Anzahl von verschiedenen Typen akkretierender weißer Zwerge und der Raten von Typ Ia Supernova. Wir zeigen, dass eine genaue Behandlung des Massentransfers essentiell für

Populations-Synthese-Berechnungen ist. Wir benutzen unseren erweiterten Code, um zu zeigen, dass die Verteilung der Zeitverzögerung von Typ Ia Supernovae im einfach entarteten Szenario inkonsistent mit Beobachtungen ist. Aus unseren Berechnungen ergibt sich die Typ Ia Supernova Rate in unserer Galaxie wesentlich geringer als in Beobachtungen - in Übereinstimmung mit früheren Studien.

Basierend auf den obigen Resultaten und einfachen Annahmen bezüglich der Emission von akkrederenden weißen Zwergen untersuchen wir die weiche Röntgen-Leuchtkraft (0.3-0.7 keV) und die H und He II ionisierende Leuchtkraft von akkretierenden weißen Zwergen. Zusätzlich benutzen wir detaillierte Photoionisierungs-Berechnungen um den Einfluss der Strahlung der akkretierenden weißen Zwerge auf die Linien-Emission des interstellaren Mediums in elliptischen Galaxien zu untersuchen - insbesondere He II 4686Å und Hβ. Danach vergleichen wir diese Ergebnisse mit *Chandra* und Sloan Digital Sky Survey Beobachtungen elliptischer Galaxien. Wir zeigen, dass die Resultate von Binärpopulations-Synthese-Rechnungen mit üblichen Annahmen inkonsistent mit Beobachtungen von Galaxien mit Sternaltern von $\lesssim 4-8$ Milliarden Jahren sind. Wir diskutieren verschiedene Möglichkeiten diese Diskrepanz zu beheben. Eine mögliche Lösung ist es, die Kriterien des dynamisch instabilen Masseverlustes von Riesen zu verbessern. Mit einem verbesserten Binärpopulation-Synthese Modell machen wir Vorhersagen zur Anzahl beobachtbarer überweicher Röntgenquellen in Galaxien verschiedener Arten.

Danach modellieren wir die Entstehung und Entwicklung von Nova Populationen von Galaxien mit unterschiedlichen Sternentstehungs-Geschichten mit dem verbesserten Binärpopulations-Synthese-Modell. Wir untersuchen die Eigenschaften von Nova Populationen in Galaxien mit unterschiedlichen Sternenstehungs-Geschichten. Insbesondere berechnen wir die Entwicklung der Nova Rate, die Massenverteilung von weißen Zwergen, die Massenverlust-Dauer, die Wiederaufrtritts-Periode und die maximale Magnitude von Novae. Wir finden, dass die massenspezifische Nova Rate in Spiralgalaxien etwa $10-20$ mal höher ist als in elliptischen Galaxien. Novae scheinen in elliptischen Galaxien von weißen Zwergen niedriger Masse und in Spiralgalaxien von weißen Zwergen hoher Masse zu stammen. Die Mehrzahl derzeitiger Novae in elliptischen Galaxien ist relativ lichtschwach und hat eine lange Massenverlust-Dauer und lange Wiederauftritts-Perioden. Die Ergebnisse unseres zusammengesetzten Modells, welches die Sternentstehungs-Geschichte der M31 Galaxie verwendet, sind in Übereinstimmung mit Beobachtungsdaten dieser Galaxie.

Summary

This thesis has focused on modelling population of accreting white dwarf binaries in galaxies. We adopt a hybrid binary population synthesis approach to study the formation and evolution of accreting white dwarfs. Based on results of the modelling, we predict the emission from their population in optical, UV and soft X-ray bands and properties of the nova population in galaxies with different star formation histories and compare our predictions with observations.

Accreting white dwarf binaries are binaries in which white dwarfs accrete material from non-degenerate donors. Depending on white dwarf mass and accretion rate, the H-rich material on the surface will burn stably or unstably. If the accreted material burns stably, accreting white dwarf will radiate predominantly in the soft X-ray or EUV band. The emission of these accreting white dwarfs is able to ionize the interstellar medium producing a number of characteristic recombination lines, such as He II 4686Å and forbidden lines of metals. Previous efforts have been made to use the observational results of the emission of accreting white dwarfs to constrain the progenitor model of type Ia supernovae in single degenerate scenario. These observations should be also good to constrain the accreting white dwarf population in general. On the other hand, if the material burns unstably, it will lead to nova explosions. Several previous observational studies have focused on the properties of nova population in galaxies of different Hubble types. Comparison of results of observations with the predictions of population synthesis models is a powerful tool to benchmark and verify the fundamental assumptions underlying the population synthesis calculations.

In this thesis, we model the formation and evolution of accreting white dwarfs population with a hybrid binary population synthesis approach using BSE (Binary Star Evolution) and MESA (Modules for Experiments in Stellar Astrophysics) codes. First, we use the rapid binary population synthesis code BSE to generate a population of WDs with non-degenerate companions on the verge of filling their Roche lobes. Then we follow their evolution with the detailed stellar evolution code MESA. We investigate the evolution of the number of different types of accreting white dwarfs and type Ia supernova rate. We show that the accurate treatment of mass transfer is critical for binary population synthesis calculations. Using our advanced code, we confirm that the delay time distribution of type Ia supernovae in single degenerate scenario is inconsistent with observations and the type Ia supernova rate of Galaxy in our calculation is much smaller than observation, in agreement with previous studies.

Based the above binary population synthesis results and using simple assumptions regarding the emission of accreting white dwarfs, we investigate the soft X-ray (0.3-0.7 keV) luminosity of accreting white dwarfs and their H and He II ionizing luminosity. In addition, using results of detailed photoionization calculations, we study the influence of the radiation of accreting white dwarfs on the line emission from interstellar medium in elliptical galaxies, in particular, He II 4686Å and Hβ. Then we compare these results with *Chandra* and Sloan Digital Sky Survey observations of elliptical galaxies. We demonstrate that the results of binary population synthesis with commonly adopted assumptions are inconsistent with the observation of galaxies with stellar ages of $\lesssim 4-8$ Gyr. We discuss various possibilities to resolve this discrepancy and find that the possible solution to this discrepancy is to improve the typically used criteria of dynamically unstable mass-loss for giant stars. With the improved binary population synthesis model, we make predictions about the number of observable supersoft X-ray sources in galaxies of different types.

We then model the formation and evolution of nova populations for galaxies with different star formation histories using the improved binary population synthesis model. We study the properties of nova populations in galaxies with different star formation histories. In particular, we present the evolution of nova rate, the distribution of white dwarf mass, mass loss time, recurrence period and maximum magnitude of novae. We found that the mass-specific nova rate in spiral galaxies is about $10-20$ times larger than in elliptical galaxies. The novae tend to be hosted by low mass white dwarfs in elliptical galaxies and massive white dwarfs in spiral galaxies. The majority of current novae in elliptical galaxies are relatively faint and have long mass-loss times and long recurrence periods. In spiral galaxies, on the contrary, the majority of the current nova are relatively bright and have short mass-loss times and short recurrence periods. The results of our composite model using star formation history of M31 galaxy are in agreement with observational data of this galaxy.

Chapter 1

Introduction

1.1 Formation of accreting white dwarf binaries

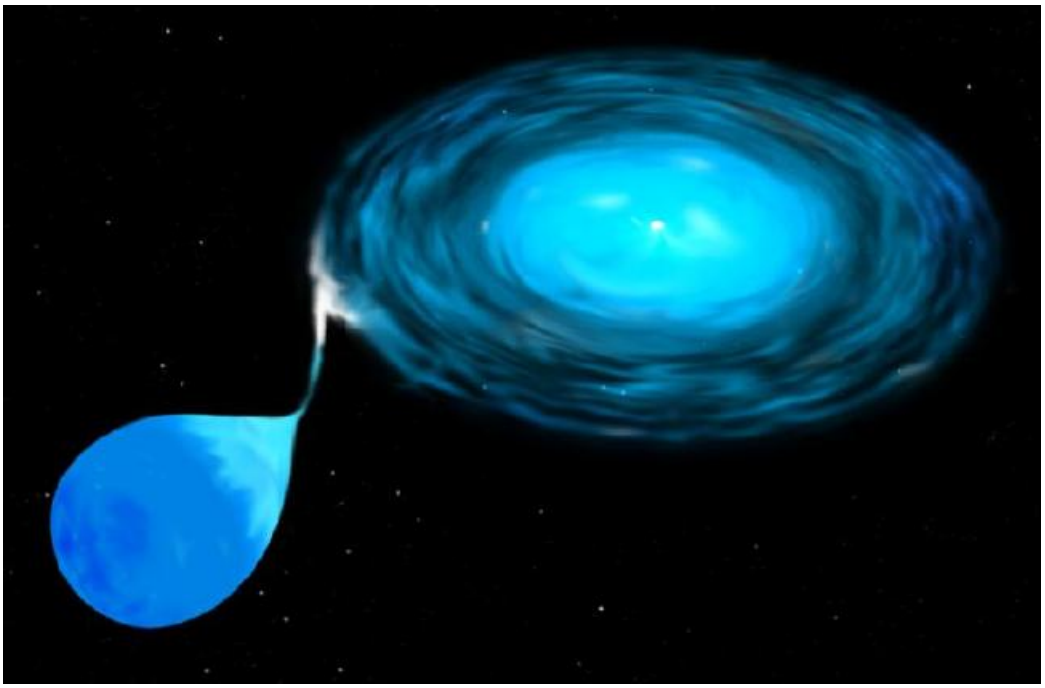

Figure 1.1: An artistic image of an accreting white dwarf with a non-degenerate secondary. The secondary fills its Roche lobe and transfers matter onto the white dwarf. A disk is formed around the white dwarf. This image can be found on the homepage of the Hubble Space Telescope.

Accreting white dwarfs are binaries in which white dwarfs accrete material from non-degenerate donors. Generally, the donor stars can be main sequence (MS), Hertzsprung gap (HG), red giant (RG) stars. The donor star can transfer matter onto the white dwarf

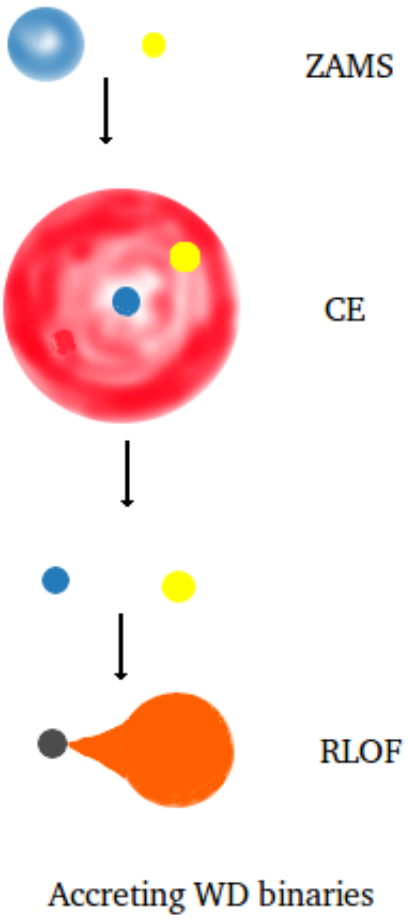

Figure 1.2: Formation of accreting white dwarf binaries (scale and color-coding are arbitrary).

through Roche lobe overflow (see Fig. 1.1)[1].

Accreting white dwarfs play an important role in the studies of binary evolution and accretion physics (see Knigge, Baraffe & Patterson 2011; Postnov & Yungelson 2014 for a review). Depending on the mass transfer rates, they can appear as cataclysmic binaries (see Warner 2003 for a review), supersoft X-ray sources (van den Heuvel et al., 1992) and rapidly accreting white dwarfs (Lepo & van Kerkwijk, 2013). In addition, they can evolve into double white dwarfs, Type Ia supernovae and binary millisecond pulsars (e.g. Whelan & Iben, 1973; Tutukov & Yungelson, 1981; Iben & Tutukov, 1984; Webbink, 1984; Taam & van den Heuvel, 1986).

Fig. 1.2 shows the formation scenario of accreting white dwarfs. In a zero age main sequence (ZAMS) binary, the massive primary evolves faster than the secondary and reaches the (super)giant branch first. If the primary fills its Roche lobe, it will begin mass transfer. Under certain condition, the mass transfer is dynamically unstable. Then a common envelope (CE) engulfs the whole binary system. If the orbital energy is large enough, the binary can survive from the CE and form a binary consisting of the core of the primary and the secondary. The core of the primary will evolve into a white dwarf. The binary will evolve into a detached binary consisting of a white dwarf and a non-degenerate secondary. As the binary evolves, the secondary will fulfill its Roche lobe and begin mass transfer. At this point, an accreting white dwarf binary is born and the secondary can be a MS, HG or RG star.

1.2 Evolution of accreting white dwarfs

Previous theoretical studies indicate that the evolution of accreting white dwarfs is strongly dependent on the accretion rate and white dwarf mass. For H-accreting white dwarfs, the accretion regimes as a function of white dwarf mass are shown in Fig. 1.3. It is widely accepted that there is a stable burning regime in which the H-rich material will burn stably (stably nuclear-burning white dwarfs, SNBWDs) and a little mass is lost (e.g. Paczynski & Zytkow, 1978; Prialnik, Shara & Shaviv, 1978; Sion, Acierno & Tomczyk, 1979; Iben, 1982; Cassisi, Iben & Tornambe, 1998; Piersanti et al., 2000; Wolf et al., 2013). If the accretion rate is above the stable burning regime, the evolution of white dwarfs is still uncertain (Hachisu, Kato & Nomoto, 1996; Cassisi, Iben & Tornambe, 1998). In the scenario of Cassisi, Iben & Tornambe (1998), the white dwarf will become a red giant, leading to the formation of a CE. On the other hand, Hachisu, Kato & Nomoto (1996) proposed that optically thick wind will occur and the excess mass will be lost in the form of optically thick wind. If the accretion rate is below the stable burning regime, it is expected that hydrogen ignites under highly degenerate condition and hydrogen burning is unstable. The hydrogen shell will undergo a thermonuclear runaway, which will lead to the ejection of the accreted material.

[1]In symbiotic stars consisting of white dwarfs and RG donors, the donor stars can transfer matter via stellar wind. We do not take them into consideration here.

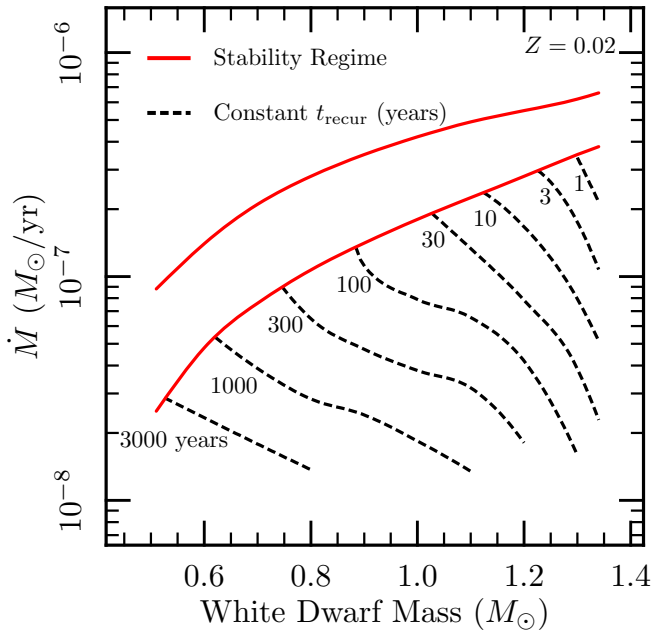

Figure 1.3: Accretion regimes of H-accreting white dwarfs as a function of white dwarf mass and accretion rate. The region between the two red lines represents the range of accretion rates in which H burning is stable. For accretion rate above the stable burning regime, the evolution of accreting white dwarfs is still uncertain (see text for more details). For accretion rate below the stable burning regime, H burning will be unstable, giving rise to novae. The dashed lines represent for novae with the same recurrence time. From Wolf et al. (2013).

These accreting white dwarfs with different accretion rates are associated with different sources and their emission spectra are also different. SNBWDs have typical effective temperatures of $10^5 - 10^6$ K. The spectra of massive white dwarfs are found to be well approximated by blackbody spectra. This means that they emit prominently in the soft X-ray and extreme ultraviolet (EUV). They can be observed as supersoft X-ray sources (SSSs) (van den Heuvel et al., 1992). Following Lepo & van Kerkwijk (2013), the white dwarfs with accretion rates above the stable burning regime are called as rapidly accreting white dwarfs (RAWDs). In the scenario of Hachisu, Kato & Nomoto (1996), RAWDs have typical effective temperatures of $10^4 - 10^5$ K and radiate predominantly in the EUV.

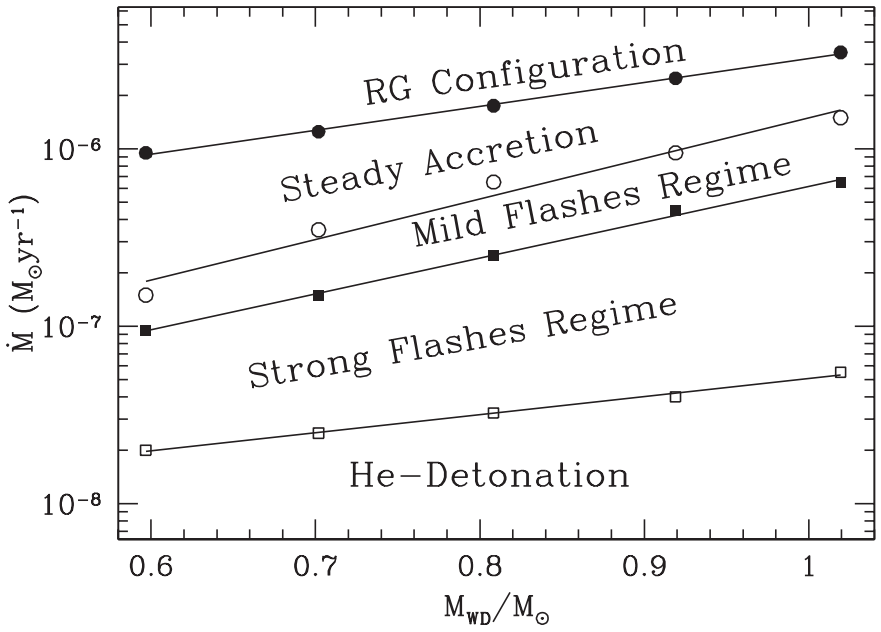

Figure 1.4: Accretion regimes of He-accreting white dwarfs as a function of white dwarf mass and accretion rate. Different lines represent the transition between different accretion regimes. From Piersanti, Tornambé & Yungelson (2014).

On the other hand, many studies devoted to the evolution of He-accreting white dwarfs (e.g. Sugimoto & Fujimoto, 1978; Nomoto & Hashimoto, 1987; Iben & Tutukov, 1991; Limongi & Tornambe, 1991; Woosley & Weaver, 1994; Shen & Bildsten, 2009; Woosley & Kasen, 2011; Piersanti, Tornambé & Yungelson, 2014; Wang et al., 2015). The possible accretion regimes of He-accreting white dwarfs are shown in Fig. 1.4. Generally, similar to the accretion regimes of H-accreting white dwarfs, there is a stable burning regime but the accretion rate is significantly higher for a same white dwarf mass. If the accretion rate is above the stable burning regime, the white dwarf may become a RG. If the accretion rate is below the stable burning regime, the helium will burn unstably. But it is worth noting that there is a He-detonation regime. In this regime, if the accretion rate is below $\sim 2 \times 10^{-8}$ $M_\odot$ yr^{-1}, helium will be ignited under highly degenerate conditions and helium detonation is induced, which may induce a supernova (e.g. Nomoto, 1982a; Iben & Tutukov,

1991; Limongi & Tornambe, 1991; Woosley & Weaver, 1994; Livne & Arnett, 1995).

During the evolution of H-accreting white dwarfs, hydrogen will burn into helium, and helium will burn into carbon and oxygen. Then the total mass accumulation efficiency of the white dwarf will be the product of the retention efficiency of hydrogen and helium. It is widely assumed that the evolution of He-shell in H-accreting white dwarfs is similar to the evolution of He-accreting white dwarfs (e.g. Toonen et al., 2013). However, Piersanti, Tornambé & Yungelson (2014) have shown that the evolution of He-shell in H-accreting white dwarfs may be different, since the He-shell will be heated by the H-burning. Then the outburst of He-burning in H-accreting white dwarfs will be milder than that in He-accreting white dwarfs. In addition, Hillman et al. (2015) simulated the long term evolution of H-accreting white dwarfs over tens of thousands of nova cycles. They found that the helium shell flash becomes weaker and weaker and finally helium burning becomes stable. Regarding this point, it is far from clear and further study is needed.

If the accreting white dwarf is a CO white dwarf and can increase its mass up to the Chandrasekhar mass limit ($\simeq 1.40$ $M_\odot$, Chandrasekhar (1931)), the white dwarf will explode as a type Ia supernovae (Whelan & Iben, 1973; Nomoto, 1982b). If the accreting white dwarf is a ONe white dwarf, the white dwarf will collapse into a neutron star and the binary will evolution into a low mass X-ray binary or binary millisecond pulsar (Michel, 1987; Canal, Isern & Labay, 1990; Nomoto & Kondo, 1991).

1.3 Type Ia supernovae

Type Ia supernovae (SNe Ia) are a type of supernova which have no hydrogen or helium lines in their spectra, but have strong Si II absorption lines around the time of maximum light (Filippenko, 1997).

The light curves of most SNe Ia have remarkable uniformity. It was found that the absolute magnitude of SNe Ia tightly correlates with the rate of decline of light curve (Phillips, 1993). With this remarkable property, SNe Ia have been successfully used as standardizable candles and used to measure cosmological parameters, providing the first evidence for the accelerating expansion of Universe (Riess et al., 1998; Perlmutter et al., 1999). Each SN Ia can produce around 0.70 $M_\odot$ of iron, enriching the interstellar medium. Given the large number of SNe Ia in galaxies, they also play an important role in galactic chemical evolution (e.g. Greggio & Renzini, 1983; Matteucci & Greggio, 1986). In spite of their great importance, the progenitor of SNe Ia is still unclear (see Wang & Han, 2012; Hillebrandt et al., 2013; Maoz, Mannucci & Nelemans, 2014, for a review).

It is widely accepted that SNe Ia are thermonuclear explosions of carbon oxygen (CO) white dwarfs in close binaries. The CO white dwarf gains mass from a companion star via mass transfer. When the white dwarf mass is close to Chandrasekhar mass ($\simeq 1.40$ $M_\odot$,Chandrasekhar 1931), it will ignite, triggering a supernova explosion. The total energy of SNe Ia is approximately the binding energy of the white dwarf. However, the nature of companion star is still unclear. Based on the mass-donor star, the progenitor model of SNe Ia may be divided into two categories. One is the single degenerate

(SD) model (e.g. Whelan & Iben, 1973; Nomoto, 1982b; Han & Podsiadlowski, 2004). The other is double degenerate (DD) model (Tutukov & Yungelson, 1981; Iben & Tutukov, 1994; Webbink, 1984; Han, 1998). In the SD model, a single CO white dwarf accretes hydrogen-rich material from a non-degenerate model, which may be a MS, HG or RG star. The white dwarf increases its mass via nuclear burning of hydrogen into helium, and helium into carbon and oxygen. In the DD model, due to the gravitational wave radiation, the orbital period of double white dwarf binary becomes shorter and shorter. This will eventually lead to the merge of two white dwarfs, giving rise to a supernova explosion.

Presently there is no consensus on the progenitors of SN Ia and different progenitor models of SNe Ia suffer from different challenges(e.g. Howell, 2011; Wang & Han, 2012; Maoz, Mannucci & Nelemans, 2014). For example, for DD scenario, it has been thought that the merger of two white dwarfs will lead to an accretion induced collapse and form a neutron star instead of a supernova (e.g. Nomoto & Iben, 1985; Saio & Nomoto, 1985). For SD scenario, Han & Podsiadlowski (2004); Wang, Li & Han (2010) found that the delay time distribution from binary population synthesis model is inconsistent with observations. Gilfanov & Bogdán (2010) estimated the X-ray emission from the progenitors of SNe Ia in SD scenario for several early type galaxies. They found that the observed X-ray luminosity is much smaller than the predicted values and claimed that the contribution of SD channel is smaller than 5 percent. Given that the emission from the progenitors of SNe Ia in SD scenario would contribute to the ionizing UV radiation from the stellar population, Johansson et al. (2014) applied the diagnostics proposed by Woods & Gilfanov (2013) and constrained the contribution of SD scenario to be < 10 percent. It is worth noticing that these observations can be used to constrain the progenitors of SNe Ia, but also useful for the study of population synthesis of accreting white dwarfs. By comparing theoretical results with these observations, we may learn something about the formation and evolution of accreting white dwarf binaries.

1.4 Novae

As we discussed above, in a accreting white dwarf binary, if the accretion rate is below the stable burning regime, the hydrogen burning is unstable, giving rise to a nova explosion. A nova explosion process is illustrated in Fig. 1.5. During the accretion, matter accumulates on the surface of the white dwarf until the pressure at the bottom of the accreted envelope becomes sufficiently high, leading to a thermonuclear runaway. The H-shell will rapidly expand and the brightness of the white dwarf will increase by ~ 10 mag, reaching the maximum luminosities around $10^{37} - 10^{38}$ erg/s. During the expansion of the envelope, a fraction of matter will be ejected. A part of the envelope may retain and return to hydrostatic equilibrium with stable hydrogen burning.

As a subclass of accreting white dwarfs, novae are important sources for binary evolution (e.g. Patterson, 1984; Knigge, Baraffe & Patterson, 2011). During the explosion, many nuclides will be produced such as ^{7}Li, ^{15}N, ^{17}O, ^{22}Na and ^{26}Al (e.g. Starrfield, Truran & Sparks, 1978; Hernanz et al., 1996; Gehrz et al., 1998; Kudryashov, Chugaĭ & Tutukov,

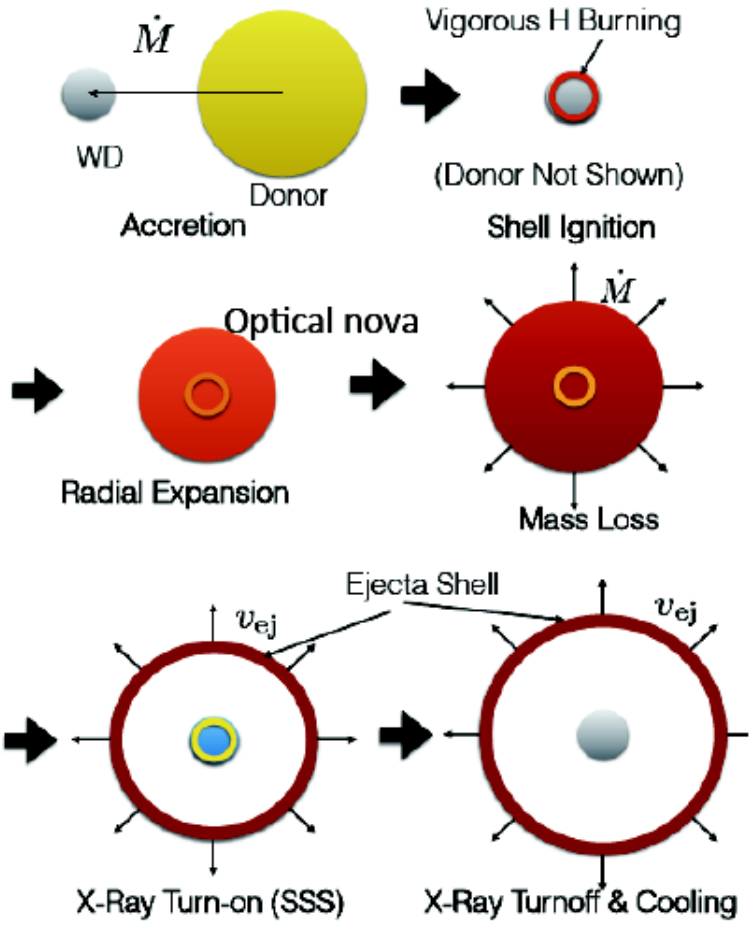

Figure 1.5: A cartoon image for the evolution of nova explosion. Image credit: Bill Wolf

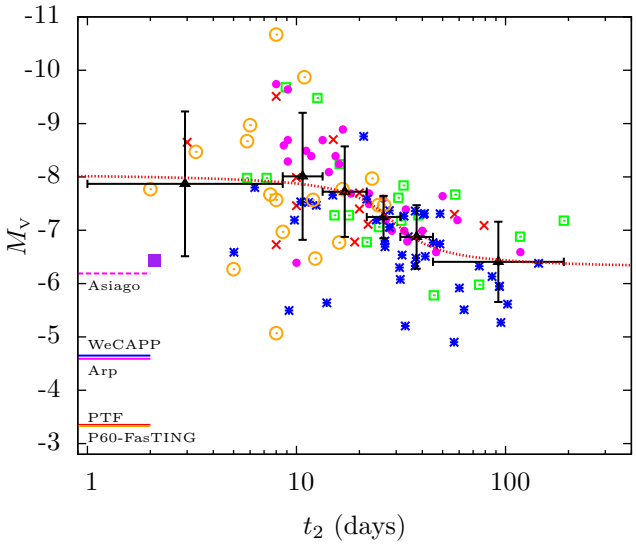

Figure 1.6: Maximum magnitude versus rate of decline relationship. Different symbols represent different observational results: PTF data – red crosses, WeCAPP – blue stars, Shafter et al. (2011) – green squares, Capaccioli et al. (1989) – magenta filled circles, Kasliwal et al. (2011) data – orange opencircles, recurrent nova M31N 2008-12a – purple square. The black triangels with error bars are the average values for different bins. The red dotted line shows the fitting results. From Soraisam & Gilfanov (2015)

2000). Thus, novae are also of great importance for the study of nucleosynthesis. If the accretion rate is close to stable burning regime, the nova explosion is relatively weak and a fraction of accreted mass will be retained, leading to the increase of white dwarf mass. It has been proposed that novae may be the progenitors of SNe Ia in SD scenario (e.g. Starrfield, Sparks & Shaviv, 1988; Yungelson et al., 1996; Hachisu & Kato, 2001). In addition, it was discovered that the absolute magnitude at maximum correlates with the rate of decline, i.e. maximum magnitude versus rate of decline relationship (see Fig. 1.6, e.g. Hubble 1929; Mclaughlin 1945; Pfau 1976; Capaccioli et al. 1990). Novae are also bright and have an average absolute blue magnitude of $M_B = -8$ at maximum(Warner, 1989). These properties make nova potential as distance indicators.

In the past, a lot of novae have been observed in galaxies of different Hubble types (e.g Ciardullo et al., 1990; Della Valle et al., 1994; Shafter, Ciardullo & Pritchet, 2000; Ferrarese, Côté & Jordán, 2003; Williams & Shafter, 2004; Coelho, Shafter & Misselt, 2008; Franck et al., 2012). Duerbeck (1990) found that the observed number counts of novae in Galaxy do not follow a unique distribution (see their Fig. 2). In addition, Della Valle et al. (1992) found that novae with short decay time concentrated at low heights above the galactic plane and novae with long decay time concentrated at high heights. Duerbeck (1990) and Della Valle et al. (1992) suggested that there are two classes of novae, i.e. 'disk novae' and 'bulge novae'. The disk novae are fast and bright, while the bulge novae are slow and faint. Such kind of classification is further supported by other observations. Based

on the study of nova spectra, Williams (1992) classified the novae into two groups: the Fe II and He/N novae. The former have prominent Fe II lines and evolve more slowly. The latter have strong lines of He and N and larger expansion velocities. Della Valle & Livio (1998) found that He/N novae tend to concentrate close to the Galactic plane and are relatively fast and bright, while Fe II novae are distributed more homogeneously enough up to heights $z \sim 1000$ pc and are relatively slow and faint. On the other hand, based on the optical and near-IR properties of interoutburst, Darnley et al. (2012) classify the nova into three groups: MS-nova, SG-nova and RG-nova according to the evolutionary state of the companion stars.

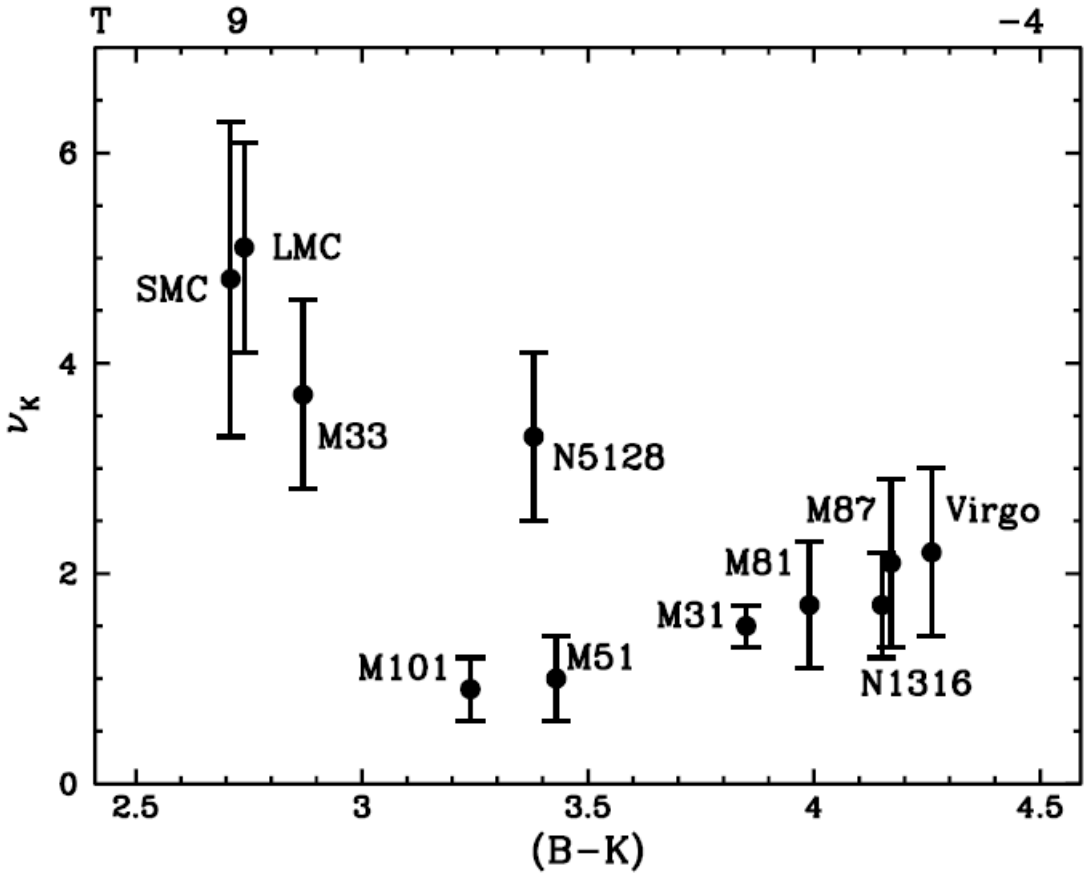

Figure 1.7: Luminosity-specific nova rate as a function of the Hubble type of galaxies. From Della Valle (2002)

Some observational studies (e.g. Ciardullo et al., 1990; Shafter, Ciardullo & Pritchet, 2000; Ferrarese, Côté & Jordán, 2003; Williams & Shafter, 2004) suggested that there is no strong dependence of mass-specific nova rate on the Hubble types of galaxies. However, Della Valle et al. (1994) found that galaxies having late Hubble type are more prolific nova producers than early type galaxies (see Fig. 1.7). In addition, it was found that some galaxies, such as the Magellanic Clouds, M33 and others, may have higher mass-specific

nova rates (e.g. Della Valle, 2002; Neill & Shara, 2005; Alis & Saygac, 2014; Shara et al., 2016). Presently, observations give contradicting results regarding the dependence of the luminosity-specific nova rate on the Hubble types of galaxy.

In order to understand and interpret these observations, it is very necessary to have nova population synthesis studies. With the binary population synthesis method, Yungelson, Livio & Tutukov (1997) found the nova rate per unit of K luminosity is higher in young stellar populations than in old stellar population. Moreover, Nelson, MacCannell & Dubeau (2004) modelled the Galactic nova population and found that their derived nova rate and orbital period distribution are consistent with observations.

1.5 Binary population synthesis approach

Binary population synthesis is an algorithm to evolve a large number of binaries at the same time. From binary evolution, we may know the properties of an individual binary system. Then we can know the properties of a type of stellar population with statistical method. With binary population synthesis approach, we can study the formation and evolution of stellar systems, such as, X-ray binaries, subdwarf, gamma-ray bursts etc. (see Han et al. (2001) for a review and references therein).

An ideal way to do binary population synthesis study is to follow the evolution of every binary system in detail from their birth up to the present moment. However, this is not feasible. The reasons are as follows. First, a stellar evolution code can not evolve different kinds of binaries from the zero-age main-sequence to remnant formation. There are a lot of process which can not be modelled with detailed codes, such as common envelope evolution. In addition, such kind of calculation is rather time-consuming and limited by the available computing power. Therefore an algorithm to evolve stars in a fast way and with reasonable precision is need and some simplified assumptions have to be made.

Generally, there are three basic algorithms applied in binary population synthesis codes. One way is to employ analytic formulae, approximating each evolutionary phase using fitting formulae from detailed calculations (e.g. Hurley, Pols & Tout, 2000; Hurley, Tout & Pols, 2002; Belczynski et al., 2008; Izzard et al., 2004). In this approach, the detailed structure of the stars are not computed. Thus, the calculation with this approach is extremely fast. Another way is to interpolate the computed stellar evolutionary tracks (e.g. Han, Podsiadlowski & Eggleton, 1995; Han et al., 1995; De Donder & Vanbeveren, 2004). In addition, one may use a 'hybrid' approach which has two steps. First, one can obtain the binary parameters of a population of semi-detached binaries at the beginning of the second mass transfer phase. In the second step, one use detailed stellar evolution code to compute a grid of binaries with different binary parameters. With this grid and some recipes, one can follow the evolution of the semidetached binary obtained in the first step. Such kind of approach has been used to study X-ray binaries, ultra luminous X-ray sources, type Ia supernovae (e.g. Pfahl, Rappaport & Podsiadlowski, 2003; Han & Podsiadlowski, 2004; Madhusudhan et al., 2008).

The binary population synthesis codes with different algorithms may have different

advantages and disadvantages. Regarding the same problem, one may get different results with different binary population synthesis algorithms. For example, it was found that the delay time distribution of type Ia supernovae computed by different groups are different (Wang & Han, 2012; Nelemans, Toonen & Bours, 2013). The reason for this difference may be due to different inherent assumptions in the codes (see Toonen et al. (2014) for a detailed comparison of binary population synthesis codes).

1.6 Outline of this work

The aim of this thesis is to model the population of accreting white dwarfs. With these models, we study the soft X-ray and UV emission of accreting white dwarf populations and the influence of their radiation on the line emission from the warm interstellar medium. Comparing these results with observations, we improve our model. Then we study the properties of nova population in galaxies of different Hubble types.

The thesis is structured as follows. In Chapter 2, with a hybrid binary population synthesis approach employed BSE and MESA codes, we have modelled the formation and evolution of accreting white dwarfs. We investigate the evolution of the number of rapidly accreting white dwarfs and stably nuclear-burning white dwarfs, and compute the SNe Ia rate in single degenerate scenario. This work is published in *Monthly Notices of the Royal Astronomical Society* (Chen et al. 2014). In Chapter 3, based on the results of previous chapter and using simple assumptions regarding the emission of accreting white dwarfs, we study the X-ray and UV emission of the population of accreting white dwarfs and their contribution to the radiation of elliptical galaxies in the He II 4686 Å and Hβ emission lines. Then we compare these results with *Chandra* and Solan Digital Sky Survey (SDSS) observations of elliptical galaxies and improve our population synthesis model. This work is published in *Monthly Notices of the Royal Astronomical Society* (Chen et al. 2015). In Chapter 4, using the hybrid binary population synthesis approach described in Chapter 2, we have modelled the nova population for elliptical-like galaxies, spiral-like galaxies and M31-like galaxies. We have calculated the nova rates and the nova properties, such as the distribution of mass-loss time distribution, maximum magnitude. Then we compare these results with the observational results of M31 galaxy. This work is published in *Monthly Notices of the Royal Astronomical Society* (Chen et al. 2016). In the final chapter, we have a brief summary.

Bibliography

Alis S., Saygac A. T., 2014, in Astronomical Society of the Pacific Conference Series, Vol. 490, Stellar Novae: Past and Future Decades, Woudt P. A., Ribeiro V. A. R. M., eds., p. 95

Belczynski K., Kalogera V., Rasio F. A., Taam R. E., Zezas A., Bulik T., Maccarone T. J., Ivanova N., 2008, ApJS, 174, 223

Canal R., Isern J., Labay J., 1990, ARA&A, 28, 183

Capaccioli M., della Valle M., D'Onofrio M., Rosino L., 1990, ApJ, 360, 63

Capaccioli M., Della Valle M., Rosino L., D'Onofrio M., 1989, AJ, 97, 1622

Cassisi S., Iben, Jr. I., Tornambe A., 1998, ApJ, 496, 376

Chandrasekhar S., 1931, ApJ, 74, 81

Ciardullo R., Tamblyn P., Jacoby G. H., Ford H. C., Williams R. E., 1990, AJ, 99, 1079

Coelho E. A., Shafter A. W., Misselt K. A., 2008, ApJ, 686, 1261

Darnley M. J., Ribeiro V. A. R. M., Bode M. F., Hounsell R. A., Williams R. P., 2012, ApJ, 746, 61

De Donder E., Vanbeveren D., 2004, New A Rev., 48, 861

Della Valle M., 2002, in American Institute of Physics Conference Series, Vol. 637, Classical Nova Explosions, Hernanz M., José J., eds., pp. 443–456

Della Valle M., Bianchini A., Livio M., Orio M., 1992, A&A, 266, 232

Della Valle M., Livio M., 1998, ApJ, 506, 818

Della Valle M., Rosino L., Bianchini A., Livio M., 1994, A&A, 287, 403

Duerbeck H. W., 1990, in Lecture Notes in Physics, Berlin Springer Verlag, Vol. 369, IAU Colloq. 122: Physics of Classical Novae, Cassatella A., Viotti R., eds., p. 34

Ferrarese L., Côté P., Jordán A., 2003, ApJ, 599, 1302

Filippenko A. V., 1997, ARA&A, 35, 309

Franck J. R., Shafter A. W., Hornoch K., Misselt K. A., 2012, ApJ, 760, 13

Gehrz R. D., Truran J. W., Williams R. E., Starrfield S., 1998, PASP, 110, 3

Gilfanov M., Bogdán Á., 2010, Nature, 463, 924

Greggio L., Renzini A., 1983, A&A, 118, 217

Hachisu I., Kato M., 2001, ApJ, 558, 323

Hachisu I., Kato M., Nomoto K., 1996, ApJ, 470, L97

Han Z., 1998, MNRAS, 296, 1019

Han Z., Eggleton P. P., Podsiadlowski P., Tout C. A., 1995, MNRAS, 277, 1443

Han Z., Eggleton P. P., Podsiadlowski P., Tout C. A., Webbink R. F., 2001, in Astronomical Society of the Pacific Conference Series, Vol. 229, Evolution of Binary and Multiple Star Systems, Podsiadlowski P., Rappaport S., King A. R., D'Antona F., Burderi L., eds., p. 205

Han Z., Podsiadlowski P., 2004, MNRAS, 350, 1301

Han Z., Podsiadlowski P., Eggleton P. P., 1995, MNRAS, 272, 800

Hernanz M., Jose J., Coc A., Isern J., 1996, ApJ, 465, L27

Hillebrandt W., Kromer M., Röpke F. K., Ruiter A. J., 2013, Frontiers of Physics, 8, 116

Hillman Y., Prialnik D., Kovetz A., Shara M. M., 2015, ArXiv e-prints

Howell D. A., 2011, Nature Communications, 2

Hubble E. P., 1929, ApJ, 69

Hurley J. R., Pols O. R., Tout C. A., 2000, MNRAS, 315, 543

Hurley J. R., Tout C. A., Pols O. R., 2002, MNRAS, 329, 897

Iben, Jr. I., 1982, ApJ, 259, 244

Iben, Jr. I., Tutukov A. V., 1984, ApJS, 54, 335

Iben, Jr. I., Tutukov A. V., 1991, ApJ, 370, 615

Iben, Jr. I., Tutukov A. V., 1994, ApJ, 431, 264

Izzard R. G., Tout C. A., Karakas A. I., Pols O. R., 2004, MNRAS, 350, 407

Johansson J., Woods T. E., Gilfanov M., Sarzi M., Chen Y.-M., Oh K., 2014, MNRAS, 442, 1079

Kasliwal M. M., Cenko S. B., Kulkarni S. R., Ofek E. O., Quimby R., Rau A., 2011, ApJ, 735, 94

Knigge C., Baraffe I., Patterson J., 2011, ApJS, 194, 28

Kudryashov A. D., Chugaĭ N. N., Tutukov A. V., 2000, Astronomy Reports, 44, 170

Lepo K., van Kerkwijk M., 2013, ApJ, 771, 13

Limongi M., Tornambe A., 1991, ApJ, 371, 317

Livne E., Arnett D., 1995, ApJ, 452, 62

Madhusudhan N., Rappaport S., Podsiadlowski P., Nelson L., 2008, ApJ, 688, 1235

Maoz D., Mannucci F., Nelemans G., 2014, ARA&A, 52, 107

Matteucci F., Greggio L., 1986, A&A, 154, 279

Mclaughlin D. B., 1945, PASP, 57, 69

Michel F. C., 1987, Nature, 329, 310

Neill J. D., Shara M. M., 2005, AJ, 129, 1873

Nelemans G., Toonen S., Bours M., 2013, in IAU Symposium, Vol. 281, IAU Symposium, Di Stefano R., Orio M., Moe M., eds., pp. 225–231

Nelson L. A., MacCannell K. A., Dubeau E., 2004, ApJ, 602, 938

Nomoto K., 1982a, ApJ, 257, 780

Nomoto K., 1982b, ApJ, 253, 798

Nomoto K., Hashimoto M., 1987, Ap&SS, 131, 395

Nomoto K., Iben, Jr. I., 1985, ApJ, 297, 531

Nomoto K., Kondo Y., 1991, ApJ, 367, L19

Paczynski B., Zytkow A. N., 1978, ApJ, 222, 604

Patterson J., 1984, ApJS, 54, 443

Perlmutter S. et al., 1999, ApJ, 517, 565

Pfahl E., Rappaport S., Podsiadlowski P., 2003, ApJ, 597, 1036

Pfau W., 1976, A&A, 50, 113

Phillips M. M., 1993, ApJ, 413, L105

Piersanti L., Cassisi S., Iben, Jr. I., Tornambé A., 2000, ApJ, 535, 932

Piersanti L., Tornambé A., Yungelson L. R., 2014, MNRAS, 445, 3239

Postnov K. A., Yungelson L. R., 2014, Living Reviews in Relativity, 17, 3

Prialnik D., Shara M. M., Shaviv G., 1978, A&A, 62, 339

Riess A. G. et al., 1998, AJ, 116, 1009

Saio H., Nomoto K., 1985, A&A, 150, L21

Shafter A. W., Ciardullo R., Pritchet C. J., 2000, ApJ, 530, 193

Shafter A. W. et al., 2011, ApJ, 734, 12

Shara M. M., Doyle T., Lauer T. R., Zurek D., Neill J. D., Madrid J. P., Welch D. L., Baltz E. A., 2016, ArXiv e-prints

Shen K. J., Bildsten L., 2009, ApJ, 699, 1365

Sion E. M., Acierno M. J., Tomczyk S., 1979, ApJ, 230, 832

Soraisam M. D., Gilfanov M., 2015, A&A, 583, A140

Starrfield S., Sparks W. M., Shaviv G., 1988, ApJ, 325, L35

Starrfield S., Truran J. W., Sparks W. M., 1978, ApJ, 226, 186

Sugimoto D., Fujimoto M. Y., 1978, PASJ, 30, 467

Taam R. E., van den Heuvel E. P. J., 1986, ApJ, 305, 235

Toonen S., Claeys J. S. W., Mennekens N., Ruiter A. J., 2013, ArXiv e-prints

Toonen S., Claeys J. S. W., Mennekens N., Ruiter A. J., 2014, A&A, 562, A14

Tutukov A. V., Yungelson L. R., 1981, Nauchnye Informatsii, 49, 3

van den Heuvel E. P. J., Bhattacharya D., Nomoto K., Rappaport S. A., 1992, A&A, 262, 97

Wang B., Han Z., 2012, New A Rev., 56, 122

Wang B., Li X.-D., Han Z.-W., 2010, MNRAS, 401, 2729

Wang B., Li Y., Ma X., Liu D.-D., Cui X., Han Z., 2015, A&A, 584, A37

Warner B., 1989, in Classical Novae, Bode M. F., Evans A., eds., pp. 1–16

Warner B., 2003, Cataclysmic Variable Stars

Webbink R. F., 1984, ApJ, 277, 355

Whelan J., Iben, Jr. I., 1973, ApJ, 186, 1007

Williams R. E., 1992, AJ, 104, 725

Williams S. J., Shafter A. W., 2004, ApJ, 612, 867

Wolf W. M., Bildsten L., Brooks J., Paxton B., 2013, ApJ, 777, 136

Woods T. E., Gilfanov M., 2013, MNRAS, 432, 1640

Woosley S. E., Kasen D., 2011, ApJ, 734, 38

Woosley S. E., Weaver T. A., 1994, ApJ, 423, 371

Yungelson L., Livio M., Truran J. W., Tutukov A., Fedorova A., 1996, ApJ, 466, 890

Yungelson L., Livio M., Tutukov A., 1997, ApJ, 481, 127

Chapter 2

Population synthesis of accreting white dwarfs with a hybrid approach

Monthly Notices of the Royal Astronomical Society, 445, 3024, 2014
Chen, H.-L., Woods, T. E., Yungelson, L. R., Gilfanov, M., & Han, Z.

2.1 Abstract

Accreting, nuclear-burning white dwarfs have been deemed to be candidate progenitors of type Ia supernovae, and to account for supersoft X-ray sources, novae, etc. depending on their accretion rates. We have carried out a binary population synthesis study of their populations using two algorithms. In the first, we use the binary population synthesis code BSE as a baseline for the "rapid" approach commonly used in such studies. In the second, we employ a "hybrid" approach, in which we use BSE to generate a population of white dwarfs (WD) with non-degenerate companions on the verge of filling their Roche lobes. We then follow their mass transfer phase using the detailed stellar evolution code MESA. We investigate the evolution of the number of rapidly accreting white dwarfs (RAWDs) and stably nuclear-burning white dwarfs (SNBWDs), and estimate the type Ia supernovae (SNe Ia) rate produced by "single-degenerate" systems (SD). We find significant differences between the two algorithms in the predicted numbers of SNBWDs at early times, and also in the delay time distribution (DTD) of SD SNe Ia. Such differences in the treatment of mass transfer may partially account for differences in the SNe Ia rate and DTD found by different groups. Adopting 100% efficiency for helium burning, the rate of SNe Ia produced by the SD-channel in a Milky-way-like galaxy in our calculations is $2.0 \times 10^{-4}\mathrm{yr}^{-1}$, more than an order of magnitude below the observationally inferred value. In agreement with previous studies, our calculated SD DTD is inconsistent with observations.

2.2 Introduction

Type Ia supernovae (SNe Ia) have been used with great success as standardizable candles, allowing for the measurement of cosmological parameters (Riess et al. 1998; Perlmutter et al. 1999). SNe Ia are also of great importance for galactic chemical evolution (e.g. Matteucci & Greggio, 1986). It is widely accepted that they are thermonuclear explosions of carbon-oxygen (CO) white dwarfs (WDs). The compact, degenerate structure of the exploding stars in SNe Ia was recently confirmed by early-time multiwavelength observations of SN2011fe (Nugent et al., 2011; Bloom et al., 2012). However, the nature of SNe Ia progenitors is still unclear (see Hillebrandt et al. 2013 for a recent review). The models for the progenitors of SN Ia fall into two categories: the single degenerate (SD) model (Whelan & Iben, 1973) and the double degenerate (DD) model (Tutukov & Yungelson, 1981; Iben & Tutukov, 1984; Webbink, 1984). In the standard SD-model a WD accretes matter from a non-degenerate companion, which may be a main-sequence, subgiant, or red giant star. In order to grow, a WD must accumulate mass via nuclear-burning of hydrogen into helium, and helium into carbon and oxygen. When the WD mass reaches $M_{\rm Ch}$, the WD explodes as an SN Ia.

However, theoretical and observational challenges persist for both scenarios. The fundamental difficulty for the SD-model is the narrow range of accretion rates ($\sim$few$\times 10^{-7}$ $\mathrm{M_\odot\ yr^{-1}}$) for which steady nuclear-burning and efficient accumulation of mass by the WD is possible (Paczynski & Zytkow, 1978). This requires specific combinations of donor and accretor masses, restricting the typical delay time between formation of a binary and a SN Ia by $\sim$1 Gyr, and similarly the peak production of SNe Ia in this channel within a similar delay time. Another problem is the treatment of the excess matter which cannot be processed through steady nuclear-burning. This is typically *assumed* either to form an extended envelope around the WD, leading to the formation of a common envelope, or to be lost from the system in the form of an optically thick wind.

Therefore, the viability of the SD-scenario depends critically on the treatment of mass transfer and resulting accretion rate, which defines whether the WD may, presumably grow in mass. White dwarfs with different accretion rates are associated with different sources and phenomena, e.g. supersoft X-ray sources (SSSs) and novae. Comparing observations with the number of SSSs and the nova rate predicted by population synthesis models can be used to verify calculations, and also to constrain the SD-channel.

Because of the relatively high mass transfer rates needed to sustain steady nuclear burning, these sources are almost always associated with mass transfer on the donor's thermal timescale (thermal timescale mass transfer, TTMT). In binary population synthesis codes, TTMT is typically accounted for using a simple analytic treatment. However, such analysis typically assumes implicitly that the donor star remains in *thermal equilibrium*, with the entire star (or at least its entire envelope) responding at once, despite mass transfer being driven by the *thermal disequilibrium* of the donor (e.g Yungelson et al., 1995; Ruiter, Belczynski & Fryer, 2009; Bours, Toonen & Nelemans, 2013). This is particularly important in treating mass loss from red giants – detailed calculations reveal that the rapid expansion of the donor envelope in response to mass transfer, expected in the simplified treatment

of adiabatic models (Hjellming & Webbink, 1987), does not necessarily occur (Woods & Ivanova, 2011). This is critical in determining the circumstances under which a binary will undergo a common envelope (CE) phase. In those cases where the binary will undergo a CE regardless, it is also possible that some mass may be accreted prior to this phase, and any accreting WD may appear briefly as an SSS. This is unaccounted for in the traditional treatment of mass transfer in population synthesis.

In this paper (Paper I), we investigate in detail mass transfer in the semidetached systems with nuclear-burning WD (NBWD) accretors and main-sequence, Hertzsprung gap and red-giant donors. We pay special attention to the systems in which WDs burn hydrogen steadily (SNBWDs) and to the systems with accretion rates exceeding the upper limit for steady burning, but too low for the formation of a common envelope, ("rapidly accreting white dwarfs" (RAWDs), Lepo & van Kerkwijk, 2013) [1]. For this, we produce a grid of $\sim 3 \times 10^4$ evolutionary sequences of close binary models with different initial combinations of WD accretors and nondegenerate donors, and with differing orbital periods at the onset of Roche lobe overflow, calculated by the detailed stellar evolutionary code MESA (Paxton et al., 2011, 2013). Our models are compared with the ones obtained using analytic descriptions of mass-transfer. In order to relate our work to observations, we compare the predicted evolution of the numbers of SNBWD, RAWD, and the rates of SNe Ia given two star formation histories: an instantaneous burst of star formation, and a constant star formation rate for 10 Gyr, approximating early and late type galaxies respectively. In a subsequent paper (hereafter Paper II), we will incorporate spectral models for nuclear-burning white dwarfs. This will allow us to more meaningfully test the predictions of our model.

We describe the method of calculations in §2.3, highlight the effect of varying treatments of TTMT in §2.4, follow with a discussion of how some observables vary with changing MT treatment in §3.5, in particular the predicted populations of RAWDs, SNBWDs, and SNe Ia. Summary and conclusions are presented in §2.6.

2.3 The method of calculations

2.3.1 Mass loss treatment in binary population synthesis

The method applied to study different populations of binary stars and the products of their evolution is binary population synthesis (BPS). In population synthesis, one convolves the statistical data on initial parameters and birthrates of binaries with scenarios for their evolution. This allows one to study birthrates and numbers of binaries of different classes and their distributions over observable parameters.

There are two basic algorithms applied to study semidetached stages of evolution in BPS

[1] It was shown by Paczyński (1971) that putting a $\simeq 10^{-3}\,M_\odot$ hydrogen-helium envelope atop a hot ($\log T_e = 5.0$) carbon-oxygen WD transforms it into a red giant ($\log T_e = 3.6$); this may be avoided, if excess of the matter is removed by postulated optically-thick stellar wind (Hachisu, Kato & Nomoto, 1999).

codes. The "rapid" one employs analytic formulae, approximating each evolutionary phase using simple fits from detailed calculations. Mass transfer is accounted for by calculating the radial response of the donor star and its Roche radius. Alternatively, one may employ a "hybrid" approach which entails two steps. Relevant to our present study, first we obtain the population of WD binaries with nondegenerate donors at the onset of mass transfer by means of a BPS code. Here we use the publicly available code BSE[2] (Hurley, Tout & Pols, 2002), which we have modified slightly (see below). In the second step, in order to obtain an accurate description of post-RLOF mass-loss rates, we compute the mass transfer rate and response of the donors in this population by drawing from a grid of 3×10^4 evolutionary sequences of models for WDs with MS, HG or FGB companions computed by MESA (Paxton et al., 2011, 2013), in practice, using about ∼4000 such tracks. The advantage of this approach is the possibility to describe $\dot{M}$ accounting for the response of the donor. This also allows one to avoid the exclusion of any short evolutionary stages.

It is known from the earliest studies of close interacting binaries (see, e.g. Morton, 1960; Paczyński, Ziólkowski & Zytkow, 1969) that, depending on the evolutionary status of the Roche-lobe-overflowing star (the donor) and the mass ratio of the components, the donor may lose mass on a timescale defined by the dynamical, thermal, or nuclear evolution of the donor, or the loss of angular momentum. In practice, this means that the mass-loss rate depends on relations between the response of the Roche lobe radius to mass loss $\zeta_{RL} \equiv \left(\frac{\partial \ln R_{RL}}{\partial \ln M_1}\right)$, the adiabatic hydrostatic response of the stellar radius $\zeta_{ad} \equiv \left(\frac{\partial \ln R}{\partial \ln M_1}\right)_{ad}$, the thermal-equilibrium response of the same $\zeta_{th} \equiv \left(\frac{\partial \ln R}{\partial \ln M_1}\right)_{th}$, the nuclear evolution of the radius, and finally the angular momentum loss timescale. If $\zeta_{ad} > \zeta_{RL} > \zeta_{th}$, the star remains in hydrostatic equilibrium, but does not remain in thermal equilibrium; in this case mass loss occurs on the thermal timescale of the star. If $\zeta_{RL} > \zeta_{ad}$, the star cannot remain in hydrostatic equilibrium, and mass loss proceeds on the dynamical timescale. If $\zeta_{ad}, \zeta_{th} > \zeta_{RL}$, mass loss occurs due to the expansion of the star during its evolution on the nuclear timescale, or due to the shrinkage of the Roche lobe owed to angular momentum losses.

Dynamical or thermal timescale mass loss is common for initial stages of mass exchange. In "rapid" BPS codes it is assumed that, if RLOF leads to dynamical mass loss (according to some assumed criteria), then the formation of a common envelope is unavoidable. In this case, no further computations of the mass transfer rate or the response of the donor star are carried out. Mass loss is assumed to occur on the thermal timescale if, after removal of an infinitesimally small amount of mass, the radius of the star in thermal equilibrium is predicted to be larger than the (volume-averaged) Roche lobe radius. In the simplest formulation, the mass loss rate is approximated as

$$\dot{M}_{\rm th} = M/\tau, \tag{2.1}$$

where M is the mass of the Roche -lobe filling star and τ is an estimate of the thermal timescale. In general, the definition of $\dot{M}_{\rm th}$ is not unique and differs between codes because

[2]http://astronomy.swin.edu.au/ jhurley/bsedload.html

of our present lack of understanding of what fraction of the star is involved in mass exchange (i.e. to what depth to we evaluate $\tau_{\rm th}$?). Then, typically, one writes $\dot{M}_{\rm th} = k \cdot R_{\rm d} L_{\rm d}/GM'$, where, in the simplest cases, $k \sim 1$, M' is the instantaneous total mass of the star or the mass of the stellar envelope. In slightly more sophisticated cases, k may be a function of the mass-radius response functions of the donor and its Roche radius (e.g. Ivanova & Taam, 2004). Moreover, for R_d and L_d the values corresponding to stars in **thermal equilibrium** are usually taken, despite mass transfer being driven by the **thermal disequilibrium** of the donor star. As a result, just after RLOF $\dot{M}$ is constant or slowly declining as M_d falls (see Fig. 2.2 below). However, Langer et al. (2000) (see also Podsiadlowski, Rappaport & Pfahl 2002) clearly showed that equations similar to Eq. (2.1) provide only the order of magnitude of the mass transfer rate.

Although detailed calculations accounting for the response of the donor are preferable, the use of the "hybrid" technique has so far been limited by the available computing power. If too crude a grid of evolutionary models is used, it may result in spurious effects. Only recently, with the advent of the rapid and robust stellar evolutionary code MESA, has it become possible to increase the number of sufficiently detailed tracks by an order of magnitude, to several $10,000$, which can be used to adequately describe the evolution of a parental population of $\sim 100,000$ systems.

Earlier, grids of detailed evolutionary tracks leading to the systems or events of desired type were combined with detailed BPS codes, e.g., by Pfahl, Rappaport & Podsiadlowski (2003) for low and intermediate mass X-ray binaries, Han & Podsiadlowski (2004) for SNe Ia in semidetached systems, Madhusudhan et al. (2008) for ultraluminous X-ray sources. Advantages of this method were recently discussed by Nelson (2012). In this paper, we present the first attempt to use grids of tracks computed by MESA to investigate accreting WDs.

2.3.2 Binary population synthesis for NBWDs

In this paper, we employ both the "hybrid" approach and the "rapid" approach described above. In either case, each evolutionary track for every binary must be scaled by a relative "weight" which accounts for the total number of binaries the track represents. To evaluate the relative "weight" of a binary, we take the IMF of primaries from Kroupa (2001) with lower and upper mass cutoffs $m_L = 0.1\,M_\odot$ and $m_U = 100 M_\odot$. We adopt a flat mass ratio distribution (Kraicheva et al., 1979). Binary separations in the range between $10 R_\odot$ and $10^6 R_\odot$ are drawn from a flat distribution in logarithmic space (Abt, 1983). We assume 50%-binarity, i.e., 2/3 of stars are components of binary systems (Duquennoy & Mayor, 1991).

Using the latest version of BSE, we computed the evolution of binaries for a regular grid of stars with primary masses varying from $0.9 M_\odot$ to $12 M_\odot$ in logarithmic steps of 0.0125, mass ratio of components between 0 and 1 in steps of $\Delta q = 0.0125$, and separations of components from $10\,R_\odot$ to $10^4\,R_\odot$ in logarithmic steps of 0.025. Altogether, this gives us a grid of $864,000$ systems. As a subset of this grid, we obtain the total population of WD binaries with nondegenerate donors at the onset of mass transfer.

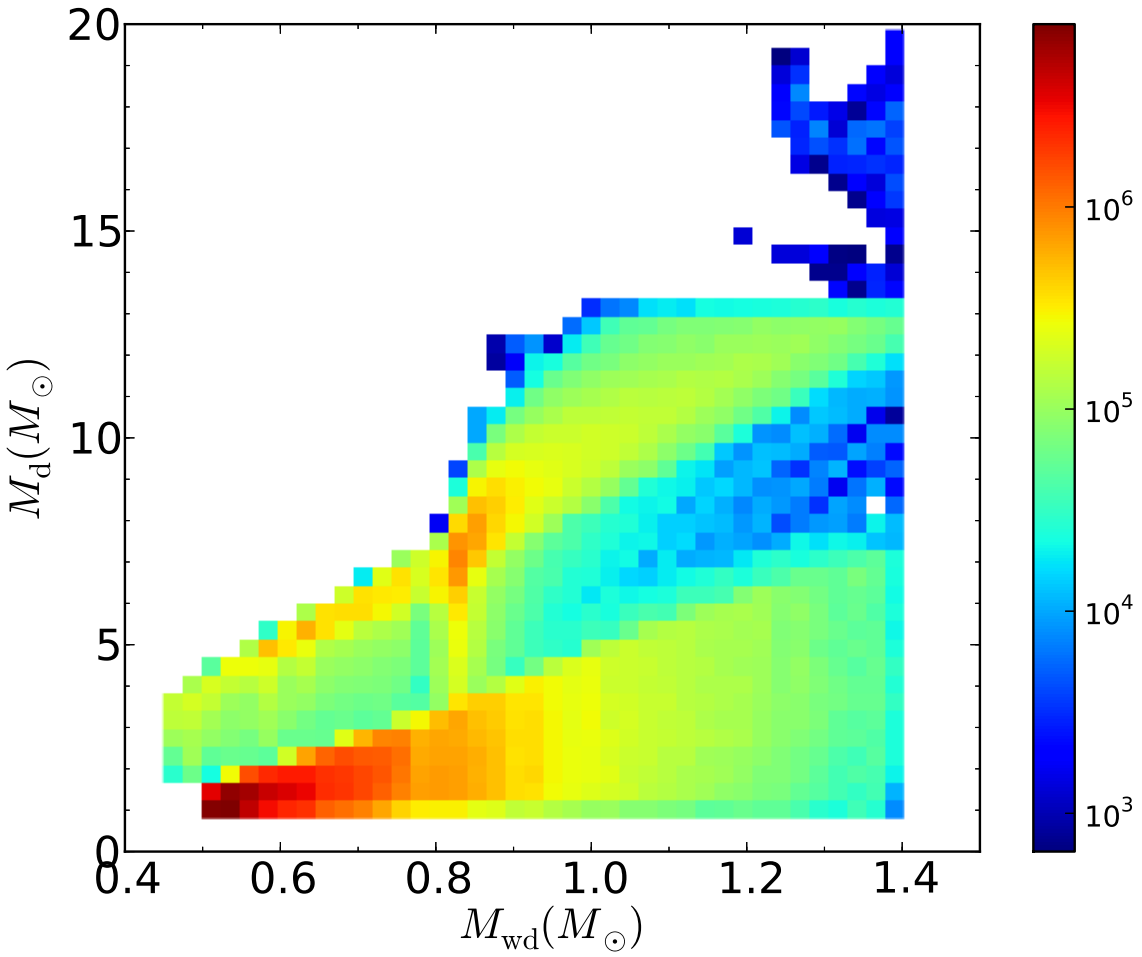

Figure 2.1: WD and donor masses distribution for the population of WD+(nondegenerate companion) binaries with different orbital periods at the onset of mass transfer for a $10^{11}\,M_\odot$ galaxy in the model B1+M (see table 2).

The WD masses at the onset of mass transfer range from $0.50\,M_\odot$ to $1.40\,M_\odot$ and companion masses – from $0.8\,M_\odot$ to $20\,M_\odot$ (see Fig. 2.1), which are consistent with other binary population synthesis studies (see Fig 3. and 4. in Toonen et al. 2013). For the systems with primary masses or donor masses $\leq 1.4\,M_\odot$ we replaced the original BSE implementation of magnetic braking by the prescription suggested by Rappaport, Verbunt & Joss (1983, Eq. (34) with $\gamma = 3$); this is identical to the magnetic braking law implemented in MESA.

To describe common envelope evolution, we use the prescription suggested by Webbink (1984), with the inclusion of the "binding energy parameter" (de Kool, 1990):

$$\alpha_{ce}\left(\frac{Gm_{\rm d,f}m_{\rm a}}{2a_{\rm f}} - \frac{Gm_{\rm d,i}m_{\rm a}}{2a_{\rm i}}\right) = \frac{Gm_{\rm d,i}m_{\rm d,e}}{\lambda R_{\rm d,r}}. \tag{2.2}$$

Here $m_{\rm d,i}$ and $m_{\rm d,f}$ are initial and final donor mass, respectively, $m_{\rm d,e}$ is the donor envelope mass, m_a is the accretor mass, $a_{\rm i}$ and $a_{\rm f}$ are the initial and final binary separations, $R_{\rm d,r}$ is the Roche lobe radius of the donor at the onset of mass transfer, α_{ce} is the fraction of the orbital energy used to eject the common envelope and λ is a parameter which characterizes the binding energy of the donor's envelope. The long-standing problem of the formalism given by Eq. (2.2) is that a_f/a_i depends on the product of $\alpha_{ce} \times \lambda$ and these two still uncertain parameters cannot be separated (see Ivanova et al., 2013, for the latest detailed discussion). It is evident that λ should not be constant along the evolutionary track of a star (e.g Dewi & Tauris, 2000). It remains uncertain whether a fraction of the binding energy of the donor may contribute to expelling the envelope and whether there are any other sources contributing to this process.

Davis, Kolb & Willems (2010) computed λ's for 1 - 8 $M_\odot$ AGB stars with varying radii, postulating that the core-envelope interface is located at the position within the star with hydrogen abundance $X_c = 0.1$. Then they found that, assuming $\alpha_{\rm CE} > 0.1$, it is possible to account for the population of post common envelope binaries found by the Sloan Digital Sky Survey (SDSS). A similar approach led Zorotovic et al. (2010) to constrain the common envelope efficiency to $0.2 < \alpha_{\rm CE} < 0.3$[3] Ricker & Taam (2012), based on results of 3D hydrodynamical calculations, limited $\alpha_{\rm CE}$ from above by 0.4 - 0.5.

Having these uncertainties in mind, we produced a set of WD+(nondegenerate companion) models using BSE, with all CE events following Eq. (2.2) assuming a constant $\alpha_{ce} \times \lambda$=0.25. In another set of computations, we used fitting formulae for λ (Loveridge, van der Sluys & Kalogera, 2011) and α_{ce}=0.25.

In the MESA grid, WD masses range from $0.5M_\odot$ to $1.3M_\odot$ with an interval of $0.1M_\odot$, with an additional final step at $1.35M_\odot$. The donor masses range from $0.9M_\odot$ to $2.5M_\odot$ with an interval of $0.025M_\odot$, with an interval of 0.1 $M_\odot$ from $2.6M_\odot$ to $3.5M_\odot$, with an interval of 0.50 from 4.0 $M_\odot$to 10.0 $M_\odot$, and with an interval of 1.0 $M_\odot$ from 10.0 $M_\odot$ to 15 $M_\odot$. Initial orbital periods $\log(P_{\rm orb}/{\rm day})$ cover the range from -0.3 to 2.9 with a logarithmic step of 0.1. If the parameters of a binary produced in the first step are out of this grid, we computed it individually. In the second step, for every binary we choose the nearest track in grid of MESA calculations in order to follow the evolution of the system.

The tracks are computed for typical Population I composition with initial hydrogen abundance X = 0.70, helium abundance Y = 0.28 and metallicity Z = 0.02.

The retention efficiency of matter accumulated by WDs was estimated on the basis of several "critical" accretion rates. Accreted hydrogen burns stably if $\dot{M}_{\rm cr} \leq \dot{M}_{\rm a} \leq \dot{M}_{\rm max}$, where, we employ the following approximations to the results of Iben & Tutukov (1989)

$$\log(\dot{M}_{\rm max}) \approx -4.6 \times {\rm M}_{\rm WD}^4 + 17.9 \times {\rm M}_{\rm WD}^3 - 26.0 \times {\rm M}_{\rm WD}^2 + 17.5 \times {\rm M}_{\rm WD} - 11.1, \quad (2.3)$$

$$\log(\dot{M}_{\rm cr}) \approx -1.4 \times {\rm M}_{WD}^2 + 4.1 \times {\rm M}_{\rm WD} - 9.3. \quad (2.4)$$

[3] Note, their sample of post-CE binaries consisted of WD with M-type main-sequence companions. For more massive companions the energetics of the CE phase may differ, see the quoted paper and Zorotovic, Schreiber & Parsons (2014).

Masses are in units of $M_\odot$ and rates in units of $\mathrm{M_\odot\ yr^{-1}}$. For $\dot{M}_\mathrm{a} > 10^{-4}\ \mathrm{M_\odot\ yr^{-1}}$, an optically thick wind can not be sustained (Hachisu, Kato & Nomoto, 1999) and a CE is formed. If $\dot{M}_\mathrm{max} < \dot{M}_\mathrm{a} \leq 10^{-4}\ \mathrm{M_\odot\ yr^{-1}}$, the excess of unburned matter is isotropically reemitted from the system by an optically thick wind. If $\dot{M}_\mathrm{cr} > \dot{M}_\mathrm{a} \geq 10^{-8}\ \mathrm{M_\odot\ yr^{-1}}$, H burns in mild flashes. Below $10^{-8}\ \mathrm{M_\odot\ yr^{-1}}$ burning flashes are strong and may even erode the dwarf. We apply in this regime a fitting formula for the mass retention efficiency η_H based on the results of Prialnik & Kovetz (1995) and Yaron et al. (2005):

$$\eta_\mathrm{H} = -0.075 \times (\log(\dot{M}_\mathrm{a}))^2 - 1.21 \times \log(\dot{M}_\mathrm{a}) - 4.95. \tag{2.5}$$

Note, η_H is based on the results for WD temperature $\mathrm{T_{WD}} = 3 \times 10^7\mathrm{K}$. We neglect weak dependence of η_H on WD mass.

To summarize (rates are in $\mathrm{M_\odot\ yr^{-1}}$):

$$\eta_\mathrm{H} = \begin{cases} \mathrm{CE} & \dot{M}_\mathrm{a} > 10^{-4} \\ \dot{M}_\mathrm{max}/\dot{M}_\mathrm{a} & \dot{M}_\mathrm{max} < \dot{M}_a \leq 10^{-4} \\ 1.0 & \dot{M}_\mathrm{cr} \leq \dot{M}_a \leq \dot{M}_\mathrm{max} \\ \text{linear interpolation} & \\ \text{between 1 and Eq. (2.5)} & 10^{-8} < \dot{M}_a < \dot{M}_\mathrm{cr} \\ \text{Eq. (2.5)} & 10^{-12} \leq \dot{M}_\mathrm{a} \leq 10^{-8}. \end{cases} \tag{2.6}$$

The ranges of WD masses and accretion rates of steady or unsteady burning regimes of H and He are not identical (see, e.g., Iben & Tutukov, 1989). For this reason, in population synthesis studies retention efficiency of He, η_He, is considered as a function of M_WD and the rate of H-accumulation. Then, total mass accumulation efficiency is taken as $\eta_\mathrm{H} \times \eta_\mathrm{He}$. The value of η_He is especially uncertain (Bours, Toonen & Nelemans, 2013; Idan, Shaviv & Shaviv, 2013; Newsham, Starrfield & Timmes, 2014; Wolf et al., 2013). We assumed, for simplicity, $\eta_\mathrm{He} = 1$. This provides a strict upper limit on the SNe Ia rate.

In the "rapid" approach, the following mass-ratio based criteria for the formation of a CE were applied: $q = 3$ for MS donors, $q = 4$ for HG donors. These values are supported by detailed binary evolution studies (Han & Podsiadlowski, 2004; Wang, Li & Han, 2010). If the donor stars are on the FGB and AGB, we use the prescription of Hjellming & Webbink (1987), despite the fact that this underestimates the stability of mass transfering red giants (Woods & Ivanova, 2011), for lack of an alternative prescription. A summary of the NBWDs population models computed in this paper is presented in Table 2.1. The use of four different models allow us to compare our results for differing treatment of the second mass transfer phase (analytic or MESA) with that of our choice in CE parameterization (fixed $\alpha\lambda$, or an analytic fit of λ from detailed evolutionary calculations with fixed α).

2.4 Comparison of mass transfer treatments

Here we present examples of computations using two simplified prescriptions for mass transfer and compare them with the results of our detailed stellar evolution calcula-

Table 2.1: Computed models

model	λ	α	code
B1	fit[a]	0.25	BSE only
B1+M	fit[a]	0.25	BSE + MESA
B2	$\alpha \times \lambda = 0.25$		BSE only
B2+M	$\alpha \times \lambda = 0.25$		BSE + MESA

[a] The fitting formula from Loveridge, van der Sluys & Kalogera (2011) for $Z = Z_\odot$.

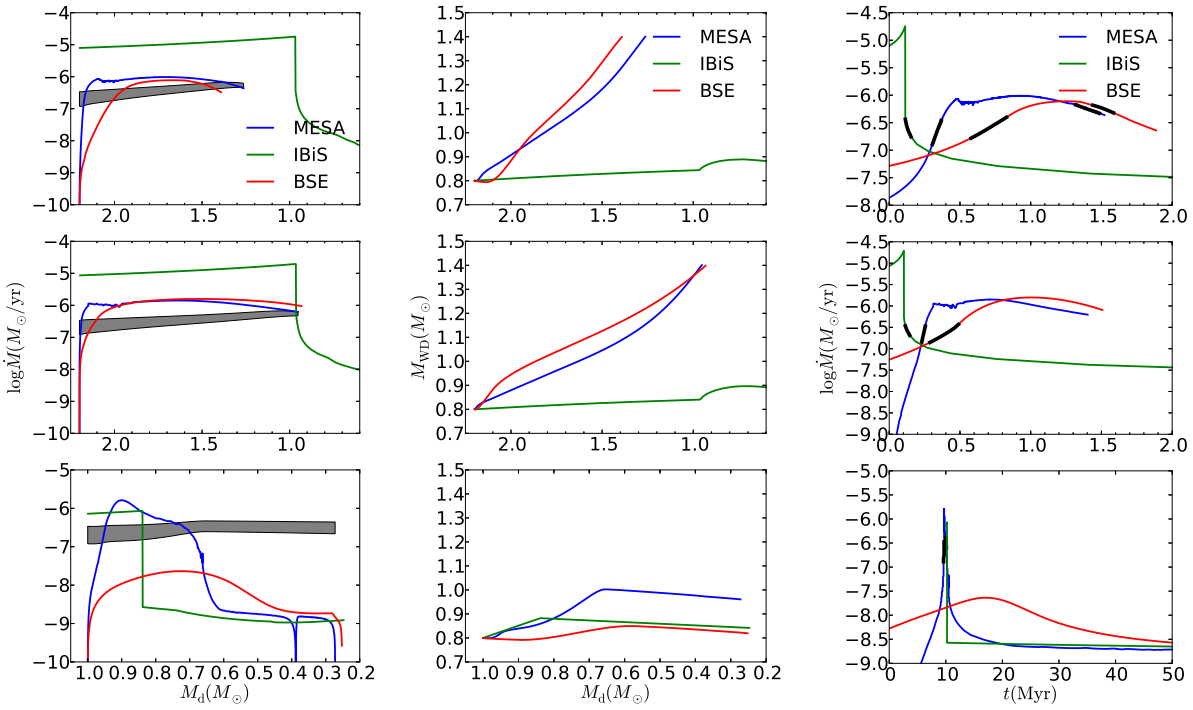

Figure 2.2: Comparison of the evolution of mass transfer rate and mass of the accretor as a function of donor mass (left and middle panels). The right set shows the dependence of $\dot{M}$ on time. At the onset of mass transfer $M_{\rm WD} = 0.80\,M_\odot$, $M_{\rm d} = 2.20\,M_\odot$, $P_{\rm orb}$= 0.80, 2.0 days in the upper and middle panels, respectively. In the lower panel, the binary parameters are $M_{\rm WD} = 0.8\,M_\odot$, $M_{\rm d} = 1.00\,M_\odot$, $P_{\rm orb}$= 3.0 days. For these three binaries, mass transfer begins on the MS, HG and RG branch, respectively. In the right set, the thick black line shows the time spent in the stable burning regime.

tions using MESA. First, we apply the prescription used in BSE. In solar units, the "thermal timescale" mass transfer rate is defined as $10^{-7} M_{\rm d,0} RL/M'$ $\rm M_\odot\ yr^{-1}$, where $M' = M_{\rm d} - M_c$, M_c is the mass of stellar core. This mass transfer rate is compared to the "nuclear timescale" mass transfer rate given by an *ad hoc* formula $\dot{M} = 3 \times 10^{-6} \left[\min(M_{\rm d}, 5.0)\right]^2 \left[\ln(R/R_{\rm RL})\right]^3$ $\rm M_\odot\ yr^{-1}$. Then, the minimum of two values for $\dot{M}$ is chosen. In the illustrative cases presented below, $\dot{M}$ corresponds to the first of these two formulae.

As the second prescription, we use the formulation applied in the code IBiS (e. g. Yungelson & Livio, 1998). If $\zeta_{th} < \zeta_{\rm RL}$, $\dot{M} = 3.15 \times 10^{-7} RL/M_{\rm d}^2$ $\rm M_\odot\ yr^{-1}$. Otherwise, if mass transfer is thermally stable, $\dot{M}$ is defined by the timescale of growth of the degenerate He-core of the donor. The stabilizing effect of an optically thick wind of from the WD is taken into account in the high-$\dot{M}$ regime.

Finally, in the detailed stellar evolutionary code MESA, $\dot{M}$ is computed as a stationary subsonic isothermal flow through the vicinity of L_1, with an additional assumption that $(R - R_{\rm RL})/H_p \approx 1$, folllowing Ritter (1988). Here H_p is the pressure scale height.

In Fig. 2.2, we show example tracks for three cases of binary evolution, where in each case we have either used one of the two simplified algorithms described above, or MESA. In the upper and middle rows of Fig. 2.2, the initial white dwarf mass is $M_{\rm WD} = 0.80 M_\odot$, the initial donor mass is $M_{\rm d} = 2.2 M_\odot$, and the initial orbital periods are $P_{\rm orb} = 0.80$ (upper) & 2.20 days (middle row). In the lower set of panels, $M_{\rm WD} = 0.80 M_\odot$, $M_{\rm d} = 1.00\ M_\odot$, $P_{\rm orb} = 3.0$ days. In these three cases, the binaries begin mass transfer on the MS, HG and FGB, respectively. In the initial stage of mass transfer in all three systems $\zeta_{th} < \zeta_{\rm RL}$ and mass transfer should proceed on thermal timescale. These binaries should not be considered representative of the total population; rather, we aim here to represent those systems in which a WD reaches $M_{\rm Ch}$. Note in particular that WD binaries in which the companion overflows its Roche lobe on the late main-sequence or Hertzsprung gap constitute the overwhelming majority of "successful" progenitors of SNe Ia in all sets of our calculations.

Note that the binary illustrated in the lower row of Fig. 2.2 would, upon overfilling its Roche lobe on the RGB, form a CE if the Hjellming & Webbink (1987) criterion for stability of mass-transfer were applied (for the purposes of comparison we ignore this criterion here). Although this criterion is widely used, it may overestimate the number of systems which undergo unstable mass-transfer (Woods & Ivanova, 2011; Passy, Herwig & Paxton, 2012). In the RG case, the binary has short thermal timescale mass transfer phases in the IBiS and MESA-based calculations. Apparently, the formal choice of lower mass transfer mass rate in BSE, ignores existence of TTMT-stage in this case.

In table 2.2, we present the duration of the RAWD and SNBWD phases, as well as the mass lost by the donor, and the mass accreted in each phase, for each example.

It is worth noting that, with different mass transfer prescriptions, the mass accreted by the WD and the duration of the RAWD and SNBWD phases in different codes are quite different. Compared to the detailed stellar evolution calculations, BSE usually overestimates the duration of the SNBWD phase and underestimates the RAWD phase. The

Table 2.2: Comparison of the duration of RAWD and SNBWD phases, accreted mass ΔM_{WD} in RAWD and SNBWD phases, mass lost by the donors for the three examples shown in Fig. 2.2. Note that these numbers do not represent the typical values in the population, which will be addressed in a subsequent paper.

	MS donor			HG donor			RG donor		
Example	BSE	IBiS	MESA	BSE	IBiS	MESA	BSE	IBiS	MESA
Duration of RAWD phase (Myr)	0.576	0.114	0.954	0.926	0.108	1.14	0.0	0.204	0.268
Duration of SNBWD phase (Myr)	0.397	0.040	0.233	0.201	0.035	0.039	0.0	0.0	0.196
ΔM_{WD} in SNBWD phase ($M_\odot$)	0.1516	0.0089	0.1068	0.049	0.0087	0.010	0.0	0.0	0.059
ΔM_{WD} in RAWD phase ($M_\odot$)	0.3088	0.0435	0.4723	0.5480	0.0417	0.5885	0.0	0.0816	0.0997
$\Delta M_{d,ml}$ of donor star ($M_\odot$)	0.8498	1.8860	0.93674	1.3264	1.8728	1.2475	0.7476	0.7515	0.7276

IBiS code underestimates both of them in the MS and HG donor cases. In the MS and HG cases, the amounts of mass accreted during RAWD phase are comparable in BSE and MESA calculations, while they are an order of magnitude smaller in IBiS calculations. In the RG case, ΔM_{WD} during the RAWD phase is comparable in IBiS calcultions and in MESA calculations. In addition, in all three cases, the amount of mass accreted during the RAWD phase is larger than that in the SNBWD phase.This points again to the need for a proper understanding of accretion at rates exceeding $\dot{M}_{max}$. The primary reason for the difference between IBiS calculations and BSE or MESA calculations is that the duration of the phase of effective mass-accumulation ($\dot{M}_a > \dot{M}_{cr}$) in IBiS is about one order of magnitude smaller than that in BSE and MESA.

The difference between IBiS and BSE calculations is partially due to the fact that approximations for $\dot{M}$ in IBiS are based on results of calculations for binary stars, while in BSE approximations are based on computations for single stars. Both of them produce results different from those, obtained using MESA. Evidently, the difference in mass transfer rate behaviour has an important impact on the results of binary population synthesis for NBWDs. Below, we will show this by using different BPS algorithms.

2.5 Results and Discussion

2.5.1 Population synthesis of accreting WDs

We model two cases of star formation:
(I) A starburst — stellar population with mass $M_t = 10^{11} M_\odot$ is formed at $t = 0$.
(II) Constant star formation rate — a galaxy has a constant star formation rate of $1 M_\odot$/yr for 10 Gyr.

The Number of SNBWD

Figures 3.12 and 2.4 show the evolution of the number of SNBWD per unit mass and their bolometric luminosity, respectively, in different models. Note immediately, that the

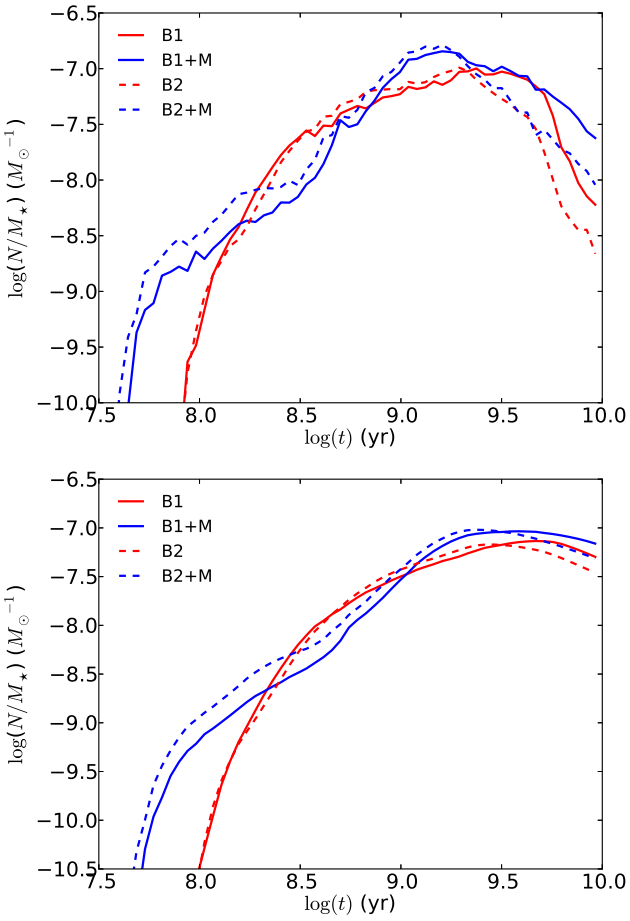

Figure 2.3: The number of SNBWDs normalised to the total stellar mass for starburst case (upper panel) and constant SFR case with SFR $= 1\,M_{\odot}/\mathrm{yr}$ (lower panel). The blue and red lines show the results computed with BSE+MESA and BSE only, respectively.

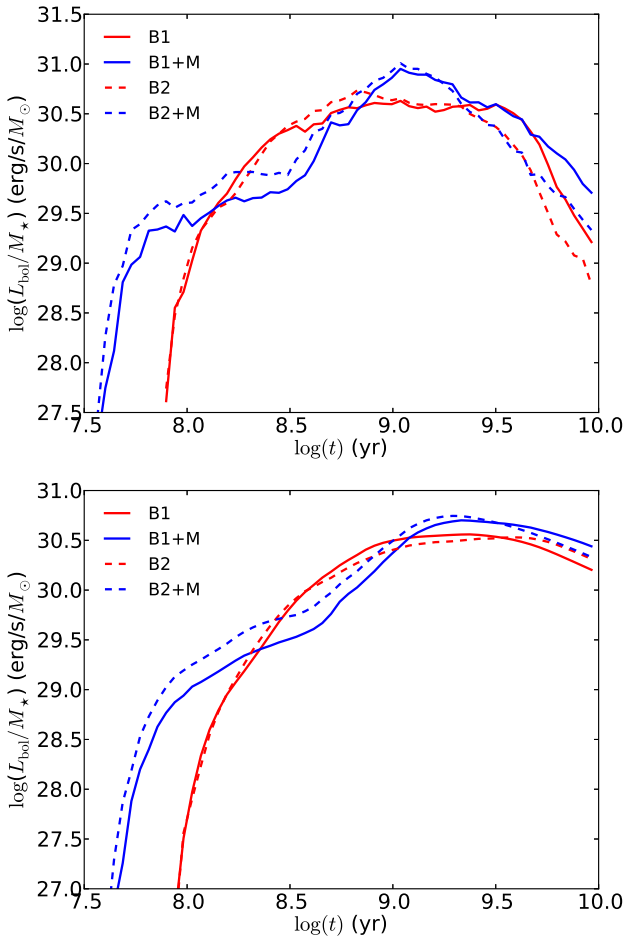

Figure 2.4: Similar to Fig. 3.12, but for bolometric luminosity. Upper panel — starburst case, lower panel — the case of constant SFR (SFR = $1M_\odot$/yr). The blue and red lines show the results computed with BSE+MESA and BSE only, respectively.

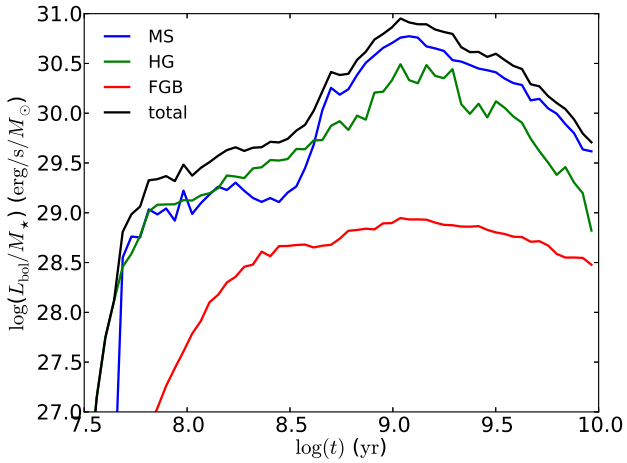

Figure 2.5: Bolometric luminosity of SNBWDs with different types of donors for starburst case in model B1+M.

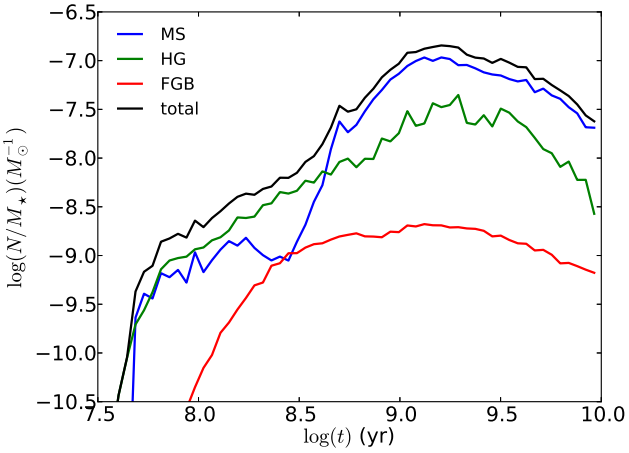

Figure 2.6: Similar to Fig. 2.5 but for the number of SNBWDs.

difference is not dramatic between models with precomputed binding energy parameter λ and a fixed α_{ce} and models with constant product $\alpha_{ce} \times \lambda$ in the common envelope equation. This is unsurprising, given that for relatively low-mass stars $\lambda < 1$, and does not vary as strongly with evolutionary state as for high-mass stars (Xu & Li, 2010; Loveridge, van der Sluys & Kalogera, 2011).

As expected from previous studies (Yungelson, 2010), the normalized number of SNBWD in case I (starburst) is larger than that for case II (constant SFR) at early age and smaller at late times. In the starburst case, the number of SNBWDs is sharply decreasing after 2 Gyr, as the reservoir of binaries with "proper" combinations of accretor and donor masses is exhausted. In the constant SFR case, SNBWDs form with a delay of about 1 Gyr respective to star formation and then "die" in about 2 Gyr, while the galaxy mass continuously increases. This is the reason for the decrease of $(N/M_\star)$ in the lower panel of Fig. 3.12. At 10 Gyr, the number of SNBWDs in BSE+MESA models may be as high as 4550 - 6550 in a $10^{11} M_\odot$ spiral "galaxy" and 750 - 1900 in an elliptical one of the same mass. The number of SNBWDs in an elliptical galaxy at $t = 10$ Gyr in our model is comparable to the number in the model of Yungelson (2010), while for a spiral galaxy in our model it is a little larger. Given that most of the soft X-ray emission from SNBWD is easily absorbed by interstellar gas, not all SNBWDs will be observed as SSSs. So we must emphasize that the number of SSS in the model may be estimated only after analysis of the spectra of SNBWDs (Paper II, in preparation).

If hydrogen burns steadily on the surface of a WD, its nuclear burning luminosity is

$$L_{\rm nuc} = \epsilon_{\rm H} X_{\rm H} \dot{M}_{\rm acc}, \tag{2.7}$$

where $\epsilon_{\rm H} = 6.4 \times 10^{18}$erg/g is the nuclear energy release per unit mass of hydrogen, $X_{\rm H}$ is the mass fraction of hydrogen, and $\dot{M}_{\rm acc}$ is the accretion rate.

In Figure 2.4, we present the dependence of the nuclear luminosity of the SNBWDs population on time. As may be expected, it follows the evolution of the number of SNBWDs. In addition, we should note that helium burning contributes little to the total bolometric luminosity, since it is only 10% as efficient as hydrogen burning.

In Figs. 2.5 and 2.6, we show the normalized bolometric luminosity and numbers of systems with donors of different types in a starburst "galaxy". We find that at very early times, the number of SNBWDs and their bolometric luminosity are dominated by HG systems, but after about 300 Myr (approximately the lifetime of a $3\,M_\odot$ star on the MS) the population becomes dominated by systems with MS-donors. Relative to MS- and HG- donor systems, those binaries which begin mass transfer on the RGB do not play a significant role at any epoch. This is due to the short time they spend in the steady hydrogen burning regime. However, in describing the number of HG donors, we should note that the donor type is defined at the onset of mass transfer. In fact, many donors which begin mass transfer on the HG reach the RGB before the end of mass transfer phase. So, this result can not be directly compared with observation.

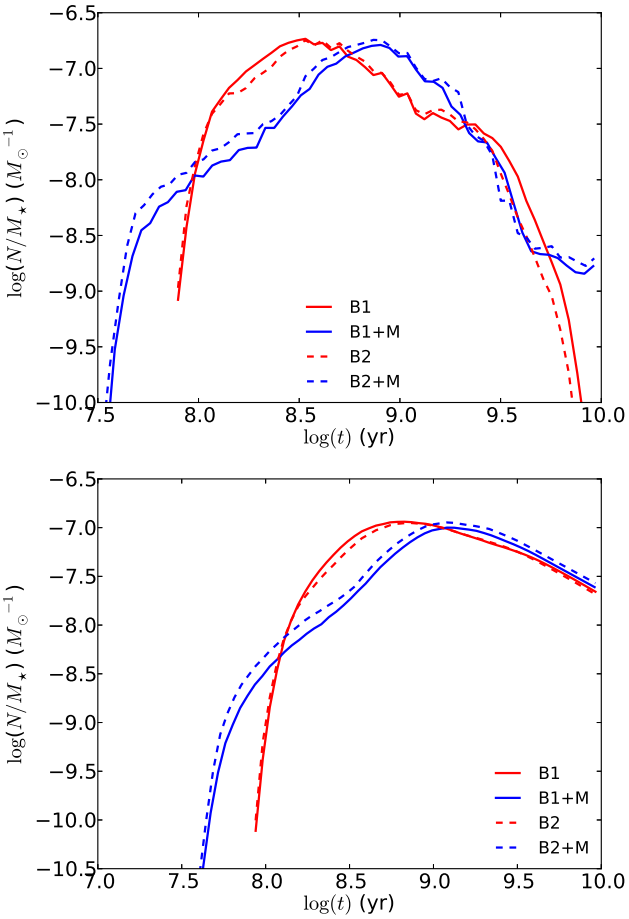

Figure 2.7: The number of RAWDs normalized to the total stellar mass at the given time for starburst case (upper panel) and constant SFR case with SFR $= 1\ M_\odot$/yr (lower panel) as a function of time. The blue and red lines show the results computed with BSE+MESA and BSE only, respectively.

The Number of Rapidly Accreting WDs

The rate of mass transfer is highest at the initial stages of mass transfer and some NBWD should pass through a RAWD phase (Fig. 2.2). In Fig. 2.7, we show the evolution of the number of RAWDs in each model. It is evident that the choice in prescription for the binding parameter λ (whether fixed or found from an analytic fit to stellar models) does not lead to the difference in numbers exceeding $\simeq 3$ for RAWDs.

The "delay" found between initial star formation and the formation of RAWDs is shorter in those models which use detailed calculation of post-RLOF evolution. This is a consequence of the difference in the common-envelope formation criterion: in our BSE-only models systems with massive donors are immediately rejected by the stability criterion, while in the BSE+MESA model they contribute to the number of RAWDs at very early epochs. The use of the stability criterion from Hjellming & Webbink (1987) in our BSE-only models likely results in the lower number of RAWD and NBWD compared to the BSE+MESA-based calculations.

The origin of another feature — the finite time in which RAWDs may exist in any starburst "galaxy" in models B1, B2 — may have the same reason: while BSE immediately rejects RG-donors on the base of the Hjellming & Webbink (1987) criterion for dynamically unstable mass loss, the hybrid algorithm always follows the increase of $\dot{M}$ before the formation of a CE, and RAWDs and SSSs should inevitably be present in the model, albeit with short lifetimes.

Since the existence of a RAWD phase is based on the assumption that WDs may lose mass through optically thick winds, it was suggested that they may be observable as low-luminosity Wolf-Rayet stars (possibly WR nuclei of PN?) or V Sge type cataclysmic binaries with numerous emission lines of highly ionized species in their spectra (see Lepo & van Kerkwijk, 2013, and references therein). Our "spiral" model galaxies with mass $10^{11} M_{\odot}$, suggest the existence of 2250 - 2500 RAWDs at 10 Gyr, while in the models of early-type "galaxies" with the same mass, the number of RAWDs is 160 - 180 at 10 Gyr. RAWDs are absent at 10 Gyr in our BSE-only models, while they remain present in our models where the response of the donor is followed throughout the mass transfer phase.

This suggests that RAWDs in nearby ellipticals, such as M32, can be observed. A search for RAWDs in the central core of the Small Magellanic Cloud (Lepo & van Kerkwijk, 2013) did not discover a single RAWD candidate system. Because it is still uncertain whether WD may lose mass via optically thick winds, and the appearance of RAWD has never been modeled in detail, the nondetection of RAWDs does not provide constraints on the SD model of SNe Ia.

Given that accreting WDs spend a significant time as RAWDs, they can increase mass significantly and become progenitors of SNe Ia. During the RAWD phase, the WD photosphere will inflate significantly and emit predominantly in the extreme UV. Given that this EUV radiation will ionize the surrounding ISM, Woods & Gilfanov (2013, 2014) suggested that observations of emission lines, in particular in He II 4686Å, may serve to constrain the presence of high-temperature ionizing sources. In order to explore this prediction, Johansson et al. (2014) selected $\sim$ 11500 emission line galaxies and searched for a HeII emission

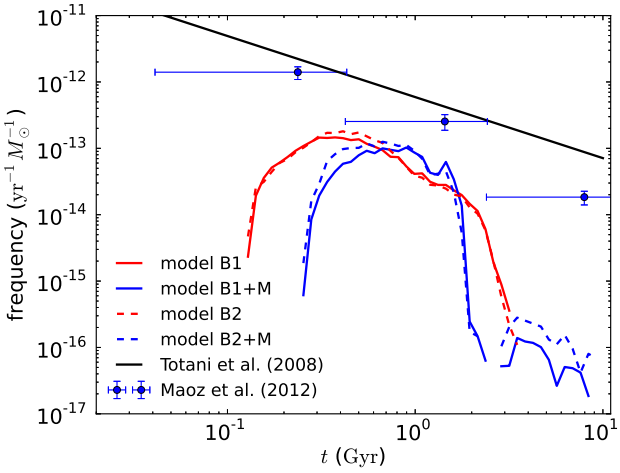

Figure 2.8: Evolution of the SNe Ia rate as a function of galaxy age for elliptical-like galaxy. The power-law line is the fitting formula from Totani et al. (2008) and the points with errorbars are the observed data from Maoz & Mannucci (2012).

feature. They found that it is significantly weaker than expected if the SD-scenario would be the primary channel for the production of SNe Ia. In particular, they found that the contribution of the SD-channel to the total SN Ia rate in early-type galaxies with the age $1\text{Gyr} \leq t \leq 4\text{Gyr}$ must be $< 5\%$.

2.5.2 SNe Ia rates

Figure 2.8 shows the SNe Ia rate as a function of age for a starburst galaxy. Since the delay time distribution (DTD) is the SN rate as a function of the time elapsed between the formation of a binary and the explosion of a SN Ia, the plot also presents the DTD.

For comparison, we show the empirical DTDs found by Totani et al. (2008) and Maoz, Mannucci & Brandt (2012). From Totani et al. (2008), we have used their fit obtained assuming solar abundance and a Salpeter IMF for the stellar population. Although we have used different IMF, inspection of their table 4 reveals that the result of Totani et al. (2008) does not strongly depend on the IMF. Maoz, Mannucci & Brandt (2012) use Kroupa IMF. Similar to other studies, the SNe Ia rate produced by the SD-scenario in our models falls well below the observed one, with a DTD which does not follow the simple power-law distribution suggested by observations. It is worth noting that the peak in the DTD for our BSE+MESA models is shifted to later times, closer to 1 Gyr, compared to the BSE models. This is mainly due to the difference in mass-transfer rate treatment, as discussed in the previous subsection.

Our peak calculated SNe Ia rate for the starburst case is still smaller than the observed rate, even though we have adopted 100% accumulation efficiency for helium burning. Figure 2.9 shows the SNe Ia rate for a spiral-like "galaxy" with constant SFR $= 1.0 M_\odot/\text{yr}$. Given that the current and likely for the last many Gyrs SFR in the Milky

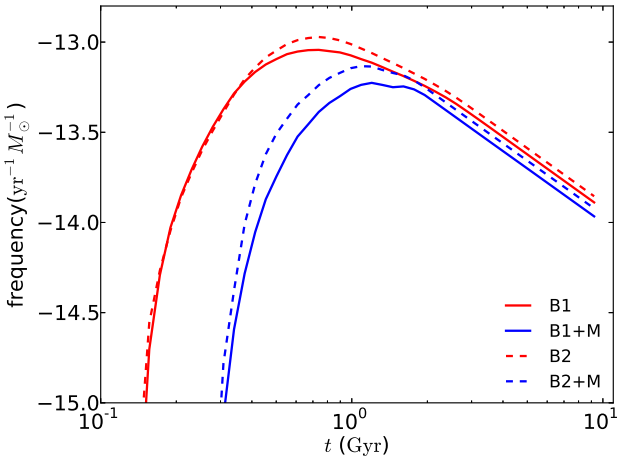

Figure 2.9: Evolution of the SNe Ia rate for spiral-like galaxy with SFR = $1.0 M_\odot$/yr.

Way is ~ 2 M$_\odot$ yr^{-1} (Chomiuk & Povich, 2011; Kennicutt & Evans, 2012)[4], the SD SNe Ia rate in our simulation is 2.0×10^{-4}yr^{-1} at $t = 10$ Gyr. This is $\approx$ 15–20 times lower than the rate inferred for Milky Way like galaxies $(3-4) \times 10^{-3}$/yr (Cappellaro, Evans & Turatto, 1999). Note that past estimates of the rate of SNe Ia from the SD-channel (e.g., Han & Podsiadlowski, 2004) produced larger values partially due to a higher assumed SFR: 3-5$M_\odot$/yr.

Han & Podsiadlowski (2004); Wang, Li & Han (2010); Meng & Yang (2010) adopted a similar method to investigate the SNe Ia rate produced by WD+MS/HG binaries, but under different assumptions on SFR, binarity fraction, common envelope ejection efficiency, retention efficiency and magnetic braking. If we renormalize the rates of SNe Ia found in these papers to a SFR of 2 M$_\odot$ yr^{-1} and binary fraction 50%, they do not exceed 3.6×10^{-4}yr^{-1} which is not significantly different from the rate which we derive. Meng & Yang (2010) also investigated the effect of mass stripping and accretion-disk instability, as suggested by Hachisu, Kato & Nomoto (2008) and King, Rolfe & Schenker (2003); these hypothetical effects may increase the rate of SNe Ia by a factor of 3-4.

In order to verify the influence of the RAWD phase on the SNe Ia rate, we also calculated the latter assuming that the WD binaries will enter CE when mass accretion rate is larger than the maximum rate for stable hydrogen burning. We find that SNe Ia rate becomes negilible in elliptical and spiral galaxies, in accordance with the estimates made before the introduction of optically thick winds as a stabilizing effect on mass transfer (e.g., Yungelson et al., 1996).

In Figure 2.10, we show the distribution of binary parameters at the onset of mass transfer for successful progenitors of SNe Ia in the starburst case. Here we only show four different WD mass ranges, since there are far fewer SNe Ia produced outside of these

[4] As shown by Chomiuk & Povich (2011), modern estimates of current Galactic SFR cluster around 1.9 ± 0.4 M$_\odot$ yr^{-1}, if normalized to the same assumptions about the IMF of the stellar population and similar assumptions about stellar evolution are adopted (see Table 1 in the quoted paper).

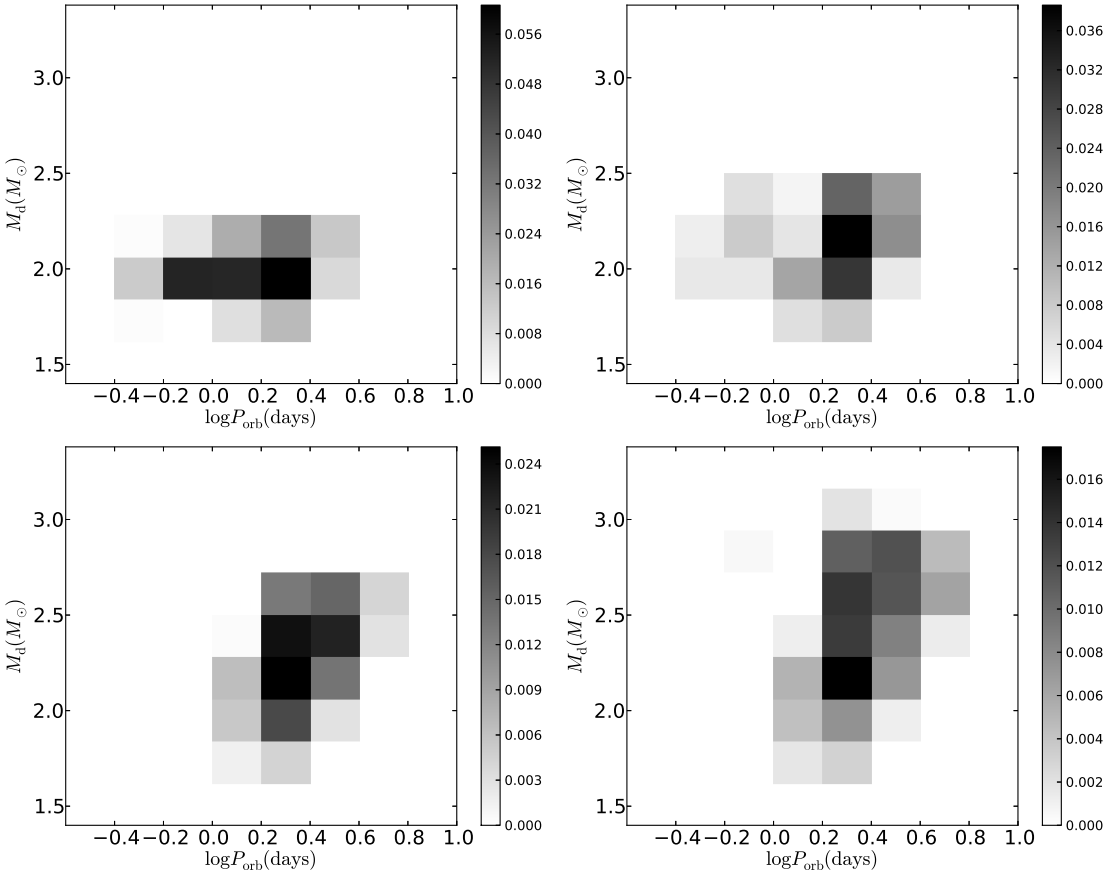

Figure 2.10: The $P_{\rm orb} - M_{\rm d}$ distribution at the onset of mass transfer of all successful progenitors of SNe Ia for starbust case in model B1+M for different ranges of WD masses: $0.65 <= M_{\rm WD} < 0.75$ (upper left panel), $0.75 <= M_{\rm WD} < 0.85$ (upper right), $0.85 <= M_{\rm WD} < 0.95$ (lower left) and $0.95 <= M_{\rm WD} < 1.05$ (lower right). The gray scale shows the relative contribution of each pixel to the total rate of SNe Ia.

ranges. It is interesting to find that most of the SNe Ia come from binaries with initially less massive WDs, which is consistent with Meng, Chen & Han (2009) (see their Fig. 9). This is not difficult to understand, since most white dwarf binaries in the post-CE white dwarf binary population have relatively small-mass WDs (Han, Podsiadlowski & Eggleton, 1995). Moreover, the lower mass WDs can accrete more mass in binaries with the same donor mass and orbital periods (Langer et al., 2000). Note that contribution of systems with red giant donors is insignificant in our calculation. Note, in our calculations, we do not consider possible atmospheric mass loss (Plavec, Ulrich & Polidan, 1973) or enhancement of stellar winds of RG close to ROLF (Podsiadlowski & Mohamed, 2007), which may delay embedding of the potentially unstable system into common envelope at the instant of RLOF (e.g. Podsiadlowski & Mohamed, 2007).

2.5.3 Uncertainty of common envelope evolution

It is widely understood that the outcome of CE evolution suffers from many uncertainties, such as the available sources of energy (e.g. Ivanova et al., 2013; Zorotovic, Schreiber & Parsons, 2014). In our calculation, we adopt $\alpha = 0.25$ and a fitting formula for λ. In the fitting formula for λ, the internal energy such as thermal energy of the gas and radiation energy are included (see Eq. (1) in Loveridge, van der Sluys & Kalogera, 2011). Given the uncertainty of CE evolution, we performed a set of calculations of the model B1 increasing α to 1. In Fig. 2.11, we compare the evolution of SNBWDs and SNe Ia rate in the starburst case for $\alpha = 0.25$ and $\alpha = 1.0$. We found that there is no dramatic difference between $\alpha = 1.0$ and $\alpha = 0.25$. For $\alpha = 1.0$, SNBWD, as well as SN Ia events appear slightly later than for $\alpha = 0.25$, since after the first common envelope episode systems are wider. A similar effect was noted before by Wang, Li & Han (2010). We also found no significant difference for RAWDs, which are not shown here.

2.5.4 Remarks about the noise in population synthesis calculations

In the above plots, especially Fig. 2.5, 2.6 and 2.8, one may note that the curves are noisy. This problem is commonly seen in population synthesis studies. There are several reasons for that, both in our BSE-only calculation as well as in our BSE+MESA calculation, the primary causes being:

- In our BSE-only calculation, one cause for the noise is that we have adopted several different CE criteria for different binaries. This is especially important for those binaries that begin mass transfer on the HG, which evolve to the RG phase prior to the end of the mass transfer phase. Typically, our HG-donor tracks end abruptly when they violate the stability condition of Hjellming & Webbink (1987). However, just prior to this, many tracks "dip back" into the stable burning regime. Whether this occurs or not does not depend smoothly on the time of onset of mass transfer,

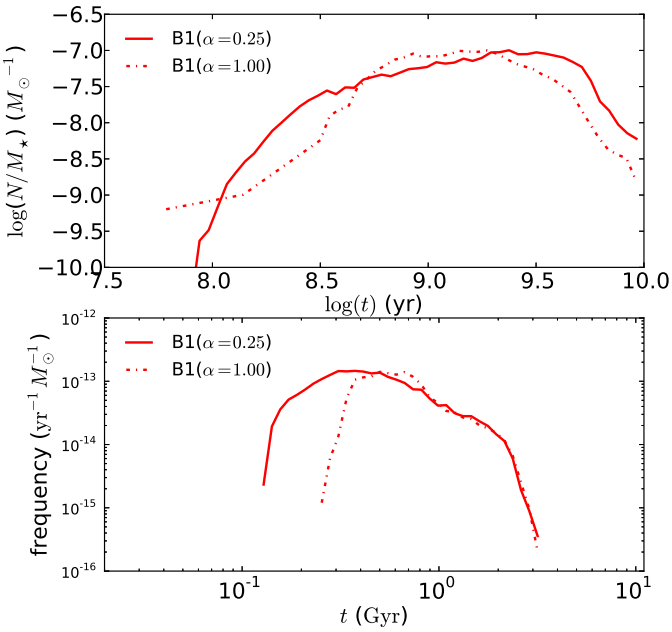

Figure 2.11: Comparision of mass-normalized SNBWDs number (upper panel) and SNe Ia rate (lower panel) for starburst case in the default configuration (solid line) and assuming $\alpha = 1.0$ (dash-dotted line).

therefore introducing small variations in the numbers and luminosity of SNBWDs predicted in our calculations.

- In addition to this, the limited number of tracks in the calculation will also contribute to the noise. In particular, in our BSE+MESA calculations, we perform a mapping from a set of $\sim$ 100,000 tracks produced by BSE, to one of $\sim$ 30,000 tracks produced by MESA. The discontinuous transition from our BSE grid to a much coarse grid of MESA tracks introduces unphysical variability in our output.

- Finally, the noise in the Fig. 2.8 is primarily due to the small number of binary tracks which explode as SNe Ia.

2.6 Summary and Conclusions

In this work, we combined the population synthesis code BSE with the detailed stellar evolutionary code MESA for the first time, in order to study the population of accreting WDs. We also compared the output from this with the results obtained applying a "rapid" algorithm, using BSE alone. With these two BPS algorithms, we investigated the evolution of the number of rapidly accreting white dwarfs, stable nuclear burning white dwarfs and the SNe Ia rate in elliptical and spiral-like galaxies. In addition to confirming that the SD

channel is subdominant in producing the overall SN Ia rate, we also evaluated the effect of implementing differing treatments of mass transfer for the results of BPS calculations.

Comparing the two versions of our binary population synthesis calculations, we found that the mass transfer prescription in BPS is especially important for calculating the number and total luminosity of nuclear-burning white dwarfs in elliptical galaxies at early and late epochs (from initial starburst). We argue that this also partially explains the differences in SNe Ia rates and DTD obtained by different binary population synthesis groups. We found that RAWDs appear earlier in our BSE+MESA model compared with BSE-only, due to the accreting WDs with massive donors found in the former.

We find that there is a factor of ≈ 3 difference between the results of our calculations using a fitting formula for the binding parameter λ (Loveridge, van der Sluys & Kalogera, 2011) and a constant $\alpha_{\rm ce} = 0.25$, and our calculations using a constant $\alpha_{\rm ce} \times \lambda = 0.25$.

In our BSE+MESA model, we found that the number of RAWDs at 10 Gyr is $160-180$ for an elliptical galaxy of $10^{11}\,M_{\odot}$ and $2250-2500$ for a spiral-like galaxy of the same mass. This result is in stark contrast with zero RAWDs predicted in our calculation for a model elliptical galaxy using BSE alone.

We find that the number of SNBWD is $750-1900$ in our model elliptical-like galaxy and $4550-6550$ in our model spiral-like galaxy (both with $M = 10^{11}\,M_{\odot}$ at 10 Gyr).

The predicted SD SNe Ia rate for a Milky-Way-like galaxy is found to be $\simeq 2.0 \times 10^{-4}{\rm yr}^{-1}$, more than an order of magnitude lower than the observationally inferred total Galactic SNe Ia rate. Our DTD for the SD-model is inconsistent with the observed DTD $\propto t^{-1}$. If we assume that RAWDs do not exist, but rather that a common envelope is formed if the accretion rate onto a WD is larger that the upper limit for stable hydrogen burning, then the rate of SNe Ia produced by the SD-channel becomes negligible.

To conclude our discussion of the significance of the SD-channel for the production of SNe Ia, we note the following. Since WDs in the steady burning phase can effectively accumulate mass, it is widely suggested that SSSs be identified with the progenitors of SNe Ia and, therefore, observations of SSSs may be useful for constraining the SD model. Gilfanov & Bogdán (2010) estimated the expected X-ray flux from the progenitors of SNe Ia in the SD-scenario for elliptical galaxies based on the observed supernova rate. They found that the observed X-ray flux from six nearby elliptical galaxies is $30-50$ times smaller than the predicted value, and constrain the contribution of the SD-channel to $< 5\%$. In a similar way, Di Stefano (2010) found that there are too few SSSs to account for the SNe Ia rate. Even if accreting WDs radiate at significantly lower temperatures (T$\approx 10^5 K$), due to the inflation of their photospheres, the SD channel may still be limited to providing $< 10\%$ of the SNe Ia rate (Woods & Gilfanov, 2013; Johansson et al., 2014).

Yungelson et al. (1996), Di Stefano (2010), and Yungelson (2010) considered the possibility that some SSSs may reside in wind-accreting systems which later produce double-degenerate systems (symbiotic stars), and estimated their number in the Galaxy as $\sim 10^3$, while the estimate by Nielsen et al. (2014) is even lower: $\sim 10^2$. Though several 10^3 SNB-WDs in the model is apparently a large number, it is still about 2 orders of magnitude lower than that necessary to be consistent with the observationally inferred Galactic SNe Ia rate. Lü, Yungelson & Han (2006) and Nielsen et al. (2014) estimated that in wind-fed systems

WD typically accrete no more than $\approx 0.1 M_{\odot}$.

Acknowledgments

We would like to thank an anonymous referee for useful comments, which helped to improve the paper. HLC acknowledges the computing time granted by the Yunnan Observatories and provided on the facilities at the Yunnan Observatories Supercomputing Platform.

Bibliography

Abt H. A., 1983, ARA&A, 21, 343

Bloom J. S. et al., 2012, ApJL, 744, L17

Bours M. C. P., Toonen S., Nelemans G., 2013, A&A, 552, A24

Cappellaro E., Evans R., Turatto M., 1999, A&A, 351, 459

Chomiuk L., Povich M. S., 2011, AJ, 142, 197

Davis P. J., Kolb U., Willems B., 2010, MNRAS, 403, 179

de Kool M., 1990, ApJ, 358, 189

Dewi J. D. M., Tauris T. M., 2000, A&A, 360, 1043

Di Stefano R., 2010, ApJ, 719, 474

Duquennoy A., Mayor M., 1991, A&A, 248, 485

Gilfanov M., Bogdán Á., 2010, Nature, 463, 924

Hachisu I., Kato M., Nomoto K., 1999, ApJ, 522, 487

Hachisu I., Kato M., Nomoto K., 2008, ApJ, 679, 1390

Han Z., Podsiadlowski P., 2004, MNRAS, 350, 1301

Han Z., Podsiadlowski P., Eggleton P. P., 1995, MNRAS, 272, 800

Hillebrandt W., Kromer M., Röpke F. K., Ruiter A. J., 2013, Frontiers of Physics, 8, 116

Hjellming M. S., Webbink R. F., 1987, ApJ, 318, 794

Hurley J. R., Tout C. A., Pols O. R., 2002, MNRAS, 329, 897

Iben, Jr. I., Tutukov A. V., 1984, ApJS, 54, 335

Iben, Jr. I., Tutukov A. V., 1989, ApJ, 342, 430

Idan I., Shaviv N. J., Shaviv G., 2013, MNRAS, 433, 2884

Ivanova N. et al., 2013, Astron. Astrophys. Rev., 21, 59

Ivanova N., Taam R. E., 2004, ApJ, 601, 1058

Johansson J., Woods T. E., Gilfanov M., Sarzi M., Chen Y.-M., Oh K., 2014, MNRAS, 442, 1079

Kennicutt R. C., Evans N. J., 2012, ARA&A, 50, 531

King A. R., Rolfe D. J., Schenker K., 2003, MNRAS, 341, L35

Kraicheva Z. T., Popova E. I., Tutukov A. V., Yungelson L. R., 1979, SvA, 23, 290

Kroupa P., 2001, MNRAS, 322, 231

Langer N., Deutschmann A., Wellstein S., Höflich P., 2000, A&A, 362, 1046

Lepo K., van Kerkwijk M., 2013, ApJ, 771, 13

Loveridge A. J., van der Sluys M. V., Kalogera V., 2011, ApJ, 743, 49

Lü G., Yungelson L., Han Z., 2006, MNRAS, 372, 1389

Madhusudhan N., Rappaport S., Podsiadlowski P., Nelson L., 2008, ApJ, 688, 1235

Maoz D., Mannucci F., 2012, PASA, 29, 447

Maoz D., Mannucci F., Brandt T. D., 2012, MNRAS, 426, 3282

Matteucci F., Greggio L., 1986, A&A, 154, 279

Meng X., Chen X., Han Z., 2009, MNRAS, 395, 2103

Meng X., Yang W., 2010, ApJ, 710, 1310

Morton D. C., 1960, ApJ, 132, 146

Nelson L., 2012, Journal of Physics Conference Series, 341, 012008

Newsham G., Starrfield S., Timmes F. X., 2014, in Astronomical Society of the Pacific Conference Series, Vol. 490, Stellar Novae: Past and Future Decades, Woudt P. A., Ribeiro V. A. R. M., eds., p. 287

Nielsen M. T. B., Nelemans G., Voss R., Toonen S., 2014, A&A, 563, A16

Nugent P. E. et al., 2011, Nature, 480, 344

Paczyński B., 1971, Acta. Astron., 21, 417

Paczyński B., Ziólkowski J., Zytkow A., 1969, in Astrophysics and Space Science Library, Vol. 13, Mass Loss from Stars, Hack M., ed., p. 237

Paczynski B., Zytkow A. N., 1978, ApJ, 222, 604

Passy J.-C., Herwig F., Paxton B., 2012, ApJ, 760, 90

Paxton B., Bildsten L., Dotter A., Herwig F., Lesaffre P., Timmes F., 2011, ApJS, 192, 3

Paxton B. et al., 2013, ApJS, 208, 4

Perlmutter S. et al., 1999, ApJ, 517, 565

Pfahl E., Rappaport S., Podsiadlowski P., 2003, ApJ, 597, 1036

Plavec M., Ulrich R. K., Polidan R. S., 1973, PASP, 85, 769

Podsiadlowski P., Mohamed S., 2007, Baltic Astronomy, 16, 26

Podsiadlowski P., Rappaport S., Pfahl E. D., 2002, ApJ, 565, 1107

Prialnik D., Kovetz A., 1995, ApJ, 445, 789

Rappaport S., Verbunt F., Joss P. C., 1983, ApJ, 275, 713

Ricker P. M., Taam R. E., 2012, ApJ, 746, 74

Riess A. G. et al., 1998, AJ, 116, 1009

Ritter H., 1988, A&A, 202, 93

Ruiter A. J., Belczynski K., Fryer C., 2009, ApJ, 699, 2026

Toonen S., Claeys J. S. W., Mennekens N., Ruiter A. J., 2013, ArXiv e-prints

Totani T., Morokuma T., Oda T., Doi M., Yasuda N., 2008, PASJ, 60, 1327

Tutukov A. V., Yungelson L. R., 1981, Nauchnye Informatsii, 49, 3

Wang B., Li X.-D., Han Z.-W., 2010, MNRAS, 401, 2729

Webbink R. F., 1984, ApJ, 277, 355

Whelan J., Iben, Jr. I., 1973, ApJ, 186, 1007

Wolf W. M., Bildsten L., Brooks J., Paxton B., 2013, ApJ, 777, 136

Woods T. E., Gilfanov M., 2013, MNRAS, 432, 1640

Woods T. E., Gilfanov M., 2014, MNRAS, 439, 2351

Woods T. E., Ivanova N., 2011, ApJL, 739, L48

Xu X.-J., Li X.-D., 2010, ApJ, 716, 114

Yaron O., Prialnik D., Shara M. M., Kovetz A., 2005, ApJ, 623, 398

Yungelson L., Livio M., 1998, ApJ, 497, 168

Yungelson L., Livio M., Truran J. W., Tutukov A., Fedorova A., 1996, ApJ, 466, 890

Yungelson L., Livio M., Tutukov A., Kenyon S. J., 1995, ApJ, 447, 656

Yungelson L. R., 2010, Astronomy Letters, 36, 780

Zorotovic M., Schreiber M. R., Gänsicke B. T., Nebot Gómez-Morán A., 2010, A&A, 520, A86

Zorotovic M., Schreiber M. R., Parsons S. G., 2014, A&A, 568, L9

Chapter 3

X-ray and UV emission of populations of accreting white dwarfs

Monthly Notices of the Royal Astronomical Society, 453, 3024, 2015
Chen, H.-L., Woods, T. E., Yungelson, L. R., Gilfanov, M. & Han, Z.

3.1 Abstract

Accreting white dwarfs (WDs) with non-degenerate companions are expected to emit in soft X-rays and the UV, if accreted H-rich material burns stably. They are an important component of the unresolved emission of elliptical galaxies, and their combined ionizing luminosity may significantly influence the optical line emission from warm ISM. In an earlier paper we modeled populations of accreting WDs, first generating WD with main-sequence, Hertzsprung gap and red giant companions with the population synthesis code BSE, and then following their evolution with a grid of evolutionary tracks computed with MESA. Now we use these results to estimate the soft X-ray (0.3-0.7keV), H- and He II-ionizing luminosities of nuclear burning WDs and the number of super-soft X-ray sources for galaxies with different star formation histories. For the starburst case, these quantities peak at ~ 1 Gyr and decline by $\sim 1-3$ orders of magnitude by the age of 10 Gyr. For stellar ages of ~ 10 Gyr, predictions of our model are consistent with soft X-ray luminosities observed by Chandra in nearby elliptical galaxies and He II $4686\mathring{A}/\mathrm{H}\beta$ line ratio measured in stacked SDSS spectra of retired galaxies, the latter characterising the strength and hardness of the UV radiation field. However, the soft X-ray luminosity and He II $4686\mathring{A}/\mathrm{H}\beta$ ratio are significantly overpredicted for stellar ages of $\lesssim 4-8$ Gyr. We discuss various possibilities to resolve this discrepancy and tentatively conclude that it may be resolved by a modification of the typically used criteria of dynamically unstable mass loss for giant stars.

3.2 Introduction

Accreting white dwarfs (WDs) are important for the study of binary evolution and accretion physics (see Postnov & Yungelson 2014; Maoz, Mannucci & Nelemans 2014 for a recent review). Depending on the accretion rates, they are deemed to be components of cataclysmic binaries (see Warner, 2003, for a comprehensive review) and supersoft X-ray sources (van den Heuvel et al., 1992). Under differing initial conditions, they are the progenitors of components of future double white dwarfs, type Ia supernovae and binary millisecond pulsars (e.g. Whelan & Iben, 1973; Tutukov & Yungelson, 1981; Webbink, 1984; Iben & Tutukov, 1984; Taam & van den Heuvel, 1986). Although they are widely studied, there remain many uncertainties concerning their formation and evolution. One avenue to constrain this problem is to invoke binary population synthesis. This allows one to compare the observed numbers and characteristics of these objects with that which are expected given our present understanding of binary evolution and accretion physics.

Hydrogen-rich material accreted by a WD from its companion may burn at its surface either stably or unstably. The result is strongly dependent on the mass transfer rate and mass of the WD (Paczynski & Zytkow, 1978; Sion, Acierno & Tomczyk, 1979). If the accretion rate corresponds to the stable nuclear burning regime, accreting white dwarfs (henceforth, SNBWD) have typical effective temperatures of $10^5 - 10^6$K, emitting prominently in the soft X-ray and EUV. In this regime, not all accreting WDs can be observed as SSSs, as this depends on their intrinsic luminosity, effective temperature and the column density of the gas along the line of sight. In the present paper, we refer to SNBWDs with observed soft X-ray (0.30-0.70 keV) luminosity $L_{\rm x} > 10^{36}$ erg/s as SSSs. For accretion rates below the stability limit, hydrogen burning occurs only in unstable flashes, observable as novae. There will be little X-ray emission in this regime, except in the post-novae SSS phase (Truran & Glasner (1995); Wolf et al. (2013), Soraisam et al. (in prep.)). If the accretion rate is larger than the maximum rate for stable nuclear-burning, the result is still unclear (Cassisi, Iben & Tornambe, 1998; Hachisu, Kato & Nomoto, 1996). In the scenario of Cassisi, Iben & Tornambe (1998), the WD will become a red giant after accreting a small amount of mass (Paczyński, 1971). On the other hand, Hachisu, Kato & Nomoto (1996) proposed that in this regime the excess mass is lost as an optically thick wind. Following Lepo & van Kerkwijk (2013), the WDs in this regime are dubbed rapidly accreting white dwarfs (RAWDs). In this scenario, an accreting WD's photosphere will expand modestly, lowering their effective temperatures such that they radiate predominantly in the EUV.

In addition to the emission from X-ray binaries dominating the X-ray radiation in most galaxies, extended emission in soft X-ray band is widely observed in galaxies of different morphologies. However, the origin of the extended emission is still unclear. Bogdán & Gilfanov (2008) demonstrated that the emission from accreting WDs should be an important component of the unresolved emission.

A population of accreting WDs with effective temperatures $T_{\rm eff} > 10^5$K should be capable of ionizing the interstellar medium. Rappaport et al. (1994) were the first to model ionization nebulae around SSSs, for the simple case of spherical symmetry and blackbody spectra. They found that these nebulae should have strong He II λ4686, [O

III] λ5007, and [O I] λ6300 emission lines. Woods & Gilfanov (2013) demonstrated that accreting WDs may provide a significant, or even dominant, contribution to the ionizing background, particularly in early-type galaxies with passively-evolving stellar populations (those with negligible ongoing star formation). Depending on their numbers, this could significantly impact the ionization state of the warm ISM in gas-rich early-type galaxies. Serra et al. (2012) found that many early type galaxies (at least 40% outside the Virgo cluster) host a detectable mass of HI, i.e. $\sim (10^8 - 10^9) M_{\odot}$. Morphologically, this gas is found in regular HI discs, rings and irregularly distributed clouds. Most common are HI discs and rings, which may extend to tens of kpc, suggesting a covering factor of $\sim$1/2 for the ionizing radiation from the stellar population.

Although emission from populations of accreting WDs is important, it has been seldom studied. In Paper I (Chen et al., 2014), we conducted a population synthesis study of accreting white dwarfs. We found that it is important to have a realistic prescription for mass transfer and investigated the number of RAWDs, SNBWDs and the SNe Ia rate in the single degenerate (SD) scenario. In this paper, based on the results of our binary population synthesis of Paper I, we study the soft X-ray and UV emission of the population of accreting WDs and their contribution to the radiation of elliptical galaxies in the He II 4686$\mathring{A}$ and Hβ emission lines. These results are then compared with observations.

The paper is structured as follows. In section 3.3, we describe how we calculate the emission spectra of accreting WDs. In section 4.3, we briefly outline the typical assumptions underlying our population synthesis. In section 3.5, we present the soft X-ray (0.3-0.7keV) luminosity, H ionizing luminosity, and He II ionizing luminosity from the population of accreting WDs as a whole. We also compute the expected ratio He II4686$\mathring{A}$/Hβ as a function of age for a starburst stellar population and compare with observations of early type galaxies in the Sloan Digital Sky Survey (SDSS; Johansson et al., 2014). In section 4.5, we discuss the uncertainties in our standard model and present a potential solution to resolve the discrepancy between the results found in our standard model and observations. In addition, we show the evolution of SSS number as a function of stellar age. Finally, we summarize our results and conclude in section 4.6.

3.3 Emission spectra of accreting white dwarfs

Detailed synthetic spectral models for accreting WDs can be produced using a non-local thermodynamic equilibrium (NLTE) stellar atmosphere model (e.g. Werner, 1986, 1989; Rauch, 2003), which is known to approximately reproduce SSSs spectra (e.g. Rauch et al., 2010). In Fig. 3.1, we compare the emission spectra of a SNBWD computed by means of a NLTE model[1] with the blackbody approximation. Except for some absorption lines, the difference is not dramatic, particularly near the H and He II absorption edges. The difference in soft X-ray (0.3-0.7) keV luminosity between the blackbody approximation and NLTE models is smaller for accreting WDs with high temperatures and greater for

[1] http://dc.g-vo.org/theossa

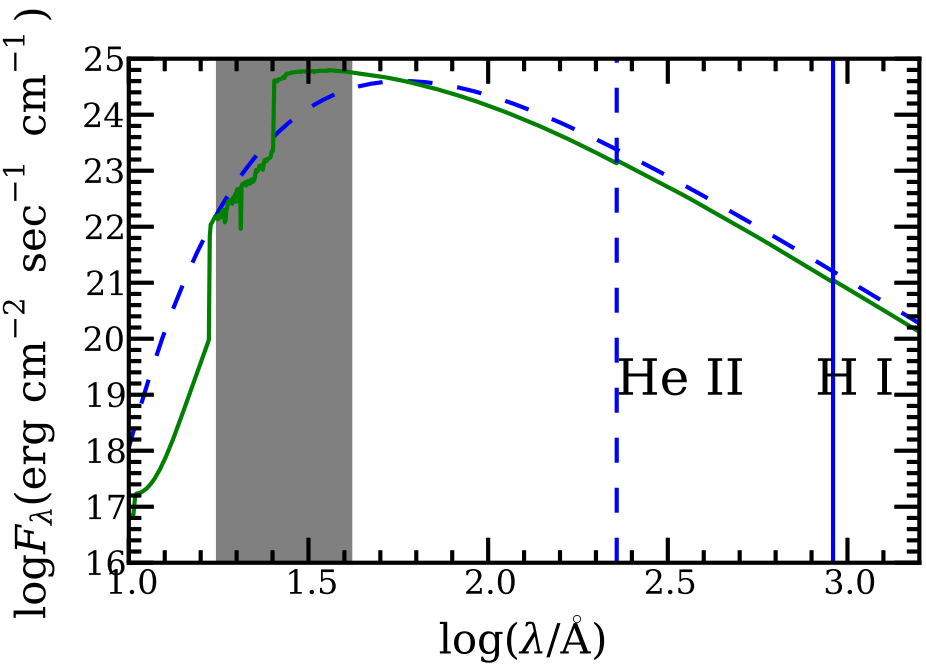

Figure 3.1: Comparison of an accreting WD spectrum computed by means of a NLTE model (green solid line, Werner (1986, 1989); Rauch (2003)) with that found from the blackbody approximation (blue dashed line) for a WD with effective temperature $T_{\rm eff}$ = 5.0×10^5 K, log(g/cm/s^2) = 8.0. The two vertical lines represent the H I and He II photoionizing limits. The edges around 25 Å and 15 Å are the C VI (25.30Å) and O VII (16.77Å) absorption edges, respectively. The shaded area denotes the soft X-ray band (0.3-0.7keV) in our calculation. The NLTE spectrum was retrieved from TheoSSA (http://dc.g-vo.org/theossa).

low temperatures. With this discrepancy in mind, we adopt the blackbody approximation for SNBWD spectra in this paper.

For a SNBWD, the nuclear burning luminosity is

$$L_{\rm nuc} = \epsilon_{\rm H} X_{\rm H} \dot{M}_{\rm acc}, \tag{3.1}$$

where $\epsilon_{\rm H} = 6.4 \times 10^{18}$ erg/g is the nuclear energy release per unit mass of hydrogen, $X_{\rm H}$ is the mass fraction of hydrogen and $\dot{M}_{\rm acc}$ is the accretion rate. We ignore the accretion luminosity in the stable-burning regime, since it is much lower (less than 10% for $M_{\rm WD} < 1.2 M_{\odot}$ and 20% for $1.20 M_{\odot} < M_{\rm WD} < 1.4 M_{\odot}$) compared with the nuclear burning luminosity.

Detailed models of SNBWDs show that their photospheric radii are about $1-8$ times as large as the radius of a cool WD (depending on the accretion rates, Iben, 1982; Wolf et al., 2013). Wolf et al. (2013) simulated the evolution of accreting WDs with different accretion rates using the MESA code (Paxton et al., 2011, 2013). From their results, we know the dependence of the photospheric radius on the accretion rates in the stable-burning regime. For any given WD mass and accretion rate, we find the radius by linear interpolation of the results of Wolf et al. (2013) between WD mass and accretion rate. Then the effective temperature of SNBWDs is found from the Stefan-Boltzmann law.

RAWDs with accretion rates larger than the maximum stable burning rate, expand as the WD loses mass and the effective temperature decreases. Hachisu, Kato & Nomoto (1999) investigated the optically-thick wind solution for different white dwarfs with different accretion rates. They showed the dependence of photospheric radius and effective temperature on the accretion rate (see their Figs. 3, 4). By linear fitting of their results and linear interpolation among different WD masses, we can find the radius and the effective temperature for any combination of white dwarf mass and accretion rate. It has been shown that RAWDs with typical mass accretion rates (less than $4.0 \times 10^{-6} M_{\odot} {\rm yr}^{-1}$) and effective temperatures (T $\approx$ 1–2$\times 10^5$K) can fully ionize hydrogen and helium beyond the wind photosphere (Woods & Gilfanov, 2013). For high accretion rates, the spectra of RAWDs are not well approximated by blackbody spectra because of absorption. However, high accretion rates can only be sustained for a short time and will contribute little to the total luminosity. Therefore, it is reasonable to use blackbody spectra as an approximation for RAWDs.

3.4 Binary Population Synthesis

In Paper I, we have introduced our approach to studying populations of accreting WDs, and have shown the importance of a careful treatment of the second mass transfer phase. Following the method outlined in Paper I, we carry out two sets of calculations with our BSE+MESA model. Here we briefly summarize the procedure and main assumptions of the calculation.

First, we evolve a set of binaries with different initial parameters using the BSE code (Hurley, Pols & Tout, 2000; Hurley, Tout & Pols, 2002), and obtain the binary parameters at the beginning of mass transfer for a population of WD binaries with main-sequence,

Hertzsprung gap and red giant companions. Second, we compute a WD binary evolution library by means of the detailed stellar evolution code MESA (Paxton et al., 2011, 2013), which describes the evolution of WD binaries with different parameters at the beginning of mass transfer. For each WD binary with a given WD mass, donor mass and orbital period from the set of systems obtained in the first step of computations, we select the nearest track in the WD binary evolution library in order to follow its subsequent evolution. We take 1.2 $M_\odot$ as the upper limit of the nascent CO WD, which was implemented in the BSE code, although modern estimates give $\approx 1.07 M_\odot$ for single stars with Z = 0.02 (e.g. Doherty et al., 2015). For the distribution of initial binary parameters, we use the Kroupa IMF for the primary mass (Kroupa, 2001), a flat mass ratio distribution (Kraicheva et al., 1979) and a flat distribution in logarithmic space for binary separation (Abt, 1983). To describe common envelope evolution, we employ the α-formalism (Webbink, 1984; de Kool, 1990). We use the fitting formula for the value of the binding energy parameter λ from Loveridge, van der Sluys & Kalogera (2011).

The efficiency α of the common envelope phase in ejecting the donor star's envelope remains uncertain (see Ivanova et al., 2013, for a comprehensive review). The latest studies of post-common envelope binaries (e.g. Davis, Kolb & Knigge, 2012) restrict α to a canonical value ≤ 1 with a tendency to decrease with increasing secondary mass and WD mass. Some studies (e.g. Davis, Kolb & Willems (2010); Zorotovic et al. (2010); Ricker & Taam (2012)) show that, likely, $\alpha < 0.50$. Here we adopt two values: $\alpha = 0.25$ (model a025) and $\alpha = 0.50$ (model a050), performing calculations for each. In Paper I, we verified that the population of hydrogen-accreting WDs depends relatively weakly on the assumed value of α.

Combining our binary population synthesis results for accreting white dwarfs with their predicted emission spectra, we study their X-ray and UV emission. As in Paper I, we investigate two simple but representative cases. (I) Starburst: all stars are formed at $t = 0$, after which the star formation rate is zero. (II) Constant star formation rate for 10 Gyr. These two cases provide us with simple models which are representative of elliptical-like and spiral-like galaxies, respectively.

3.5 Results

3.5.1 X-ray emission of accreting white dwarfs

Figure 3.2 shows the evolution of the mass-normalized X-ray luminosity of the population of accreting WDs in the starburst and constant SFR cases. For our predicted observable X-ray luminosity, we apply absorption with a column density $N_{\rm H} = 3.0 \times 10^{20} {\rm cm}^{-2}$, which is a typical value for the extinction within the Galaxy at high Galactic latitudes (Dickey & Lockman, 1990). In addition, for early-type galaxies we also show the observed X-ray luminosity per unit mass with column density $1.8 \times 10^{20} {\rm cm}^{-2} < {\rm N_H} < 6.7 \times 10^{20} {\rm cm}^{-2}$(the shaded region in the plot). This range of $N_{\rm H}$ corresponds to that observed for the six elliptical galaxies in Table 3.1. In the calculation, we only considered Galactic absorption,

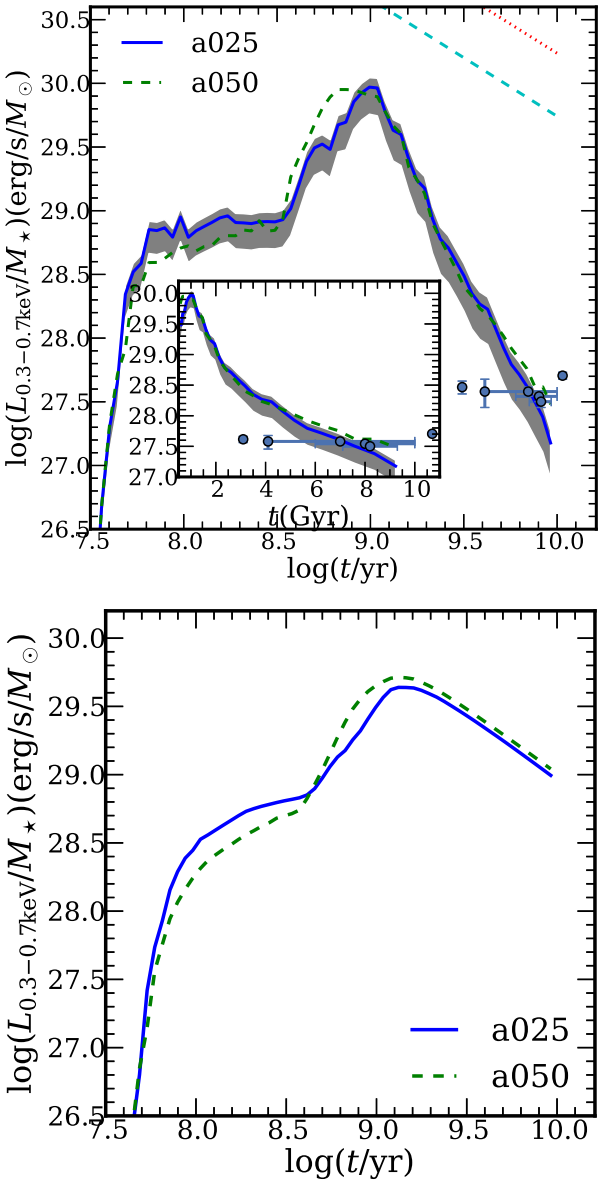

Figure 3.2: Mass-normalized X-ray luminosity (absorption applied with $N_{\rm H} = 3.0 \times 10^{20}{\rm cm}^{-2}$) in soft (0.3-0.7keV) band for starburst case (upper panel) and constant SFR case (lower panel) as a function of stellar age. In the upper panel, the shaded area shows the X-ray luminosity with $1.8 \times 10^{20}{\rm cm}^{-2} < {\rm N_H} < 6.7 \times 10^{20}{\rm cm}^{-2}$. The blue solid and green dashed lines are for models a025 and a050, respectively. The points with error bars are the observed X-ray luminosities for individual elliptical galaxies (see Table 3.1, Bogdán & Gilfanov, 2010; Zhang, Gilfanov & Bogdán, 2012). The cyan dashed line is the expected soft X-ray luminosity if all SNe Ia are produced via the SD scenario assuming $\dot{M} = 10^{-7} M_\odot$/yr, and an initial WD mass of $1.2 M_\odot$ and the delay time distribution given by Totani et al. (2008). The red dotted line is similar to the cyan dashed lines but assuming $\dot{M} = 3 \times 10^{-7} M_\odot$/yr, an initial WD mass of $1.0 M_\odot$ (cf. Gilfanov & Bogdán 2010).

Table 3.1: Comparison of the predicted X-ray luminosity in the soft X-ray band (0.3-0.7keV) in our standard model with observations. The observed X-ray luminosities for individual galaxies are taken from Bogdán & Gilfanov (2010); Zhang, Gilfanov & Bogdán (2012).

Name	age (Gyr)	$L_{\rm K}$ ($L_{\rm K,\odot}$)	$N_{\rm H}$ ($\times 10^{20}{\rm cm}^{-2}$)	$L_{\rm x}$ observed (erg/s)	$L_{\rm x}$ predicted (erg/s)	$L_{\rm x,predict}/L_{\rm x,observed}$	SSSs Num
(1)	(2)	(3)	(4)	(5)	(6)	(7)	(8)
NGC3585	3	1.5×10^{11}	5.6	3.8×10^{38}	$(2.6-3.0)\times10^{39}$	$6.8-7.9$	330-570
M32	4-10	8.5×10^{8}	6.3	1.5×10^{36}	$(1.2-1.7)\times10^{36}$	$0.8-1.1$	0
NGC3377	4	2.0×10^{10}	2.9	4.7×10^{37}	$(2.0-2.2)\times10^{38}$	$4.3-4.7$	30-60
M31 bulge	6-10	3.7×10^{10}	6.7	6.3×10^{37}	$(3.9-6.1)\times10^{37}$	$0.6-1.0$	10
M105	7-9	4.1×10^{10}	2.8	8.3×10^{37}	$(1.7-2.8)\times10^{38}$	$2.0-3.4$	10-40
NGC4278	11	5.5×10^{10}	1.8	1.5×10^{38}	$(0.88-1.98)\times10^{38}$	$0.6-1.3$	10-40

Notes. (1)-Galaxy name. (2)-Approximate stellar age of the galaxies. References-Terlevich & Forbes (2002); Coelho, Mendes de Oliveira & Cid Fernandes (2009); Olsen et al. (2006); Sánchez-Blázquez et al. (2006). (3) K-band luminosity of galaxies. (4)-Galactic absorption column density. (5)-Observed soft X-ray luminosity. (6)-Predicted soft X-ray luminosity. (7)-Predicted soft X-ray luminosity over observed soft X-ray luminosity. (8)-Predicted SSS number.

since the intrinsic absorption of these elliptical galaxies is small.

Our calculations predict that in the starburst case, the X-ray luminosity sharply decreases after 1 Gyr (Fig. 3.2). At early times (stellar age $t < 1.0$ Gyr), the X-ray luminosity in the starburst case is comparable with that in the constant SFR case for galaxies with the same mass. However, it is smaller for $t > 1.0$ Gyr. In order to compare our results with observations we use X-ray data from Bogdán & Gilfanov (2010) and Zhang, Gilfanov & Bogdán (2012) for nearby elliptical galaxies. The data and our predictions are summarised in Table 3.1 where we list the observed X-ray luminosities along with the predicted X-ray luminosities and SSS numbers for six elliptical galaxies (Bogdán & Gilfanov, 2010; Zhang, Gilfanov & Bogdán, 2012). Note that observed luminosities are total soft X-ray luminosities of unresolved emission and soft compact sources and therefore should be regarded as upper limits on the soft X-ray luminosity of nuclear burning white dwarfs (see Bogdán & Gilfanov (2010) for details). In the calculation of the predicted X-ray luminosities and SSS numbers, we have taken absorption into consideration for different galaxies with different column density values.

One can see in Fig. 3.2 that, at the ages exceeding 6 Gyr, our predicted X-ray luminosities are comparable to that which are observed in nearby ellipticals, and is roughly two orders of magnitude below the soft X-ray flux expected if all SNe Ia are produced via the SD scenario (see Gilfanov & Bogdán (2010)). This is consistent with our prediction that the SD channel does not significantly contribute to the SN Ia rate at late delay times (see Fig. 8 in Paper I). However, for the two youngest galaxies in the Bogdán & Gilfanov (2010) sample, NGC3585 and NGC3377, our standard calculations predict up to an order of magnitude larger soft X-ray luminosities than observed. The strong dependence of the X-ray luminosity on the age of the stellar population predicted by our calculation seems to contradict observations. In interpreting this result one should keep in mind that there is some controversy regarding the ages of the two youngest galaxies. Idiart, Silk & de Freitas Pacheco (2007) found that the age of NGC3377 is around 7.8 Gyr and Georgiev, Goudfrooij & Puzia (2012) listed literature values of the age of NGC3377, varying from 3.5 Gyr to 8.9 Gyr. In the case of NGC3585, Michard (2006) found a single stellar population age of 1.7 Gyr, while Hempel et al. (2007) suggested that its age should be larger than 3 Gyr. On the other hand, metallicity may be important to explain the discrepancy between model predictions and observations. O'Sullivan & Ponman (2004) and Georgiev, Goudfrooij & Puzia (2012) found that the metallicities of the two youngest galaxies, NGC3585 and NGC3377, are likely to be lower than solar metallicity. However, solar abundance is adopted in our calculation. The metallicity plays a complicated role in the evolution of accreting WDs. The metallicity influences the initial-final mass relation for stars, the stable burning limits of accreting WDs, and the evolution of mass transfer rates (Umeda et al., 1999; Meng, Chen & Han, 2008; de Mink, Pols & Yoon, 2008; Kistler et al., 2013). Therefore, any strong conclusion based on the example of these two galaxies may be premature. On the other hand, a similar discrepancy was also found in comparing predicted populations of low mass X-ray binaries with observations, based on a larger and different sample of galaxies and age determinations (Zhang, Gilfanov & Bogdán, 2012; Fragos et al., 2013).

3.5.2 UV emission of accreting white dwarfs

Since nuclear-burning white dwarfs are characteristically high temperature sources, the emission from this population will ionize the ISM and will have an important influence on the structure of the ionized gas and emission lines of a galaxy. In particular, compared with the single stellar population, accreting WDs are likely to emit predominantly beyond the He II photoionizing limit (see Fig.1 in Woods & Gilfanov 2013). So in this section, we will investigate the H ionizing and He II ionizing luminosity of accreting, nuclear-burning WDs as a binary population. In addition, we will compute the predicted ratio of two recombination lines produced in the ISM, He II λ4686Å/Hβ, and compare this with observations.

In our calculation, we assumed the binary fraction to be 50%. It has been suggested that the binary fraction may depend on the binary parameters (Kouwenhoven et al., 2009; Kraus & Hillenbrand, 2009; Sana et al., 2012). We neglect this effect, and therefore may slightly underestimate the binary fraction in our calculations. According to its standard definition, the binary fraction includes all binary stars, irrespective of their separation and evolutionary state. Our population synthesis calculations keep track of only those binaries in which one of the components is a mass accreting white dwarf. Such mass-transferring binaries are in fact a very small minority in the population (in terms of the number of systems and total mass). In accounting stars in wide binaries we assume that their emission is similar to the emission of single stars of the same spectral type. To compute emission of single stars and stars in wide binaries we use the stellar population synthesis code of Bruzual & Charlot (2003), as described below. In computing the normalisation of the stellar emission we use the total mass of stars, ignoring the small fraction (0.7% by mass) of stars in mass transferring close binaries. Hereafter, we refer to the stars in wide binaries and single stars as single population (SP) and accreting, nuclear burning WDs as binary population (BP). The total emission of the entire population is computed as a sum of emission of the SP and BP. The SP-only model represents the hypothetical case of absence of mass-accreting white dwarfs in the stellar population.

In Fig. 3.3, we show the evolution of the H-ionizing and He-ionizing luminosities as a function of stellar age in the starburst case. For the binary population, we only show the results for model a025, since we do not find a significant difference between models a025 and a050. To compute emission from the SP, we use the Bruzual & Charlot (2003) stellar population synthesis model. In running their model, we assumed solar metallicity and Chabrier (2003) IMF, as this model is not available for Kroupa IMF. This introduces only small inconsistency with our BP calculations (conducted for the Kroupa IMF). The Chabrier IMF has the same exponent as the Kroupa IMF for stellar masses above 1.0 $M_{\odot}$ and a more complicated shape at smaller masses. If the two IMFs are normalised to the same total mass, their high mass ($> 1.0M_{\odot}$) parts have the same shape and only small ($\sim 7\%$) difference in normalisation. This will result in a similarly small difference ($\sim 7\%$) in the predicted ionizing luminosity between the two IMFs, since stars with initial mass below 1.0 $M_{\odot}$ do not contribute to the ionising UV radiation. Such a small difference is insignificant given the large dynamical range of the ionising luminosities plotted in Fig. 3.3.

In Fig. 3.3, we do not show the case of a constant SFR, as in this case the H-ionizing and He-ionizing emission from accreting white dwarfs are significantly smaller than emission from the SP. This is due to the fact that in the constant SFR case there are many luminous young stars with high effective temperatures, which dominate the ionizing emission.

In the starburst case, the H-ionizing emission from the population of accreting WDs is comparable to that from the SP in the $\sim 0.3 - 2.0$ Gyr age range; it is unimportant for much earlier ages and for old galaxies. The He-ionizing emission on the contrary is predicted to dominate the ionizing UV background at ages greater than ~ 0.3 Gyr. In the SP model, massive stars dominate the ionizing UV radiation at early times. As the galaxy age increases, the main sequence turn-off mass decreases and the effective temperatures of the hottest stars in the population drops. This leads to the decrease of the ionizing luminosity seen in the Fig.3.3 at $t \lesssim 100$ Myr. Around $t \sim 100$ Myr, the first post-AGB stars appear, resulting in the sharp increase in the ionizing luminosity at $t \sim 100$ Myr, thereafter they dominate the UV emission. Note that in the SP, the He-ionizing luminosity provided by the massive stars drops very steeply and is outside the plotting range in the lower panel of Fig. 3.3. In the considered time range ($t \gtrsim 30$ Myrs), the He-ionizing luminosity of the SP becomes significant only after the first post-AGB stars appear at $t \sim 100$ Myr. Note also, that the little "bump" around 1 Gyr, which can be seen on the curves in Fig. 3.3, is due to the fact that $\sim 2M_{\odot}$ stars undergo a helium flash and their effective temperatures increase.

Woods & Gilfanov (2013, 2014) proposed that the UV emission from accreting WDs is capable of ionizing the ISM. They investigated the contribution of accreting, nuclear-burning WDs in the SD scenario (as SNe Ia progenitors) and pAGB stars to the ionizing background and their influence on the emission lines of warm ISM in early-type galaxies. They predicted that, if the SD scenario for SNe Ia is the dominant channel, SNe Ia progenitors should strongly ionize He, producing strong He recombination lines in the extended emission-line regions of early-type galaxies. Such lines are predicted to be much weaker if only single pAGB stars are considered. Using a similar line of reasoning, one implication of the large population of accreting WDs found in our results across a large range of delay-times is that there should be strong He II recombination lines (e.g. He II 4686$\mathring{A}$) detectable in stellar populations with ages larger than 0.3 Gyr but less than ~ 5 Gyr.

Among the recombination lines of He II, He II λ4686 is the strongest line in the optical band, and is not heavily absorbed by the ISM. In order to avoid the uncertainties in the covering factor, we directly compare the predicted ratio of He II 4686$\mathring{A}$/Hβ with observations. In order to predict the emission line fluxes, we make use of the photoionization code MAPPINGS III (e.g. Kewley et al., 2001; Groves, Dopita & Sutherland, 2004). The procedure is similar to that in Woods & Gilfanov (2013). Here we briefly summarize the main points and assumptions in the calculation.

Serra et al. (2012) found that the common morphology of HI gas in elliptical galaxies is a regular HI disc or ring. The HI discs may extend to several kpc well beyond the nucleus, and may or may not be confined within the stellar body of the galaxy. Given that this gas will be ionized by the combined diffuse emission of many distant sources, we assume plane-parallel geometry in our calculation. We adopt a constant hydrogen density

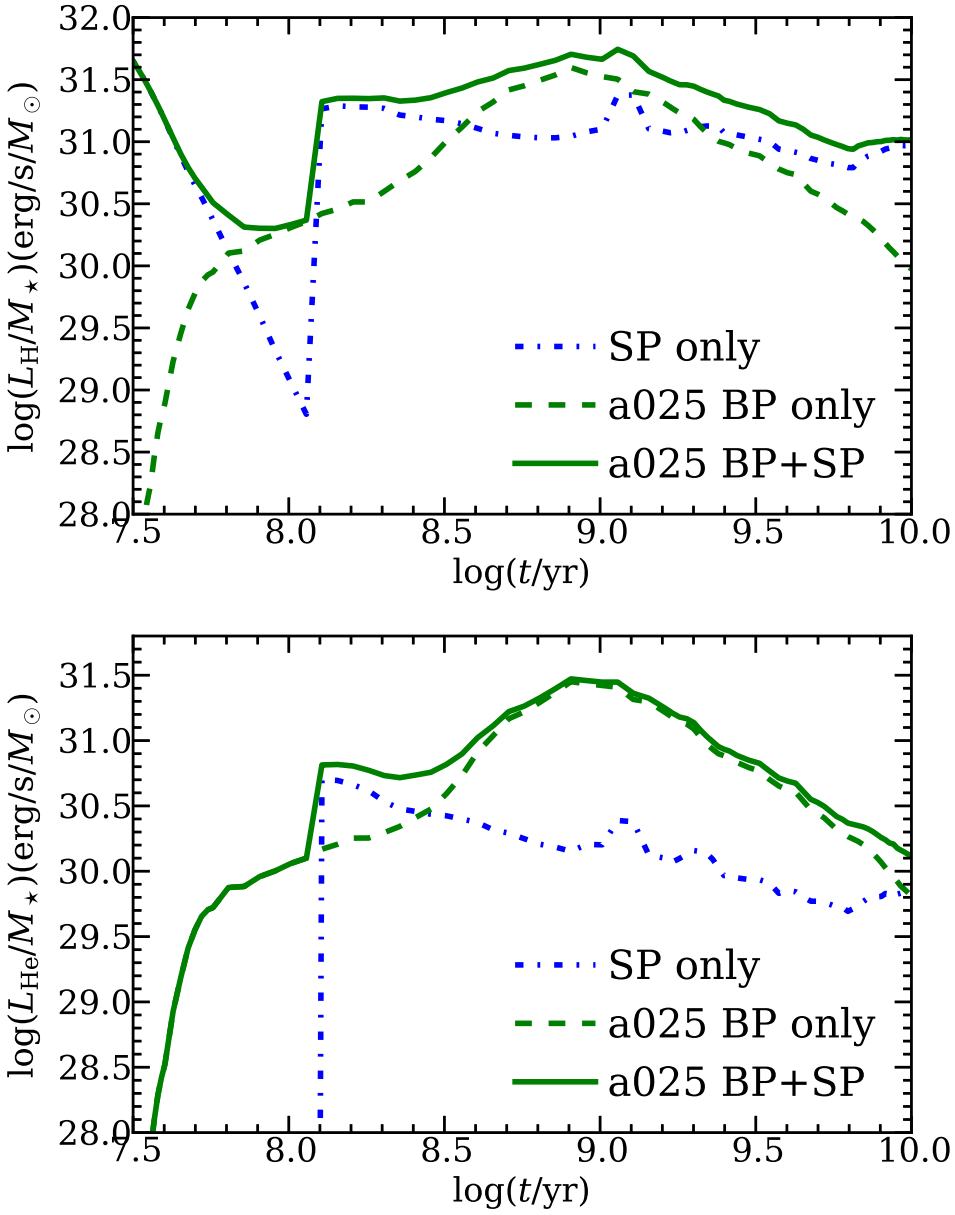

Figure 3.3: Upper panel:H-ionizing ($h\nu > 13.6$ eV) luminosity per unit mass assuming ionization by single stars alone (SP only, blue dash-dotted line), ionizing radiation of a population of accreting white dwarfs for BP model a025 (a025 BP only, green dashed line), and their combined ionizing luminosity (green solid line) as a function of galaxy age in starburst case. Lower panel: similar to the upper panel, but for He-ionizing ($h\nu > 54.4$ eV) luminosity in starburst case.

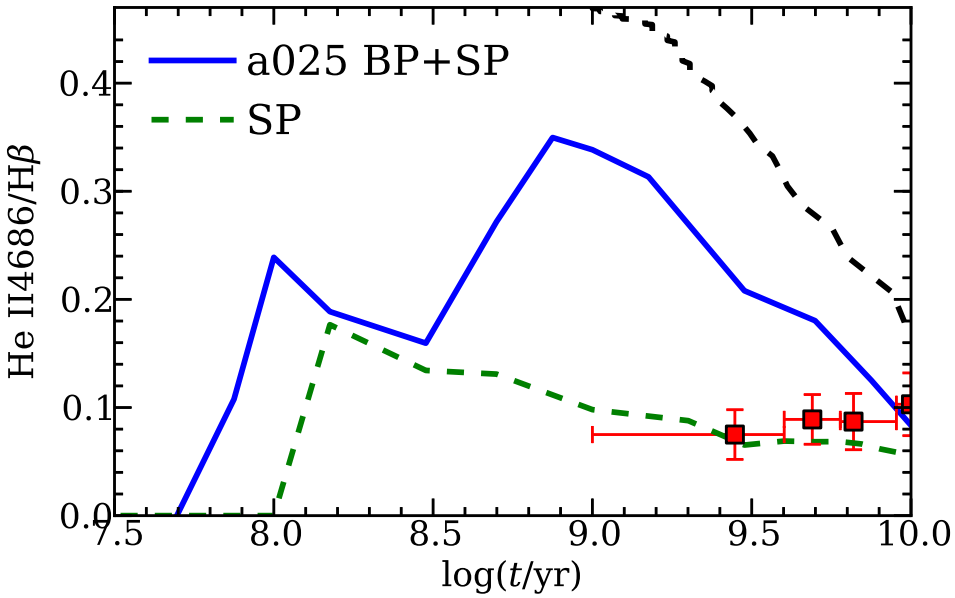

Figure 3.4: Comparison between the predicted values of He II λ4686/Hβ in our starburst models and that which is observed in (stacks of) early-type galaxies, as a function of stellar age. The blue solid line shows the predicted values of He II λ4686/Hβ for the combined populations (a025 BP+SP) and the green dashed line is for the single stellar population from (Bruzual & Charlot, 2003). The black dashed line shows the predicted values of He II λ4686/Hβ for the model combining SNe Ia progenitors in SD-scenario and post-AGB stars (similar to the model in Woods & Gilfanov (2013)). In the calculation of the emission of SNe Ia progenitors, we assumed that all the SNe Ia are produced via SD scenario, the initial WD mass $1.1M_{\odot}$, WD effective temperature $T_{\rm eff} = 2 \times 10^5$K and the delay time distribution given by Totani et al. (2008). The observed values (red squares) are data from Johansson et al. (2014). Note that for these points the vertical bars denote the error in the observed value, but the horizontal bars simply indicate the width of each age bin.

$n_{\rm H} = 100$ cm^{-3}, which agrees with the observed ratio of [SII] 6716Å/6731Å in passively-evolving galaxies (Yan & Blanton, 2012). Regarding the metallicities of the gas, which can be estimated from the oxygen abundance, Athey & Bregman (2009) found an average value of $Z_{\rm oxygen} \simeq Z_{\rm oxygen,\odot}$. So we use solar abundances in our calculation. Although the hydrogen density may be varied as the galaxy evolves or the metallicity may be different, the line ratio calculated in this work is relatively insensitive to the density and the metallicity. Following Johansson et al. (2014), we assume that the ionization parameter $\log(\rm U) \approx -3.5$, where $U = \frac{\dot{N}_{\rm ph}}{4\pi r^2 n_{\rm H} c}$. This is consistent with the [O III] λ5007/Hβ ratio found in their stacks of early-type galaxies.

In Fig. 3.4, we present the computed He II 4686Å/Hβ ratio powered by the emission from the SP together with the accreting WD population, and powered by the emission of the SP alone. At early times, the ratio begins to increase with the decrease in H-ionizing

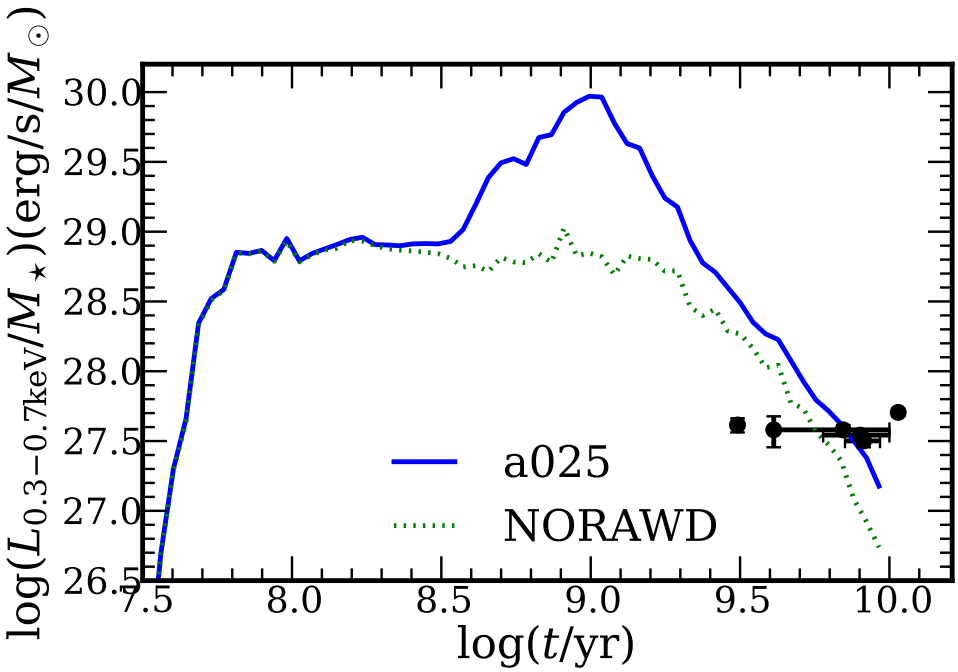

Figure 3.5: Dependence of the soft X-ray luminosity (absorption applied with $N_{\mathrm{H}} = 3.0 \times 10^{20}\mathrm{cm}^{-2}$) from different models of accreting WDs on the stellar ages in starburst case. The blue solid line is for the model a025. The green dotted line is for the model NORAWD assuming that accreting WD will enter CE instead of RAWD phases.

luminosity and increase of the He-ionizing luminosity. The ratio reaches its first maximum when the H-ionizing luminosity reaches its minimum. Around 0.15 Gyr, the H-ionizing luminosity from the SP increases and exceeds the emission from the accreting WDs by an order of magnitude, leading to the beginning of a decrease in this ratio. After that, the H-ionizing luminosity does not change significantly. Thereafter, the evolution of this ratio simply reflects the evolution of the He ionizing luminosity. The luminosity ratio at 10 Gyr is consistent with observations, but the computed ratio is larger than the observed one by a factor up to $\simeq 3$ in the age range $1 - 8$ Gyr. This comes about due to the predominance of accreting WDs in producing our predicted ionizing background at these delay times. Although the total luminosities of accreting WDs and post-AGB stars in this age range are comparable, the lack of a sharp cutoff at 54.4eV in the spectra of accreting WDs leads to a dramatically greater production of He II-ionizing photons. In particular, the He II-ionizing luminosity predicted in our a025 model exceeds that in the SP case by up to an order of magnitude at t$\sim$ 1Gyr (see Fig. 3.3).

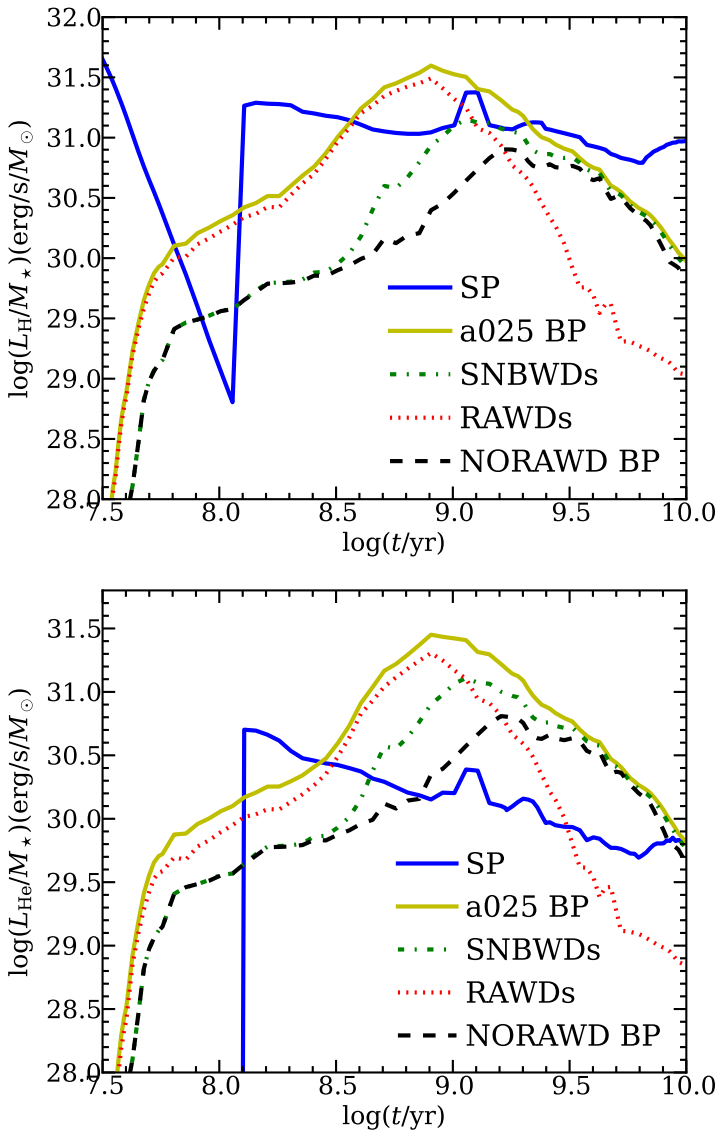

Figure 3.6: Upper panel: Evolution of H-ionizing luminosity from different subsets of accreting WDs as a function of stellar age in the starburst case. The blue solid line is for the SP model. The yellow solid line is for model a025. The green dash-dotted line and red dotted line are for the contribution of the SNBWDs and RAWDs, respectively. The black dashed line is for the model that assumes the accreting WDs will enter a CE instead of a RAWD phase. Lower panel: Similar to the upper panel, but for He-ionizing luminosity.

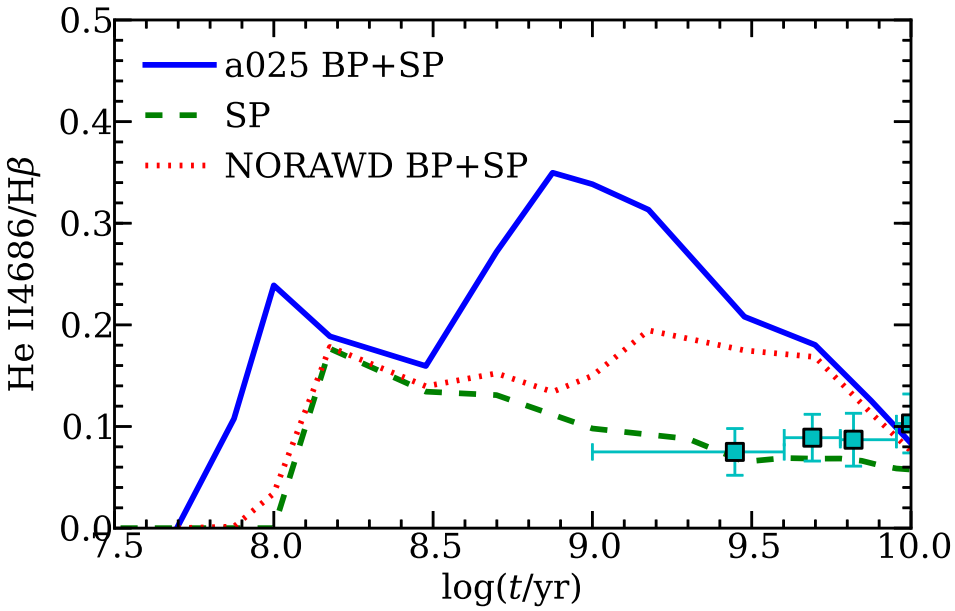

Figure 3.7: The evolution of the HeII/Hβ ratio as a function of stellar age for different model assumptions in the starburst case. The blue solid line and red dotted line show the values for the combined population in model a025 and NORAWD, respectively. The green dashed line and square data are the same as Fig. 3.4.

3.5.3 Emission from subsets of accreting WDs

In Fig. 3.5, we show the soft X-ray emission from SNBWDs in model a025 and in an additional model in which we assume that upon exceeding the maximum accretion rate for stable burning, accreting WDs enter a CE phase instead of becoming RAWDs (model NORAWD) and WDs cease to contribute to X-ray and UV output of the population. Similar to Fig. 3.5, we show the H-ionizing luminosity and He-ionizing luminosity in Fig. 3.6. For the young stellar populations with age $t < 1$Gyr, the RAWDs dominate the H and He II ionizing emission. For old stellar populations ($t > 1$ Gyr), the H and He ionizing luminosity is dominated by emission from the SNBWDs. This is due to the fact that, at early times, the binaries have massive donor stars and higher thermal timescale mass transfer rates. In contrast, at later times, the donors are less massive and the thermal mass transfer rate is lower, leading to more emission from the SNBWDs. In the model NORAWD, the soft X-ray luminosity, H-ionizing luminosity and He-ionizing luminosity are very different from that in model a025. In Paper I (see Fig. 2), we found that there are two stable burning phases for some accreting WD binaries. In model NORAWD, replacing the RAWD phase with a CE, only the first stably burning phase will contribute to the emission. So the H and He-ionizing luminosity in model NORAWD are comparable to the emission from SNBWDs at early and late times, when massive systems do not make a contribution. In Fig. 3.7, we show the computed HeII 4686Å/Hβ ratio in the model NORAWD and in model a025. The ratio reduces significantly, but it is still larger than the observed ones by a factor of 2. This corresponds to a remaining discrepancy of up to factors of 2 to 5 between our prediction for the He II-ionizing luminosity and that expected from the single stellar population alone (see Fig. 3.3).

3.6 Discussion

3.6.1 Model uncertainties

In the section above, we found that there is a strong dependence of soft X-ray luminosity $L_{0.3-0.7\mathrm{keV}}$ and the ratio He II 4686$\mathring{A}$/Hβ on stellar age for non-star-forming early-type galaxies in our calculation, in contrast with observations (Fig. 3.2 and Fig. 3.4). In producing a population synthesis model, there exist several uncertainties in both the initial conditions and the treatment of stellar evolution which may influence the results. In the following, we discuss a (partial) list of several aspects which may significantly impact our model, and their viability in providing a solution. Some of the model parameters not considered here were either tested and found to be of minimal importance (e.g. IMF, mass ratio), or are simply unlikely to be of significant impact (e.g. treatment of convective overshooting, as this only matters for massive stars).

1) One important uncertainty is the retention efficiency of accreted matter, (see Bours, Toonen & Nelemans (2013) [2]. In our calculation, we assumed that the He burning retention

[2]Note, in Yungelson (2010) He-retention efficiency is calculated differently from that quoted by Bours,

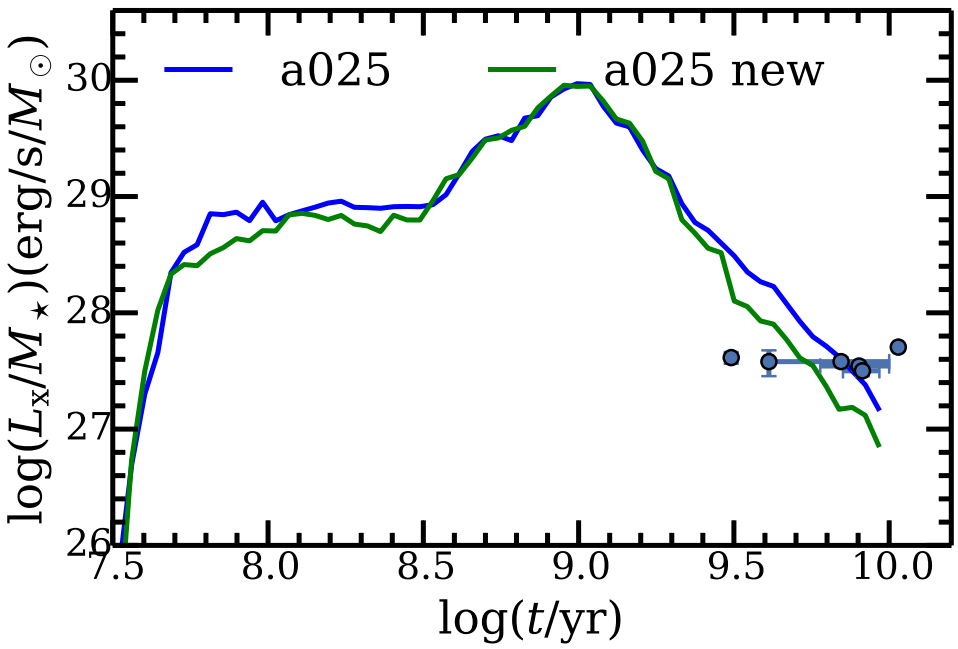

Figure 3.8: Similar to the upper panel of Fig. 3.2. The "new" model a025 is the result computed using the revised He burning retention efficiency (see text).

efficiency is 100%, which is clearly an overestimate and results in an excess of massive WDs [3], which may be partially responsible for the high H and He ionizing emission of accreting WDs. On the other hand, Piersanti, Tornambé & Yungelson (2014) have shown that the conventional assumption that the retention efficiency of matter at the surface of a WD may be computed as a product of independently calculated retentions of H and He (i.e. $\eta = \eta_{\rm H} \times \eta_{\rm He}$), results in an underestimate of η. The reason is that H-burning heats the underlying He layer and the outbursts of He-burning are milder than that in the case of accretion of pure He.

In order to check if He retention efficiency has a strong influence on our result, we recomputed our results with the He burning retention efficiency given in Hachisu, Kato & Nomoto (1999), and with the range in mass transfer rates corresponding to the stable burning regime as given in Wolf et al. (2013). In Fig. 3.8, we compare the soft X-ray luminosity from this new model with that from our standard model, and find the difference is not significant. In spite of this, we should emphasize that the retention efficiency suffers significant uncertainty, requiring further investigation. Therefore, without more precisely understood retention efficiency, we can not completely exclude the influence of this parameter.

2) In our calculations, solar abundance is adopted. As we discussed in Section 3.5.1,

Toonen & Nelemans (2013).

[3] The WD mass may also be overestimated because of the initial-final mass function used in BSE code (see Claeys et al., 2014).

some galaxies in our X-ray comparison are likely to have low metallicities, which plays a complicated and still uncertain role in the evolution of accreting WDs. On the one hand, at very low metallicities the stable-burning regime may be extended to much lower mass transfer rates (Shen & Bildsten, 2007). However, at the same time low-Z WD binaries are expected to have much higher accretion rates (Langer et al., 2000), likely pushing many more binaries into dynamically unstable mass transfer. Either of these mechanisms require very low metallicities ($< 0.01 Z_{\odot}$), unlikely to be typical of many of the relatively nearby early-type galaxies used in our study. Therefore, we leave consideration of the evolution of WD binaries at low-Z to a future study.

3) The X-ray comparison is based on a sample of six nearby galaxies (the only currently available set of measurements suitable for such a comparison). In addition, there is some controversy between different age estimates for the two youngest galaxies. However, while the incorrect age determination could in principle resolve the discrepancy in the X-ray band, it is unlikely to explain the He II 4686 $\mathring{A}$/Hβ line ratio, as demonstrated in Johansson et al. (2014).

4) It may be that our modeling of the emission spectra of nuclear burning white dwarfs is incorrect. This must involve a failure of the 1D theory, rather than any simple deviations from the black body spectral template used throughout the paper (see section 3.3). One obvious possibility is that the photospheric radii may be much larger than predicted by 1D models of the nuclear burning on the WD surface. This would shift the peak of their emission to the UV or optical bands where they would be remarkably unusual objects. However, Lepo & van Kerkwijk (2013) searched for such objects in the Small Magellanic Cloud and found no plausible candidates. Therefore this possibility seems to be unlikely.

5) One of the most important uncertainties in our calculations is the treatment of the CE phase. There are still many aspects of CE evolution which remain unclear, such as the available energy sources and the definition of the core-envelope boundary (see Ivanova et al. (2013) for a review,Hall & Tout (2014)). In addition, the criteria for the onset of a CE phase also suffer from great uncertainty. In the following subsection, we will discuss this possibility in depth and provide a possible solution to resolve the discrepancy between our computed results and observations.

3.6.2 A potential solution

In our calculations, for binaries harbouring giant donors, we adopted after Hjellming & Webbink (1987) and Webbink (1988) as the criterion for stable mass loss a critical value of mass ratio (hereafter, HW criterion):

$$q_c = 0.362 + \frac{1.0}{3.0(1 - m_c)}, \tag{3.2}$$

where m_c is the core mass fraction. For conservative mass transfer, this predicts dynamical instability for stars with a core mass fraction $\lesssim 0.45$, i.e. $q_c \lesssim 1.0$. Chen & Han (2008) (see also Han et al. (2002)), using detailed binary evolution calculations, found that the critical mass ratio can be up to ~ 2.0, depending on the evolutionary phase of the donor

star, mass and angular momentum loss from the system. Woods & Ivanova (2011) (see also Passy, Herwig & Paxton (2012)) found that this difference is due to the existence of a superadiabatic outer surface layer, which plays a critical role during the mass transfer. Following on the work of Woods & Ivanova (2011), Pavlovskii & Ivanova (2015) found that the critical mass ratio varies from 1.5 to 2.2 for conservative mass transfer. Given these recent results, we turn now to considering alternatives to the HW prescription, in particular a more stringent condition for the onset of a CE, as a possible solution to the overproduction of accreting WDs found in our standard model above. We attempt to replace the HW criteria with $q_c = 1.5$ (model a025qc15), 1.7 (model a025qc17), and 1.9 (model a025qc19), for binaries consisting of MS and giant stars. Although the mass ratio needed for the onset of a CE is understood to vary significantly for differing combinations of accretor mass, donor mass, and evolutionary state of the donor, these values are more consistent with the results of detailed numerical simulations (e.g. Pavlovskii & Ivanova, 2015), and much higher than what is typically found when implementing the HW criterion. In this section, using these new criteria, we calculated the soft X-ray, H-ionizing and He-ionizing luminosity as a function of stellar age.

In Fig. 3.9, we show the evolution of soft X-ray luminosity as a function of stellar age. Compared with our model using the HW criterion, the new criteria have larger critical mass ratios. With larger critical mass ratios, the predicted soft X-ray luminosity becomes lower. This is due to the fact that, with the requirement of a larger critical mass ratio, it will be relatively difficult for binaries to enter dynamically unstable mass transfer. Therefore, fewer binaries will enter a CE phase, and fewer accreting WDs will form. For old stellar populations, the predicted soft X-ray luminosities in model a025qc17 and model a025qc19 are lower than the observed values. Given that the observational soft X-ray luminosity is the upper limit for the emission of accreting WDs, our results are consistent with observations. Fig. 3.10 shows the evolution of the H-ionizing and He-ionizing luminosity for different models, respectively. These results are similar to model a025, but the H-ionizing and He-ionizing luminosity is lower, for the same reason as above. In Fig. 3.11, we present the dependence of line ratio HeII λ4686/Hβ on stellar age for the new models. For old stellar populations in model a025qc17 and model a025qc19, the line ratio is much smaller than that in model a025 and consistent with observations.

The use of fixed unique critical mass ratios for the onset of rapid, unstable mass transfer is not realistic (Nelemans et al., 2000; Woods & Ivanova, 2011). Numerical experiments above show that stability criteria of mass loss for giant stars play a crucial role in defining the number of SNBWD. However, stability also depends on mass of the donor, specific momentum of matter lost from the system etc. Fine-tuning of all these parameters may bring even better agreement of model and observations, but it is computer-time prohibitive.

3.6.3 Number of SSSs

As discussed in Paper I, not all SNBWDs can be detected as SSSs, since this is dependent on the luminosity and effective temperature of the source, and the column density of the gas along the line of sight. In this paper, we define SSSs as SNBWDs with soft X-ray (0.30-

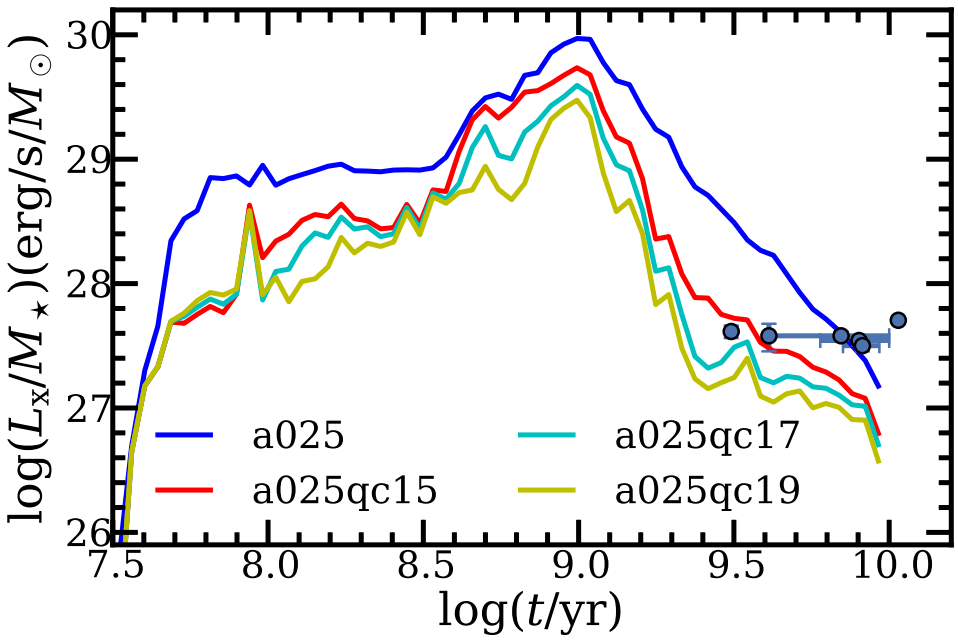

Figure 3.9: Evolution of soft X-ray luminosity (absorption applied with $N_{\rm H} = 3.0 \times 10^{20}{\rm cm}^{-2}$) as a function of stellar age in starburst case. The red, green and yellow solid lines are for model a025qc15, model a025qc17 and model a025qc19, respectively.

0.70keV) luminosity $L_{\rm x} > 10^{36}$erg/s. With this definition, we computed the evolution of the number of SSSs, which is shown in Fig. 3.12. In the starburst case, the SSS population peaks around ~ 1 Gyr and then declines by ~ 2 orders of magnitude by the age of 10 Gyr. We note that the ionizing radiation from SNBWDs has a peak at the same age range (see the figures above). A similar peak was found in earlier studies of SNe Ia rates in the single degenerate scenario (e.g. Canal, Ruiz-Lapuente & Burkert, 1996; Han & Podsiadlowski, 2004; Ruiter, Belczynski & Fryer, 2009; Yungelson, 2010). The reason for this is that main-sequence stars with mass close to $\sim 2\ M_\odot$ have lifetimes ~ 1 Gyr and radii and luminosities that enable a relatively long stage of thermal time-scale mass loss with the rate $\sim 10^{-6} M_\odot$/yr, corresponding to the stable hydrogen burning regime (see Figs. 2 and 10 in Paper I)[4]. The number of SSSs for a $10^{11} M_\odot$ galaxy at 10 Gyr is $10 - 20$ in the starburst case and $200 - 820$ in the constant SFR case assuming $N_{\rm H} = 3 \times 10^{20}{\rm cm}^{-2}$. Given the high intrinsic absorption of spiral galaxies, we also made a set of calculations assuming $N_{\rm H} = 3 \times 10^{21}{\rm cm}^{-2}$. In this case, the SSS number is $40 - 130$ for a spiral-like galaxy. Note, however, that the observable number of SSSs depends on the absorption column density, which in turn depends on the relative distribution of gas and SSSs in any

[4]If mass loss is artificially fine-tuned, e.g., by the highly uncertain effect of mass-stripping effect of donors by an accretor wind (Hachisu, Kato & Nomoto, 1999), the peak may be shifted to younger ages, e.g., Mennekens et al. (2010). The peak is smeared by the scatter in the actual parameters of WD+MS pairs - masses, mass ratios of components, and initial separations.

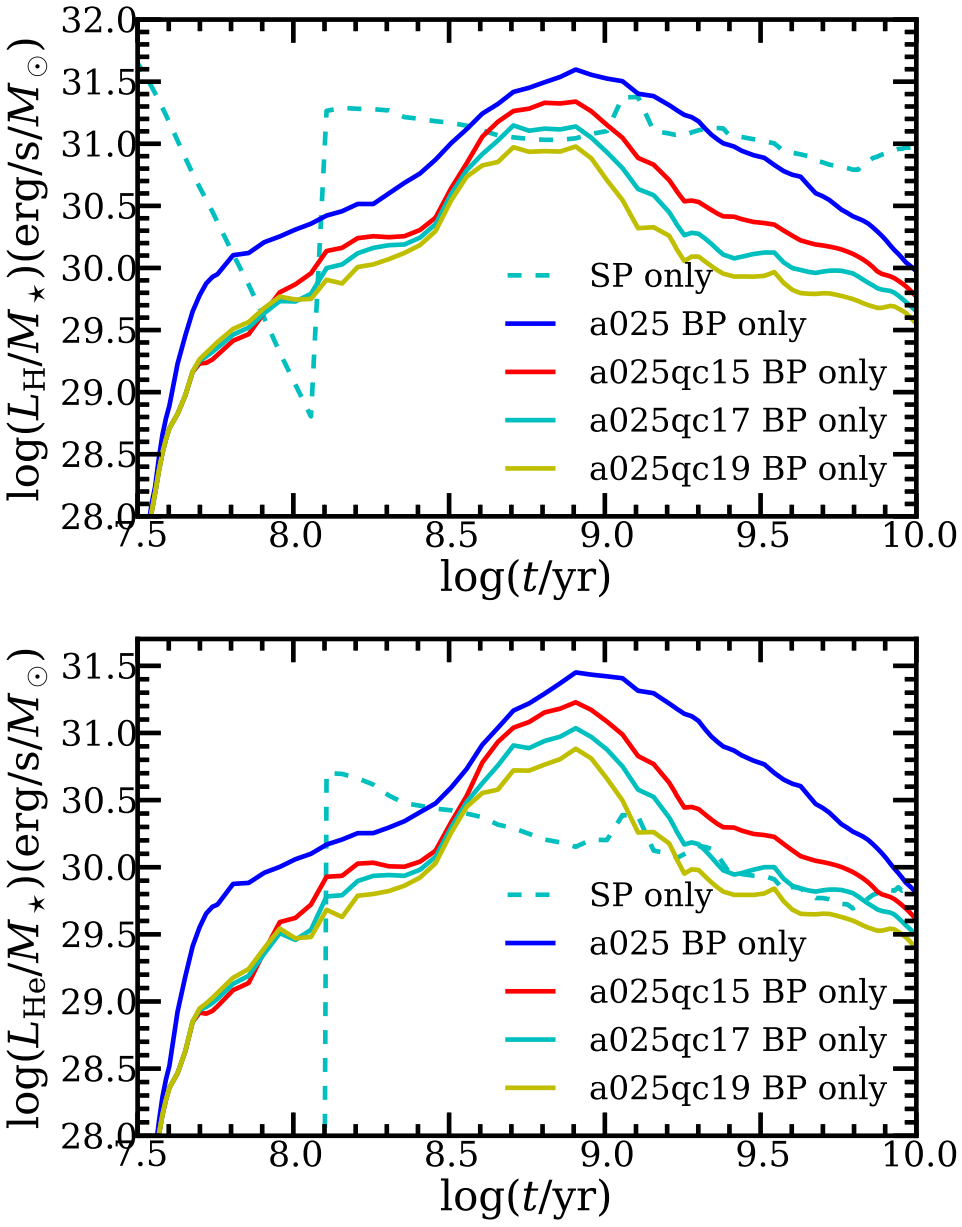

Figure 3.10: Evolution of H-ionizing (upper panel) and He-ionizing (lower panel) luminosity as a function of stellar age in different models.

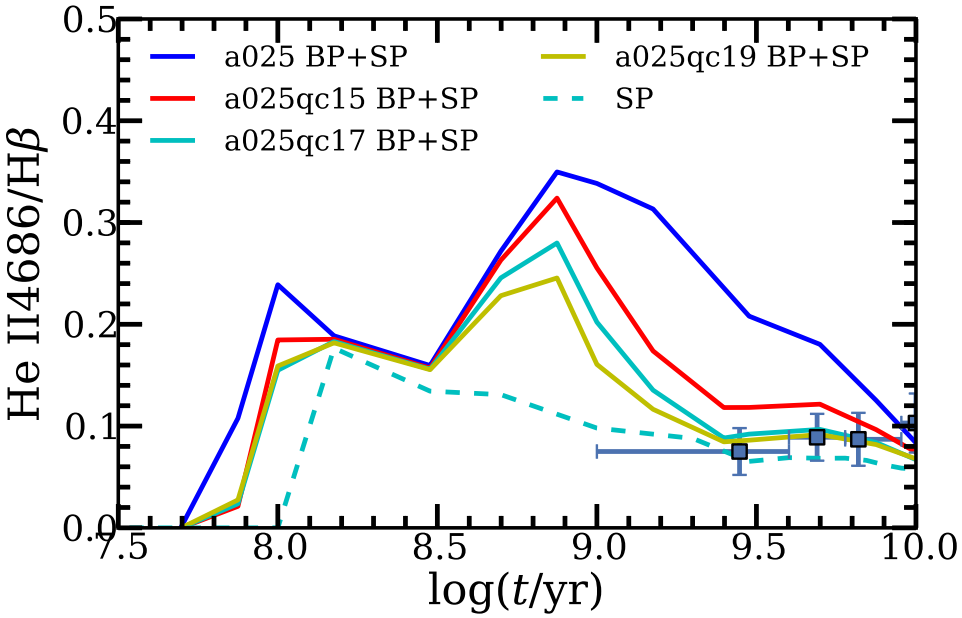

Figure 3.11: Evolution of line ratio HeII 4686/Hβ as a function of stellar age for combined population in model a025qc15, model a025qc17 and model a025qc19.

given galaxy.

3.6.4 Gaseous nebulae around SSSs

Given the hard emission of SSSs, it is suggested that they should be accompanied by ionized nebulae. Rappaport et al. (1994) modeled the ionization and temperature structure of such nebulae and predicted strong [OIII] λ5007 and He II λ4686 emission lines. Remillard, Rappaport & Macri (1995) searched for gaseous nebulae surrounding SSSs in the Large and Small Magellanic Clouds. They found only one SSS, Cal 83 (first identified as a high-excitation nebula by Pakull & Motch, 1989), with a detected nebula, with null detections among the 9 other known Magellanic SSSs. This means that either the time-averaged luminosity and/or temperature of these sources must be much lower than presently observed, or that the local ISM density around SSSs are typically too low. In fact, given that typical ISM densities are 1 – 2 orders of magnitude below that observed for the Cal 83 nebula, the latter appears more likely (see Woods & Gilfanov (submitted), who found a 70% probability that $\lesssim 1$ SSS in the LMC would have a detectable nebula). The situation is complicated further in the accretion-wind scenario – for SSSs in star-forming galaxies, a wind-blown bubble will excavate a cavity in the ISM surrounding the source which is 10 – 40 pc in radius (Badenes et al., 2007). Consequently, the ionization parameter and morphology of these nebulae will be much different.

Since the common morphology of HI gas in elliptical galaxies is a regular HI disk or ring, individual sources are not embedded in the ISM they ionize. With the above expla-

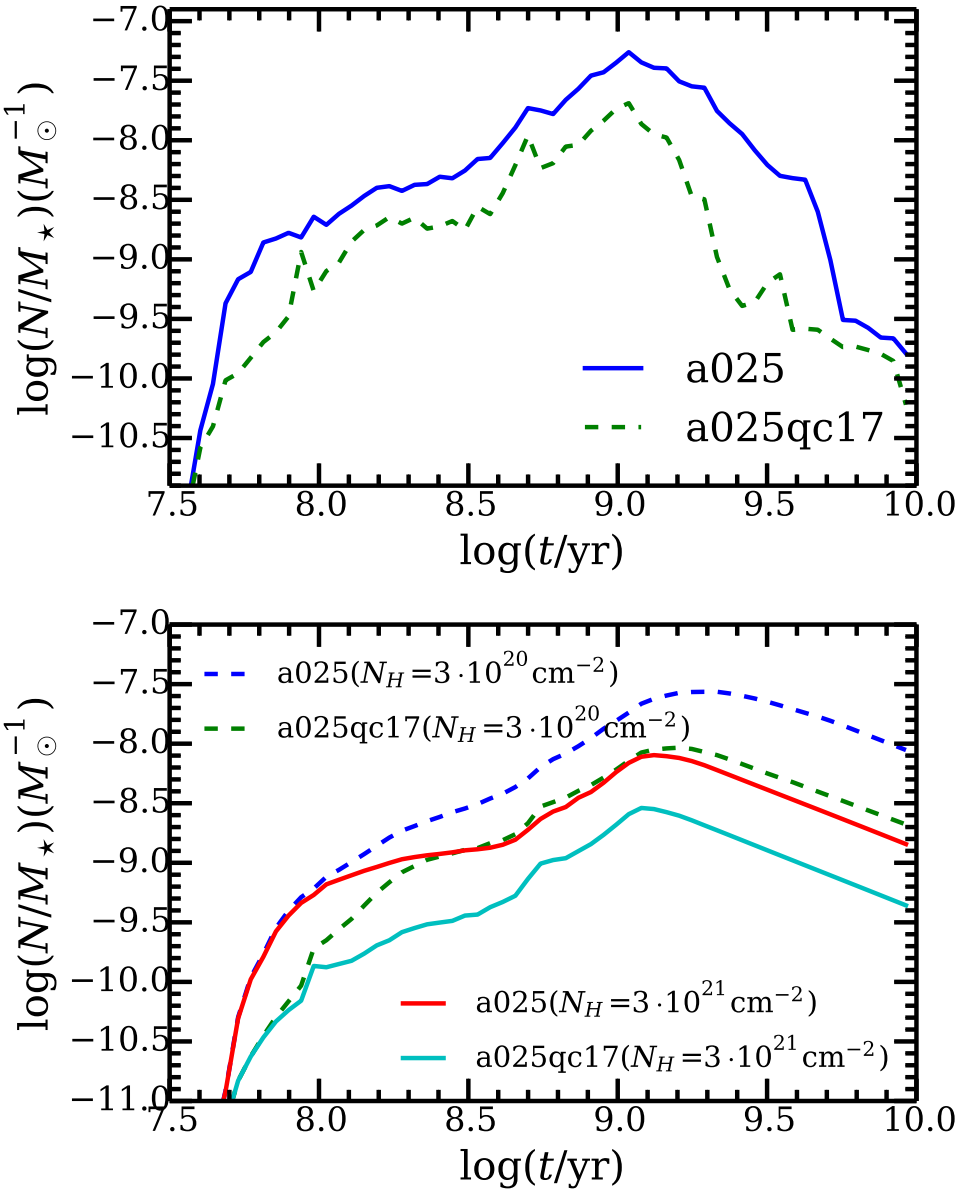

Figure 3.12: Evolution of the number of SSSs per unit stellar mass in the starburst case (upper panel) and the constant SFR case (lower panel). The blue dashed line is for model a025 and green dashed line for model a025qc17 assuming $N_{\rm H} = 3.0 \times 10^{20}{\rm cm}^{-2}$. The red and cyan solid lines in the bottom panel show the number of SSSs with $N_{\rm H} = 3.0 \times 10^{21}{\rm cm}^{-2}$ in model a025 and model a025qc17.

nation and HI gas morphology in mind, we would expect that the individual emission line luminosity in elliptical galaxies should not be influenced by any complications introduced by the impact of the accreting WD on any surrounding ISM, as is the case in star-forming galaxies.

3.7 Summary and Conclusions

Based on the results of population synthesis of accreting WDs from Paper I and using simple assumptions regarding the emission of accreting WDs, we study the number of observed SSSs, the soft X-ray luminosity of accreting WDs, and their H and He II ionizing luminosity. The main conclusions are as follows.

1. We compare predictions of our model with observations of nearby elliptical galaxies in optical and X-ray bands. To this end we use the He II 4686 $\AA$/Hβ line ratio to characterise the hardness and strength of the ionizing UV continuum. In our standard model, using commonly (although not universally) adopted assumptions, our predictions for the soft X-ray luminosity of old stellar populations are consistent with *Chandra* observations of several nearby elliptical galaxies. Likewise, for stellar ages of $\sim$ 10 Gyr, the He II 4686 $\AA$/Hβ line ratio from warm ISM predicted by our model is consistent with that measured in the stacked SDSS spectra of retired galaxies. However, for stellar ages of $\sim 4-8$ Gyrs our model significantly over-predicts the soft X-ray luminosity and the He II 4686 $\AA$/Hβ line ratio.

2. We discuss various possibilities to explain this controversy and tentatively conclude that the most likely reason is that the classical Hjellming & Webbink (1987) criterion typically used for evaluating the onset of dynamically unstable mass transfer for giant stars predicts too low critical mass ratio. Replacement of this criterion by fixed critical mass ratios ($q_c = 1.7$ or 1.9), brings the soft X-ray luminosity and line ratio He IIλ4686/Hβ in the new models to consistency with the observations. However, we stress that the critical mass ratio needed for the onset of a common envelope is actually not a fixed value, and varies in an as yet unspecified way as a function of other stellar parameters. Further effort is needed in this regard, in order to better reconcile the predictions of binary population synthesis with observations.

3. In the starburst case, the population of SNBWDs, their combined soft X-ray and UV output and the number of SSSs (SNBWDs with $L_{\rm x} > 10^{36}$erg/s) peak at $\sim$ 1 Gyr and then strongly decline with age, by $\sim (1-3)$ orders of magnitude. Assuming $N_{\rm H} = 3 \cdot 10^{20}$ cm^{-2}, the number of SSSs present at 10 Gyr in the starburst case is $10-20$ for a galaxy with mass $10^{11} M_{\odot}$. In the constant SFR case, assuming $N_{\rm H} = 3 \cdot 10^{21}$ cm^{-2}, the SSSs number at 10 Gyr is around $40-130$ for the same mass galaxy.

Acknowledgments

We would like to thank Bill Wolf for kindly providing us model data for stable-burning WDs. We are grateful to the MESA council for the MESA instrument papers and website. The TheoSSA service (http://dc.g-vo.org/theossa) used to retrieve theoretical spectra for this paper was constructed as a part of the activities of the German Astrophysical Virtual Observatory. HLC acknowledges the computing time granted by the Yunnan Observatories and provided on the facilities at the Yunnan Observatories Supercomputing Platform.

Bibliography

Abt H. A., 1983, ARA&A, 21, 343

Athey A. E., Bregman J. N., 2009, ApJ, 696, 681

Badenes C., Hughes J. P., Bravo E., Langer N., 2007, ApJ, 662, 472

Bogdán Á., Gilfanov M., 2008, MNRAS, 388, 56

Bogdán Á., Gilfanov M., 2010, A&A, 512, A16

Bours M. C. P., Toonen S., Nelemans G., 2013, A&A, 552, A24

Bruzual G., Charlot S., 2003, MNRAS, 344, 1000

Canal R., Ruiz-Lapuente P., Burkert A., 1996, ApJL, 456, L101

Cassisi S., Iben, Jr. I., Tornambe A., 1998, ApJ, 496, 376

Chabrier G., 2003, PASP, 115, 763

Chen H.-L., Woods T. E., Yungelson L. R., Gilfanov M., Han Z., 2014, MNRAS, 445, 1912

Chen X., Han Z., 2008, MNRAS, 387, 1416

Claeys J. S. W., Pols O. R., Izzard R. G., Vink J., Verbunt F. W. M., 2014, A&A, 563, A83

Coelho P., Mendes de Oliveira C., Cid Fernandes R., 2009, MNRAS, 396, 624

Davis P. J., Kolb U., Knigge C., 2012, MNRAS, 419, 287

Davis P. J., Kolb U., Willems B., 2010, MNRAS, 403, 179

de Kool M., 1990, ApJ, 358, 189

de Mink S. E., Pols O. R., Yoon S.-C., 2008, in American Institute of Physics Conference Series, Vol. 990, First Stars III, O'Shea B. W., Heger A., eds., pp. 230–232

Dickey J. M., Lockman F. J., 1990, ARA&A, 28, 215

Doherty C. L., Gil-Pons P., Siess L., Lattanzio J. C., Lau H. H. B., 2015, MNRAS, 446, 2599

Fragos T. et al., 2013, ApJ, 764, 41

Georgiev I. Y., Goudfrooij P., Puzia T. H., 2012, MNRAS, 420, 1317

Gilfanov M., Bogdán Á., 2010, Nature, 463, 924

Groves B. A., Dopita M. A., Sutherland R. S., 2004, ApJS, 153, 9

Hachisu I., Kato M., Nomoto K., 1996, ApJL, 470, L97

Hachisu I., Kato M., Nomoto K., 1999, ApJ, 522, 487

Hall P. D., Tout C. A., 2014, MNRAS, 444, 3209

Han Z., Podsiadlowski P., 2004, MNRAS, 350, 1301

Han Z., Podsiadlowski P., Maxted P. F. L., Marsh T. R., Ivanova N., 2002, MNRAS, 336, 449

Hempel M., Zepf S., Kundu A., Geisler D., Maccarone T. J., 2007, ApJ, 661, 768

Hjellming M. S., Webbink R. F., 1987, ApJ, 318, 794

Hurley J. R., Pols O. R., Tout C. A., 2000, MNRAS, 315, 543

Hurley J. R., Tout C. A., Pols O. R., 2002, MNRAS, 329, 897

Iben, Jr. I., 1982, ApJ, 259, 244

Iben, Jr. I., Tutukov A. V., 1984, ApJS, 54, 335

Idiart T. P., Silk J., de Freitas Pacheco J. A., 2007, MNRAS, 381, 1711

Ivanova N. et al., 2013, Astron. Astrophys. Rev., 21, 59

Johansson J., Woods T. E., Gilfanov M., Sarzi M., Chen Y.-M., Oh K., 2014, MNRAS, 442, 1079

Kewley L. J., Dopita M. A., Sutherland R. S., Heisler C. A., Trevena J., 2001, ApJ, 556, 121

Kistler M. D., Stanek K. Z., Kochanek C. S., Prieto J. L., Thompson T. A., 2013, ApJ, 770, 88

Kouwenhoven M. B. N., Brown A. G. A., Goodwin S. P., Portegies Zwart S. F., Kaper L., 2009, A&A, 493, 979

Kraicheva Z. T., Popova E. I., Tutukov A. V., Yungelson L. R., 1979, SvA, 23, 290

Kraus A. L., Hillenbrand L. A., 2009, ApJ, 703, 1511

Kroupa P., 2001, MNRAS, 322, 231

Langer N., Deutschmann A., Wellstein S., Höflich P., 2000, A&A, 362, 1046

Lepo K., van Kerkwijk M., 2013, ApJ, 771, 13

Loveridge A. J., van der Sluys M. V., Kalogera V., 2011, ApJ, 743, 49

Maoz D., Mannucci F., Nelemans G., 2014, ARA&A, 52, 107

Meng X., Chen X., Han Z., 2008, A&A, 487, 625

Mennekens N., Vanbeveren D., De Greve J. P., De Donder E., 2010, A&A, 515, A89

Michard R., 2006, A&A, 449, 519

Nelemans G., Verbunt F., Yungelson L. R., Portegies Zwart S. F., 2000, A&A, 360, 1011

Olsen K. A. G., Blum R. D., Stephens A. W., Davidge T. J., Massey P., Strom S. E., Rigaut F., 2006, AJ, 132, 271

O'Sullivan E., Ponman T. J., 2004, MNRAS, 349, 535

Paczyński B., 1971, Acta. Astron., 21, 417

Paczynski B., Zytkow A. N., 1978, ApJ, 222, 604

Pakull M. W., Motch C., 1989, in European Southern Observatory Conference and Workshop Proceedings, Vol. 32, European Southern Observatory Conference and Workshop Proceedings, Meurs E. J. A., Fosbury R. A. E., eds., p. 285

Passy J.-C., Herwig F., Paxton B., 2012, ApJ, 760, 90

Pavlovskii K., Ivanova N., 2015, MNRAS, 449, 4415

Paxton B., Bildsten L., Dotter A., Herwig F., Lesaffre P., Timmes F., 2011, ApJS, 192, 3

Paxton B. et al., 2013, ApJS, 208, 4

Piersanti L., Tornambé A., Yungelson L. R., 2014, MNRAS, 445, 3239

Postnov K. A., Yungelson L. R., 2014, Living Reviews in Relativity, 17, 3

Rappaport S., Chiang E., Kallman T., Malina R., 1994, ApJ, 431, 237

Rauch T., 2003, A&A, 403, 709

Rauch T., Orio M., Gonzales-Riestra R., Nelson T., Still M., Werner K., Wilms J., 2010, ApJ, 717, 363

Remillard R. A., Rappaport S., Macri L. M., 1995, ApJ, 439, 646

Ricker P. M., Taam R. E., 2012, ApJ, 746, 74

Ruiter A. J., Belczynski K., Fryer C., 2009, ApJ, 699, 2026

Sana H. et al., 2012, Science, 337, 444

Sánchez-Blázquez P., Gorgas J., Cardiel N., González J. J., 2006, A&A, 457, 809

Serra P. et al., 2012, MNRAS, 422, 1835

Shen K. J., Bildsten L., 2007, ApJ, 660, 1444

Sion E. M., Acierno M. J., Tomczyk S., 1979, ApJ, 230, 832

Taam R. E., van den Heuvel E. P. J., 1986, ApJ, 305, 235

Terlevich A. I., Forbes D. A., 2002, MNRAS, 330, 547

Totani T., Morokuma T., Oda T., Doi M., Yasuda N., 2008, PASJ, 60, 1327

Truran J. W., Glasner S. A., 1995, in Astrophysics and Space Science Library, Vol. 205, Cataclysmic Variables, Bianchini A., Della Valle M., Orio M., eds., p. 453

Tutukov A. V., Yungelson L. R., 1981, Nauchnye Informatsii, 49, 3

Umeda H., Nomoto K., Yamaoka H., Wanajo S., 1999, ApJ, 513, 861

van den Heuvel E. P. J., Bhattacharya D., Nomoto K., Rappaport S. A., 1992, A&A, 262, 97

Warner B., 2003, Cataclysmic Variable Stars

Webbink R. F., 1984, ApJ, 277, 355

Webbink R. F., 1988, The Formation and Evolution of Symbiotic Stars, Mikolajewska J., Friedjung M., Kenyon S. J., Viotti R., eds., p. 311

Werner K., 1986, A&A, 161, 177

Werner K., 1989, A&A, 226, 265

Whelan J., Iben, Jr. I., 1973, ApJ, 186, 1007

Wolf W. M., Bildsten L., Brooks J., Paxton B., 2013, ApJ, 777, 136

Woods T. E., Gilfanov M., 2013, MNRAS, 432, 1640

Woods T. E., Gilfanov M., 2014, MNRAS, 439, 2351

Woods T. E., Ivanova N., 2011, ApJL, 739, L48

Yan R., Blanton M. R., 2012, ApJ, 747, 61

Yungelson L. R., 2010, Astronomy Letters, 36, 780

Zhang Z., Gilfanov M., Bogdán Á., 2012, A&A, 546, A36

Zorotovic M., Schreiber M. R., Gänsicke B. T., Nebot Gómez-Morán A., 2010, A&A, 520, A86

Chapter 4

Modelling nova populations in galaxies

Monthly Notices of the Royal Astronomical Society, 458, 2916, 2016
Chen, H.-L., Woods, T. E., Yungelson, L. R., Gilfanov, M. & Han, Z.

4.1 Abstract

Theoretical modelling of the evolution of classical and recurrent novae plays an important role in studies of binary evolution, nucleosynthesis and accretion physics. However, from a theoretical perspective the observed statistical properties of novae remain poorly understood. In this paper, we have produced model populations of novae using a hybrid binary population synthesis approach for differing star formation histories (SFHs): a starburst case (elliptical-like galaxies), a constant star formation rate case (spiral-like galaxies) and a composite case (in line with the inferred SFH for M31). We found that the nova rate at 10 Gyr in an elliptical-like galaxy is $\sim 10-20$ times smaller than a spiral-like galaxy with the same mass. The majority of novae in elliptical-like galaxies at the present epoch are characterized by low mass white dwarfs (WDs), long decay times, relatively faint absolute magnitudes and long recurrence periods. In contrast, the majority of novae in spiral-like galaxies at 10 Gyr have massive WDs, short decay times, are relatively bright and have short recurrence periods. The mass loss time distribution for novae in our M31-like galaxy is in agreement with observational data for Andromeda. However, it is possible that we underestimate the number of bright novae in our model. This may arise in part due to the present uncertainties in the appropriate bolometric correction for novae.

4.2 Introduction

As a subclass of accreting white dwarfs, novae are important objects for the study of binary evolution and nucleosynthesis (see Patterson, 1984; Gehrz et al., 1998, for a review). Given that WDs undergoing nova eruptions may gain mass during accretion, it has been suggested

that they may be the progenitors of type Ia supernovae in some variants of the single degenerate scenario (e.g. Starrfield, Sparks & Shaviv, 1988; Yungelson et al., 1996; Hachisu & Kato, 2001). Novae are believed to be important sources of some nuclides, such as ^{7}Li, ^{15}N, ^{17}O, ^{22}Na and ^{26}Al (e.g. Starrfield, Truran & Sparks, 1978; Hernanz et al., 1996; Gehrz et al., 1998; Kudryashov, Chugaĭ & Tutukov, 2000) which in some cases have been actually observed (Tajitsu et al., 2015; Izzo et al., 2015; Tajitsu et al., 2016). Although novae have been widely studied, many questions remain unclear. In recent years, an increasing number of observational studies of novae have become available. It is vital to compare our present theoretical understanding with observations, in particular the properties of nova populations on the whole.

It is accepted that novae occur in an accreting WD binary with accretion rates below the stable burning regime, whereby the H-rich material burns unstably on the surface of the WD (e.g. Mestel, 1952a,b; Kraft, 1964; Giannone & Weigert, 1967; Tutukov & Yungel'Son, 1972; Paczynski & Zytkow, 1978; Sion, Acierno & Tomczyk, 1979; Tutukov & Ergma, 1979). But note, Idan, Shaviv & Shaviv (2013) found that in the high accretion rate regime which is conventionally considered as corresponding to 'stable' H-burning, the latter actually proceeds in small-scale short-timescale flashes. In order to understand the process underlying nova explosions, considerable effort has been made in producing simulations of nova explosions (e.g. Starrfield et al., 1972; Prialnik, Shara & Shaviv, 1978, 1979; Sion, Acierno & Tomczyk, 1979; Prialnik & Kovetz, 1995; Yaron et al., 2005). During the accretion phase, first, H-rich material will be accumulated on the surface of the WD and gradually compressed by accreted material. The H-rich shell will be heated by the compression and undergo a thermonuclear runaway (TNR), when the pressure at the bottom of the accreted envelope becomes sufficiently high and the degeneracy is lifted. The TNR will lead to ejection of the accreted mass. If the accretion rate is close to the stable burning regime, the nova explosion is relatively weak and only a fraction of the accreted mass will be ejected. If the accretion rate is low enough, nova explosions are strong and the WD will be eroded. Prialnik & Kovetz (1995) and Yaron et al. (2005) have simulated a large number of multicycle nova evolution models. They found that the properties of novae (e.g. ignition mass, maximum luminosity) are mainly determined by the WD mass, accretion rate and the interior temperature. They show different characteristics of novae for accreting WDs with different parameters within the possible ranges. Based on the results of these simulations, many general properties of individual novae can be understood.

In the past three decades, observations of novae in galaxies of different Hubble types have been undertaken (e.g. Ciardullo et al., 1990; Della Valle et al., 1994; Shafter, Ciardullo & Pritchet, 2000; Ferrarese, Côté & Jordán, 2003; Williams & Shafter, 2004; Coelho, Shafter & Misselt, 2008; Franck et al., 2012). These observations are very helpful to study nova properties in different stellar populations. Previous studies (e.g. Duerbeck, 1990; Della Valle et al., 1992) suggested that there are two kinds of nova population: the disk novae and bulge novae. The disk novae are fast and may harbour more massive WDs, compared with the bulge novae (Della Valle & Livio, 1998). Some observational studies (e.g. Ciardullo et al., 1990; Shafter, Ciardullo & Pritchet, 2000; Ferrarese, Côté & Jordán, 2003; Williams & Shafter, 2004) have suggested that luminosity-specific nova rates may not

evolve strongly with the Hubble type of galaxies and the average luminosity-specific nova rate is around $2 \times 10^{-10}\, {L_{\mathrm{K},\odot}}^{-1}\, \mathrm{yr}^{-1}$. However, several studies indicate that some galaxies, such as the Magellanic Clouds, M33 and others, may have higher luminosity-specific nova rates (e.g. Della Valle et al., 1994; Della Valle, 2002; Neill & Shara, 2005; Alis & Saygac, 2014; Mróz et al., 2016; Shara et al., 2016).

Regarding individual galaxies, novae in M31 have been intensively studied in the past (e.g Arp, 1956; Rosino, 1964, 1973; Ciardullo et al., 1987; Rosino et al., 1989; Shafter & Irby, 2001; Darnley et al., 2006). Some earlier results suggested a nova rate in M31 of $\sim 20 - 40\ \mathrm{yr}^{-1}$ (see Shafter & Irby (2001) and their table 1). Darnley et al. (2006) performed a careful analysis of the distribution and the incompleteness of novae in their survey, and derived a nova rate of $65^{+16}_{-15}\, \mathrm{yr}^{-1}$. These studies have also provided other key parameters in describing nova properties (e.g. decay time, peak magnitude), which can be directly compared with theoretical results.

With the binary population synthesis method, Yungelson, Livio & Tutukov (1997) found that the luminosity-specific nova rate should be significantly higher in younger stellar populations compared with older stellar populations. The typical WD mass of novae in young stellar populations is larger than in old stellar populations. In addition, Nelson, MacCannell & Dubeau (2004) modelled the Galactic nova population (assuming a constant SFR and 100% initial binarity) and found that their derived nova rate and orbital period distribution are in agreement with observations.

In this paper, with a hybrid binary population synthesis method, we model the nova population for galaxies with two representative star formation histories (SFHs), i.e. starburst and constant star formation rate (SFR). Moreover, in order to compare with nova surveys of M31, we have computed a composite model with a star formation history consistent with that which is presently inferred for M31 (see Robertson et al., 2004, and discussion below). We will present our predicted nova rates, as well as the characteristic distribution of novae for different models, such as the WD mass, peak magnitude, mass loss time, and compare these results with observations.

The paper is structured as follows. In section 4.3, we introduce our binary population synthesis approach and describe how we calculate the values of various nova properties in our simulation models. In section 4.4, we mainly show the results of these simulations and compare these results with observations. We have a further discussion in section 4.5, before summarizing our results in section 4.6.

4.3 Binary population synthesis

In this paper, we adopt a hybrid binary population synthesis approach, which was first introduced in Chen et al. (2014). In this approach, first, we use the BSE code (Hurley, Tout & Pols, 2002) to generate WD binaries with non-degenerate donors (i.e. main sequence (MS), Hertzsprung gap (HG), red giant (RG) stars). Then we follow the evolution of these WD binaries with a grid of detailed evolutionary tracks computed with MESA code (Paxton et al., 2011, 2013). Compared with other binary population synthesis approaches,

this method allows a careful treatment of the second mass transfer phase. Here we briefly summarize the main assumptions and ingredients in our calculation.

4.3.1 BSE calculation

We adopt the initial mass function (IMF) of Kroupa (2001) for the primary mass ranging from $0.1\,M_\odot$ to $100\,M_\odot$. We take a flat mass ratio distribution (Kraicheva et al., 1979) and a flat distribution in logarithmic space for binary separations in the range between 10 and $10^6 R_\odot$. With respect to the binary fraction, observations indicate that it may depend on the binary parameters (Kouwenhoven et al., 2009; Kraus & Hillenbrand, 2009; Sana et al., 2012). Following the suggestion of van Haaften et al. (2013), we adopt the following formula for the binary fraction (f_b):

$$f_\mathrm{b} = 0.50 + 0.25\log_{10}(M_1), \tag{4.1}$$

where M_1 is the primary mass. This is different from our previous papers (Chen et al., 2014, 2015), in which we adopt a constant binary fraction, i.e. 50%. However, this does not significantly influence our results.

With the BSE population synthesis code (Hurley, Tout & Pols, 2002), we computed the evolution of around 2×10^6 binary systems, a fraction of which may evolve into a binary system consisting of a WD and a non-degenerate donor that later stably overflows Roche lobe. We follow the evolution of these systems until the WD binaries become semi-detached and obtain the binary parameters (i.e. WD mass, donor mass, orbital period) at the onset of mass transfer.

It is worth noting that we include different types of donors (i.e. MS, HG, RG donors) in our calculation. In previous studies of nova populations (e.g. Nelson, MacCannell & Dubeau 2004), only MS donors are included. However, Darnley et al. (2014) have shown that some recurrent novae harbour HG and RG donors, though some of these may reside in symbiotic binaries. Therefore, for the first time, we include a relatively complete set of progenitors of novae binaries in a population synthesis study.

4.3.2 Binary evolution calculation

In order to follow the evolution of these WD binaries, we computed the evolution of a grid of WD binaries with varying initial parameters using the detailed stellar evolutionary code MESA (Paxton et al., 2011, 2013). In this grid, the WD mass ranges from $0.50\,M_\odot$ to $1.35\,M_\odot$ with a step $\Delta M = 0.10\,M_\odot$. We ignore He WDs in our calculation.[1] The donor mass ranges from $0.10\,M_\odot$ to $13.5\,M_\odot$ with a step $\Delta M = 0.05\,M_\odot$. The orbital period ranges (with step size $\Delta\log_{10}P_\mathrm{orb} = 0.1$) from 1000 days down to the minimum period for which the binary separation yields mass transfer which begins on the zero-age

[1] Nelson, MacCannell & Dubeau (2004) computed the nova rates from He WDs by extrapolating the results of Prialnik & Kovetz (1995) and found that He WDs contribute a very small fraction ($\lesssim 5\%$) to the total nova rates.

main sequence. With the binary parameters at the onset of mass transfer from our BSE calculations, we can select the closest track in the grid of MESA calculation and follow the evolution of any WD binaries.

In the MESA calculation, we adopt the limits for the stable burning regime from Wolf et al. (2013). We assume that the excess mass will be lost in the form of an optically thick wind (Hachisu, Kato & Nomoto, 1996) and take away the specific angular momentum of the WD, if the accretion rate is larger than the maximum stable burning rate. If the accretion rate is in the stable burning regime, we assume that no mass will be lost. If the accretion rate is below the stable burning regime, we adopt the H burning retention efficiency from Yaron et al. (2005), as approximated in Chen et al. (2014) (see their Eq. 6). Regarding the He burning retention efficiency, this suffers from considerable uncertainties (e.g. Hachisu, Kato & Nomoto, 1999; Kato & Hachisu, 2004; Piersanti, Tornambé & Yungelson, 2014; Hillman et al., 2015). Here we simply use the prescription from Hachisu, Kato & Nomoto (1999). The angular momentum lost due to mass loss during nova explosion is rather uncertain (see e.g. Livio, Govarie & Ritter, 1991; Nelemans et al., 2016; Schreiber, Zorotovic & Wijnen, 2016). Here we assume that the lost mass takes away the specific angular momentum of the WDs.

In our calculation, we adopt an initial hydrogen abundance $X = 0.70$, helium abundance $Y = 0.28$ and metallicity $Z = 0.02$.

4.3.3 Calculation of the nova rate

In our calculations, we do not compute the detailed evolution of the WDs. We consider the WD as a point mass and compute its mass evolution. From our binary evolution calculations, for any given WD binary evolutionary track, we know the accretion rate and WD mass. Yaron et al. (2005) computed multicycle nova models for WDs under differing conditions, and showed the dependence of nova properties on WD mass, accretion rate and WD temperature (see their tables 2 and 3). Under certain assumptions on the interior temperature of the WDs, we can then find the characteristics of Novae, such as the ignition and ejected mass, by interpolating their tables. The results of Townsley & Bildsten (2004) indicate that, for WD masses and accretion rates typical of cataclysmic variables, equilibrium WD core temperatures are smaller than 1.0×10^7 K. However, there is no complete computation similar to Yaron et al. (2005) for different WDs with low temperatures. Therefore, we use $T_{\rm c} = 1.0 \times 10^7$ K in our calculations. In section 4.5, we will discuss its influence on our results.

4.3.4 Common envelope evolution

For the treatment of common envelope (CE) events, we adopt the α-formalism (Webbink, 1984; de Kool, 1990) and use the fitting formula from Loveridge, van der Sluys & Kalogera (2011) for the binding energy parameter λ. The efficiency α suffers from considerable uncertainty (see Ivanova et al., 2013, for a review). Davis, Kolb & Knigge (2012) found that the value of α should be ≤ 1.0 and it may decrease with increasing WD mass and

secondary mass. By reconstructing the evolution of post CE binaries, Zorotovic et al. (2010) constrain the value of α to be in the range of $0.2 - 0.3$. A similar result is found by Ricker & Taam (2012) using hydrodynamic simulations. Davis, Kolb & Willems (2010) found that a global value of $\alpha > 0.10$ provides a good agreement with observations of post CE binaries. Therefore, in our calculation, we adopted $\alpha = 0.25$. We will discuss the influence of this value on our results in section 4.5.

By default, we adopt criteria for dynamically stable mass loss from Hjellming & Webbink (1987) and Webbink (1988) (hereafter the HW criteria) for binaries with giant stars. However, some detailed binary evolution calculations (e.g. Han et al., 2002; Chen & Han, 2008) indicate that this criteria may predict too low a critical mass ratio, and that the critical mass ratio should depend on the evolutionary phase of the donor star, mass, and adapted mode of angular momentum loss from the system. Woods & Ivanova (2011) (see also Passy, Herwig & Paxton, 2012) demonstrated that the difference is due to consideration of the superadiabatic outer surface layer, whose typical thermal timescale may be smaller than the timescale for mass transfer. The muted response of this surface layer of the donor in response to mass loss (relative to mass loss directly from the convective envelope, as in polytropic models), allows for stable mass transfer at higher mass ratios than previously considered. Recently, Pavlovskii & Ivanova (2015) found that the critical mass ratio may vary from 1.5 to 2.2.

4.3.5 Binary population synthesis models

With the uncertainties in the treatment of CE events in mind, we computed three different models: a025 model, a025qc15 model, a025qc17 model. In all of these models, we use $\alpha = 0.25$. In the first model, we use the HW criteria for giant stars. In the other models, we use critical mass ratios $q_{\rm c} = 1.5$ and 1.7 for giant stars, respectively. However, we should emphasize that the critical ratio should not be a fixed value and varies as a function of other stellar parameters, as mentioned above.

In each model, we consider three different SFHs, which may roughly represent three kinds of galaxies. (I) Elliptical-like galaxies: all stars (with initial total mass $10^{11}\,{\rm M}_{\odot}$) are formed at $t = 0$. (II) Spiral-like galaxies: a constant SFR for 10 Gyr with total stellar mass $10^{11}\,{\rm M}_{\odot}$ formed. (III) M31-like galaxies: In order to compare wtih observations of novae in M31, we make a composite model with a SFH outlined as follows. Robertson et al. (2004) simulated the formation and SFH of disk galaxies, which Olsen et al. (2006) have demonstrated to be consistent with the observationally derived SFH of M31. Given that the total stellar mass of M31 is around $1.1 \times 10^{11}\,{\rm M}_{\odot}$ (Barmby et al., 2007), we adopt the SFH from Robertson et al. (2004) as the SFH of M31 and rescale the total stellar mass to $1.1 \times 10^{11}\,{\rm M}_{\odot}$. In this model, the SFR increases from $t = 0\,{\rm Gyr}$ and peaks around $t = 2.0$ Gyr, and then declines by around one order of magnitude by 10 Gyr.

Table 4.1: The current nova rates (i.e. at 10 Gyr) for different kinds of galaxies in different models. The total stellar mass for elliptical-like and spiral-like galaxies is 10^{11} $M_\odot$ and it is 1.1×10^{11} $M_\odot$ for M31-like galaxies. The present nova rate of M31 galaxy is around $97\,yr^{-1}$ (see text).

model	α	q_c	WD temperature (T_c) (10^7 K)	nova rate (yr^{-1}) (elliptical-like)	nova rate (yr^{-1}) (spiral-like)	nova rate (yr^{-1}) (M31-like)
(1)	(2)	(3)	(4)	(5)	(6)	(7)
a025	0.25	HW criteria	1	20	413	158
a025qc15	0.25	1.50	1	14	283	105
a025qc17	0.25	1.70	1	12	207	80
a050	0.50	HW criteria	1	13	468	160
a025	0.25	HW criteria	3	42	462	198

Notes. (1) model name. (2) α value. (3) CE criteria for binaries with giant stars at the first mass transfer phase. (4) WD interior temperature. (5)-(7) nova rates at 10 Gyr.

4.4 Results

4.4.1 Evolution of nova population with stellar ages

In Fig. 4.1, we show the evolution of nova rates for elliptical-like and spiral-like galaxies in different models. The mass-normalized nova rates reach maximum around 1 Gyr in elliptical-like galaxies and around 2 Gyr in spiral-like galaxies. After the maximum, they decline by ∼2 orders of magnitude in elliptical-like galaxies and by a factor of ∼4 in spiral-like galaxies by the age of 10 Gyr. A similar behaviour in elliptical galaxies is also found in Matteucci et al. (2003). In elliptical-like galaxies, at ∼1 Gyr, the typical donor mass of WD binaries is around 2 $M_\odot$. For these binaries, WDs will efficiently accumulate mass during a thermal timescale mass transfer. These massive WDs have frequent outbursts. With increasing stellar age, the typical donor mass will decrease. The WD can not efficiently accumulate mass and the typical WD mass decreases. Therefore, the nova rate will decrease. In spiral-like galaxies, novae form with a typical delay time around 1 Gyr. Therefore, after ∼2 Gyr, the nova rate is almost constant while the stellar mass continues to increase linearly with time. Therefore, the mass-specific nova rates at old ages in the right panel of Fig. 4.1 decrease as t^{-1}.

Compared with our a025 model, the nova rates in a025qc15 and a025qc17 are smaller. In a025qc15 and a025qc17 models, the critical mass ratios for a CE in binaries with giant stars are larger than when using the HW criteria. Therefore, it will become more difficult for binaries to enter a CE and fewer accreting WD binaries will be produced. Consequently, the nova rates decrease as this critical mass ratio increases.

The nova rates at 10 Gyr in different models for different kinds of galaxies are shown in table 4.1. For an elliptical-like galaxy with $10^{11}\,M_\odot$, the nova rate is around $10 - 20\,yr^{-1}$. For a spiral-like galaxy with the same mass, the nova rate is around 10-20 times larger. These results are in line with Matteucci et al. (2003) who found that the luminosity-specific nova rates in elliptical galaxies are lower than in spiral and irregular galaxies. Yungelson,

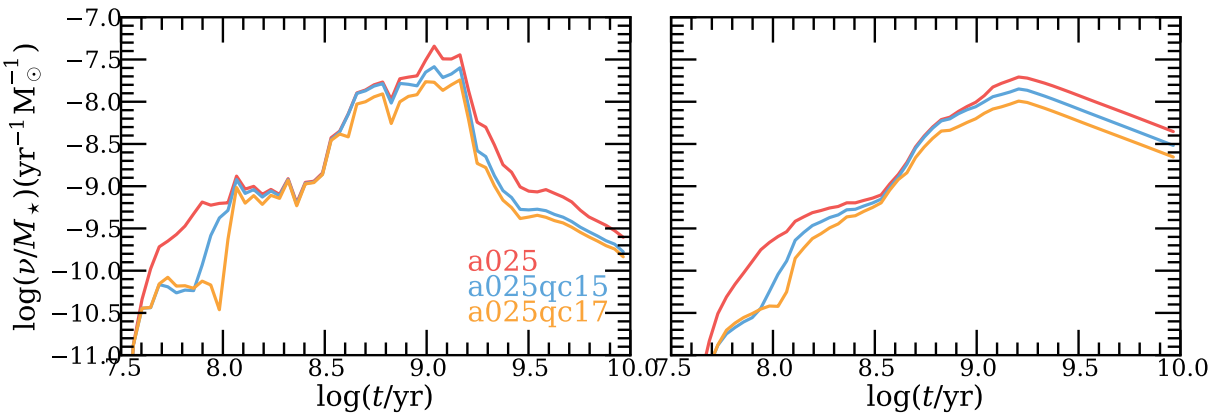

Figure 4.1: Evolution of mass-specific nova rates for elliptical-like galaxies (left panel) and spiral-like galaxies (right panel) in different models (see table 4.1). The red, blue, orange colours are for a025, a025qc15, a025qc17 model, respectively.

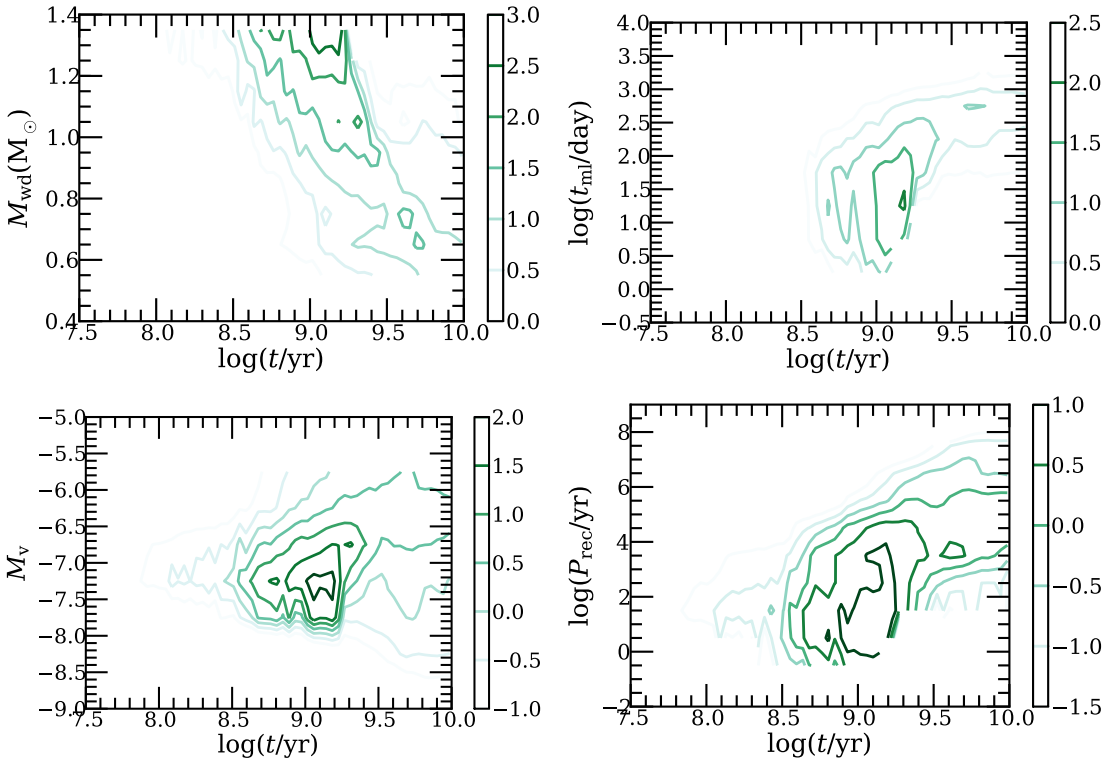

Figure 4.2: Isodensity contours for nova properties at different stellar ages for elliptical-like galaxies in a025 model. The values of different contours are for $(\partial^2 N/\partial \log t \partial M_{\rm WD})/M_\star$(upper left), $(\partial^2 N/\partial \log t \partial \log t_{\rm tml})/M_\star$ (upper right), $(\partial^2 N/\partial \log t \partial M_{\rm v})/M_\star$ (lower left), $(\partial^2 N/\partial \log t \partial \log P_{\rm rec})/M_\star$ (lower right) in logarithm scale. N is the number of nova events and $M_\star$ is the stellar mass of the galaxy.

Livio & Tutukov (1997) came to a similar conclusion using a binary population synthesis method. In M31-like galaxies, the nova rate is around $80 - 160\,\mathrm{yr}^{-1}$. Darnley et al. (2006) detected 20 classical novae in M31 and deduced a global nova rate of $65^{+16}_{-15}\,\mathrm{yr}^{-1}$ based on a thorough analysis of the completeness of novae in their survey. However, as they discussed, the novae with the shortest decay times t_2 or t_3 (the decline time of the optical light curve from the peak by 2 (3) magnitudes) in their sample are likely incomplete because of insufficient cadence of the survey. In order to get a reliable nova rate for M31, Soraisam & Gilfanov (2015) and Soraisam et al. (2016) combined the data from observations of novae with $t_2 < 20$ days by Arp (1956) with the data of novae with $t_2 > 20$ days from Darnley et al. (2006), taking the completeness into consideration. In the incompleteness analysis of Arp's survey, they ran Monte-Carlo simulations and used a template nova light curve and an observed maximum magnitude-rate of decline relation. Then they are able to get the fraction of detected novae as a function of t_2 (see Appendix of Soraisam et al. (2016) for more details). Regarding the incompleteness of Darnley's survey, we use a completeness value of $\approx 23\%$ for correction based on the result of Darnley et al. (2006) (see their table 3). The nova rate is computed as follows. $\dot{N}(t_2) = \begin{cases} \frac{N}{\eta \times 1.342 \times 6.02 \times 10^{10}}, & \text{for Arp's data} \\ \frac{N}{\eta \times 2.830 \times (0.47 \times 11 \times 10^{10})}, & \text{for Darnley's data.} \end{cases}$ where $\dot{N}(t_2)$ is in units of $\mathrm{yr}^{-1}\ {\mathrm{M}_\odot}^{-1}$, N is the observed numbers of sources at t_2 and η is the completeness. The duration of the two surveys are 1.342 yr and 2.830 yr respectively. The masses enclosed by the field of view in the two surveys are 6.02×10^{10} $\mathrm{M}_\odot$ and 5.17×10^{10} $\mathrm{M}_\odot$, respectively (see Soraisam et al. (2016) for more details). Then we obtain a global nova rate $97\,\mathrm{yr}^{-1}$ [2] for M31. Our results are in good agreement with this number. In order to make a further comparison, we compare the distributions of predicted and observed mass loss time distribution of novae in the following section.

In order to understand the evolution of nova populations with time, in Fig. 4.2, we show the isodensity contours of nova parameters at different stellar ages for elliptical-like galaxies in our a025 model. Using Yaron et al. (2005) data we can find the maximum luminosity of novae and then convert it to M_v (see the following section). From these plots, it is found that the average WD mass of a nova population decreases with increasing stellar ages, which is consistent with previous studies, e.g. Politano (1996). According to the results of Yaron et al. (2005), the mass loss times and recurrence periods of novae with massive WDs are shorter compared with novae with smaller WD mass (see also Truran & Livio, 1986; Politano et al., 1990). Therefore, it is expected that the typical mass loss time and recurrence time of populations of novae will increase with increasing stellar age. Similarly, the typical maximum magnitude of novae become lager as the stellar age increases.

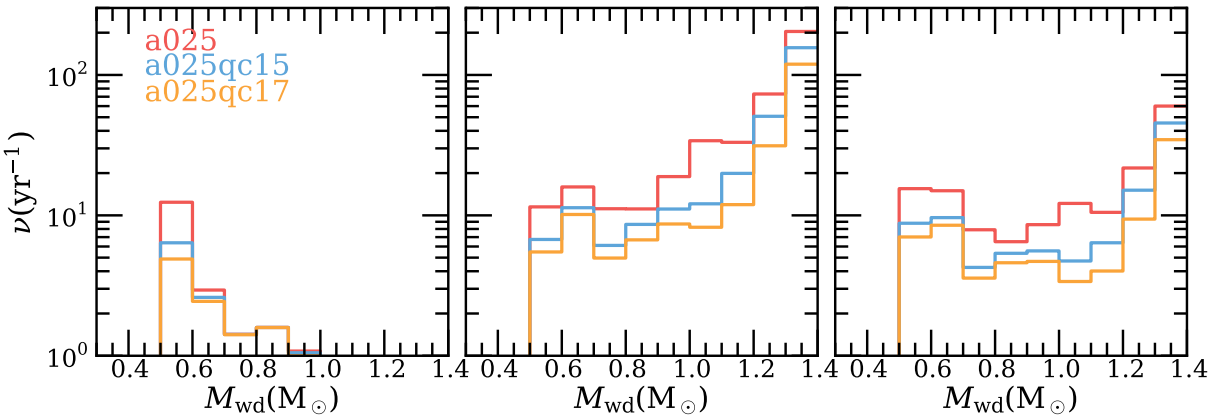

Figure 4.3: Distribution of nova rate as a function of WD mass for current nova population of elliptical-like galaxies (left panel), spiral-like galaxies (middle panel) and M31-like galaxies (right panel) in different models (see table 4.1). The red, blue, orange colours are for a025, a025qc15, a025qc17 model, respectively.

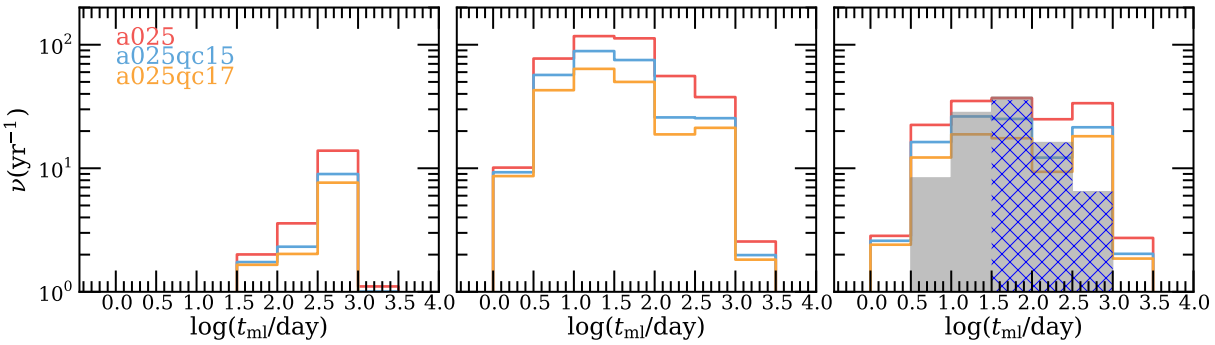

Figure 4.4: Mass loss time distribution of current nova population of elliptical-like galaxies (left panel), spiral-like galaxies (middle panel) and M31-like galaxies (right panel) in different models (see table 4.1). The red, blue, orange colours are for a025, a025qc15, a025qc17 model, respectively. The gray histogram shows the combined observational nova data from Arp (1956) and Darnley et al. (2006) taking the incompleteness into consideration (Soraisam & Gilfanov, 2015; Soraisam et al., 2016). The shaded histogram shows the observational nova data of Darnley's paper only.

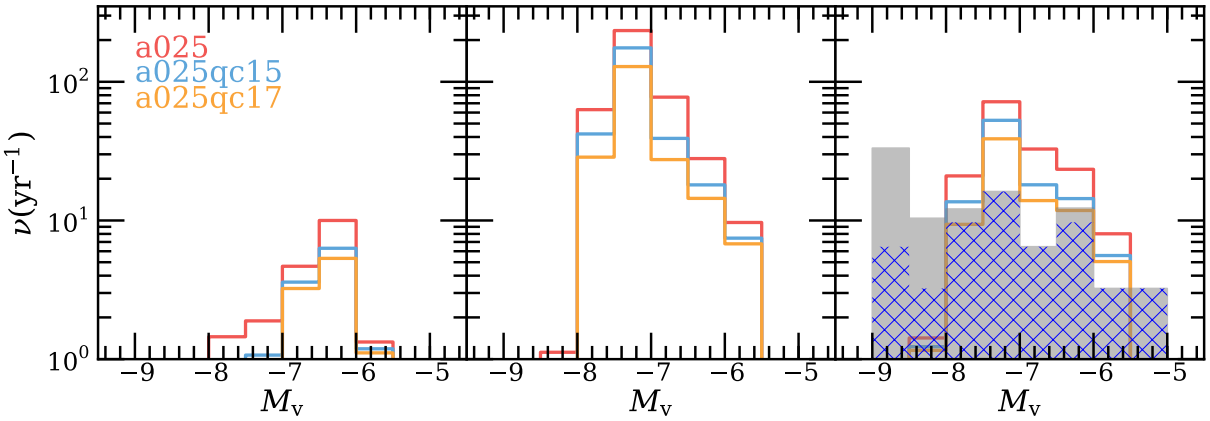

Figure 4.5: Distribution of V band maximum magnitude for current nova population of elliptical-like galaxies (left panel), spiral-like galaxies (middle panel) and M31-like galaxies (right line) in different models (see table 4.1). The red, blue, orange colours are for a025, a025qc15, a025qc17 model, respectively. The gray histogram shows the combined observational nova data from Arp (1956) and Darnley et al. (2006) taking the incompleteness into consideration (Soraisam & Gilfanov, 2015; Soraisam et al., 2016). The shaded histogram shows the observational nova data from Darnley et al. (2006) only.

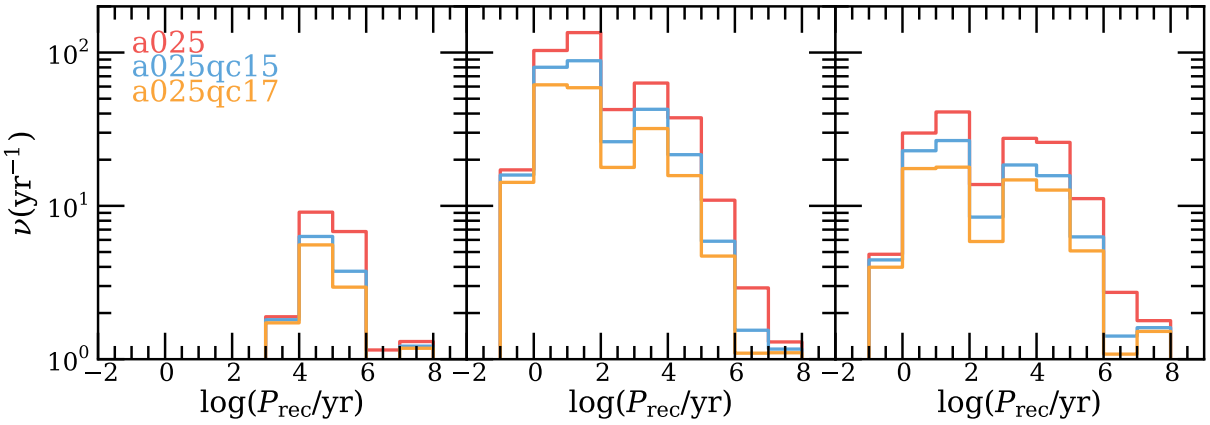

Figure 4.6: Distribution of recurrence period for current nova population of elliptical-like galaxies (left panel), spiral-like galaxies (middle panel) and M31-like galaxies (right panel) in different models (see table 4.1). The red, blue, orange colours are for a025, a025qc15, a025qc17 model, respectively.

4.4.2 Current nova population

Since the properties of novae are mainly determined by the WD mass, we show the WD mass spectra of the "current" (10 Gyr) nova population in Fig. 4.3. The WD mass peaks around $0.5 - 0.6\,\mathrm{M}_\odot$ in elliptical-like galaxies and $1.30 - 1.40\,\mathrm{M}_\odot$ in spiral-like galaxies. This is expected; in elliptical-like galaxies, WD binaries with massive WDs evolve faster and the number of massive WDs decreases. Therefore, the typical WD mass of novae at 10 Gyr is small. The cut off at the low mass side is simply due to the fact that we ignore He WDs in our calculation. In spiral-like galaxies, there are young stellar populations with massive WDs. Most of these WDs have initially small mass and have increased their mass during the thermal timescale mass transfer (see Fig. 2 of Chen et al. (2014)). From Yaron et al. (2005), we know that the ignition mass of novae for massive WDs can be smaller by $2 - 3$ orders of magnitude, compared with low mass WDs. Therefore, massive WDs can have relatively more frequent nova outbursts. In M31-like galaxies, there are two peaks in the WD spectra. The peak around low WD mass is simply due to the large number of WD binary systems with low mass WDs. The peak around massive WD mass is due to massive WDs having more frequent nova outbursts.

In Fig. 4.4, we show the mass loss time ($t_{\rm ml}$) distribution of novae for different kinds of galaxies and compare the result of M31-like galaxies with the observational data of M31. With respect to the observational data, identical to the above treatment of the observed nova rate in M31, we combine the nova data of Arp (1956) and Darnley et al. (2006). With the results of Yaron et al. (2005), we can get two timescales for each nova - the decay time of bolometric luminosity by 3 mag $t_{3,\rm bol}$ and the duration of mass loss phase $t_{\rm ml}$. It is found that $t_{\rm ml}$ is much closer to the observed t_3 than $t_{3,\rm bol}$ (Prialnik & Kovetz, 1995; Yaron et al., 2005). The following formula is used to compute the values of $t_{\rm ml}$ for observed novae (Bode & Evans, 2008).

$$t_2 = \begin{cases} t_{\rm ml}/2.1 & t_{\rm ml} < 50 \text{ days} \\ t_{\rm ml}/1.75 & t_{\rm ml} \geq 50 \text{ days} \end{cases}$$

One point worth noting is that using a higher and fixed critical mass ratio in the CE criteria does not result in an unrealistic nova population. In elliptical-like galaxies, novae have a typical mass loss time around hundreds of days. The mass loss time of novae in spiral-like galaxies peaks around several tens of days. In M31-like galaxies, the mass loss time of novae ranges from tens of days to hundreds of days. Compared with the observational data of M31, there are too many novae predicted with $t_{\rm ml} < 10$ days and $t_{\rm ml} > 300$ days. Although Soraisam & Gilfanov (2015) and Soraisam et al. (2016) have corrected for the incompleteness of the fast events, their correction was approximate and may not be accurate enough for the fastest novae. No incompleteness was applied for the longest events in our comparison. The novae with the shortest mass loss times are easily missed in observations, since observations are usually discontinuous. On the other hand,

[2]In Soraisam et al. (2016), they found a nova rate of 106 yr^{-1}, corresponding to the $\theta = 1.0$ case of Darnley et al. (2006). Here, we use the $\theta = 0.18$ case of Darnley et al. (2006). θ is the ratio of nova rates per unit r' flux of the disc and bulge population.

the novae with the longest mass loss times may be difficult to detect, because these novae are likely to be faint and the luminosity may not dramatically decline within the limited observational time.

Following Shafter et al. (2009), we assume that the colour of novae at maximum luminosity is the same as the colour of an A5V star ($T_{\rm eff} \sim 8200\,{\rm K}$). Then we can get the V band magnitude of novae for any given maximum bolometric luminosity with the data compiled by Johnson (1966). In Fig. 4.5, we show the distribution of V-band magnitude for novae at maximum luminosity. The novae are dominated by those with $M_{\rm v}$ from about -7.0 to about -6.0 in elliptical-like galaxies while absolute V-band magnitude peaks around about -8.0 to -6.5 in spiral-like and M31-like galaxies. Arp (1956) found that the maximum photographic magnitude of novae in M31 has a bimodal distribution. However, in M31-like galaxies, we do not find a bimodal distribution in the theoretical and observational results. The observational data of M31 is shown in the right panel of Fig. 4.5, which is based on the results of Arp (1956) and Darnley et al. (2006). In the Arp's survey, the photographic magnitudes were given. We correct them for the foreground extinction with $A_{\rm pg} = 0.25$ (Shafter et al., 2009). Then we convert the photographic magnitude to V-band magnitude using colours $(B - m_{\rm pg}) = 0.17$ (Arp, 1956; Capaccioli et al., 1989) and $(B - V) = 0.15$ (Shafter et al., 2009). For novae from Darnley et al. (2006), we convert the observed magnitude to V-band magnitude using colour $(V - R) = 0.16$ (Shafter et al., 2009). Compared with the observational data, we underestimate the number of very bright novae. The possible reasons for this discrepancy are as follows. First, we did not include low temperature WDs ($T_{\rm c} < 1.0 \times 10^7$ K) in our calculation. With the same code used by Yaron et al. (2005), Shara et al. (2010) (see also Schwartzman, Kovetz & Prialnik (1994)) found that some very luminous novae can be explained by low temperature WDs with low accretion rates. Additionally, as Prialnik & Kovetz (1995) discussed, the error in the maximum luminosity in their simulations can be as large as -0.75 magnitude. Finally, in our calculation of $M_{\rm v}$, we assume that the spectra of all novae at maximum are similar to normal A5V main sequence stars. However, previous studies (e.g. Bode & Evans, 2008) found that the spectra of novae at maximum resemble the spectra of stars with spectral type in the range B5 to F5. Recently, based on high quality photometric spectra of novae, Munari (2014) found that the spectra of some novae deviate from A5 main sequence stars (see his Fig. 4). For example, the colour (B-V) ranges from around 0.20 to 3.40, while (B-V) = 0.15 for A5V main sequence stars. This evidence suggests that adopting a unique spectral type may not be an accurate assumption. This will influence the colour and bolometric correction used in the above conversion.

In Fig. 4.6, we show the distribution of recurrence periods for novae in different galaxy types given different models. The novae in elliptical-like galaxies have relatively long recurrence periods, while the novae in spiral-like galaxies have predominantly shorter recurrence periods. In M31-like galaxies, there are two peaks, which correspond to the two peaks of the WD mass distribution in Fig. 4.3. The peak around massive WD produces the peak around short recurrence periods; most of these WDs have accumulated additional mass during a prior thermal timescale mass transfer phase. These massive WDs have more frequent outbursts and are also short lived (see Fig. 4.2). The peak around small WD masses

corresponds to the peak around long recurrence periods. In spiral-like galaxies, there is a large number of WD binaries with small WD mass. But these small WDs have less frequent outbursts. Given the short observational time in reality, less novae, particularly recurrent novae, will be detected in elliptical galaxies. If we take the novae with recurrence period $P_{\rm rec} < 100$ yr as recurrent novae, there will be no recurrent novae in elliptical-like galaxies. In spiral-like galaxies, the fraction of recurrent novae is around $\sim 60\% - 65\%$. In M31-like galaxies, the fraction of recurrent novae is $\sim 45\% - 50\%$. Shafter et al. (2015) performed a thorough astrometric study of novae in M31 and did a Monte Carlo analysis of the detection effficiency of recurrent novae. They suggested that as many as one in three M31 novae may be recurrent novae with $P_{\rm rec} < 100\,{\rm yr}$. Our result is not inconsistent with their results.

4.5 Discussion

4.5.1 Influence of α values

As we discussed in section 4.3, the appropriate value(s) of α suffers from considerable uncertainty. Therefore, we computed a model with $\alpha = 0.5$ (a050 model) and found no dramatic difference between the results of this model and a025 model, which is similar to what we found in Chen et al. (2014). Here we only show the distribution of recurrence periods for comparison in Fig. 4.7. The influence of α values on the evolution of the binary population is rather complicated. Qualitatively it is clear that for larger α values more binaries will survive from the first CE phase and typical binary separations of survivors will become larger. For larger binary separations, in more binary systems the mass loss of nondegenerate donors upon ROLF will be unstable and a fraction of population underlaying novae will be lost. As well, in remaining systems accretion rates will be higher and WD may spend more time as stably nuclear burning objects and less as nova progenitors (less mass will be left for unstable burning). But the last effect may be offset by the increased WD mass and lower ignition mass of WDs with higher accretion rates. As a result, the total nova rates remain comparable. A more thorough study of this issue is beyond the scope of the present paper.

4.5.2 Influence of WD interior temperatures

In the above nova calculation, we assume that the interior temperatures of WDs are constant, i.e. $T_{\rm c} = 1.0 \times 10^7\,{\rm K}$. In order to understand the influence of WD temperature on our results, we computed a model with $T_{\rm c} = 3.0 \times 10^7$ K. The other assumptions of this model are the same as in a025 model.

From Fig. 4.8, we see that there is no dramatic difference among models with different WD temperatures and nova rates are only slightly higher for WDs with higher temperatures (see also table 4.1). This can be understood since the ignition mass of novae is lower for WDs with higher temperature (Yaron et al., 2005). In elliptical-like galaxies, the difference

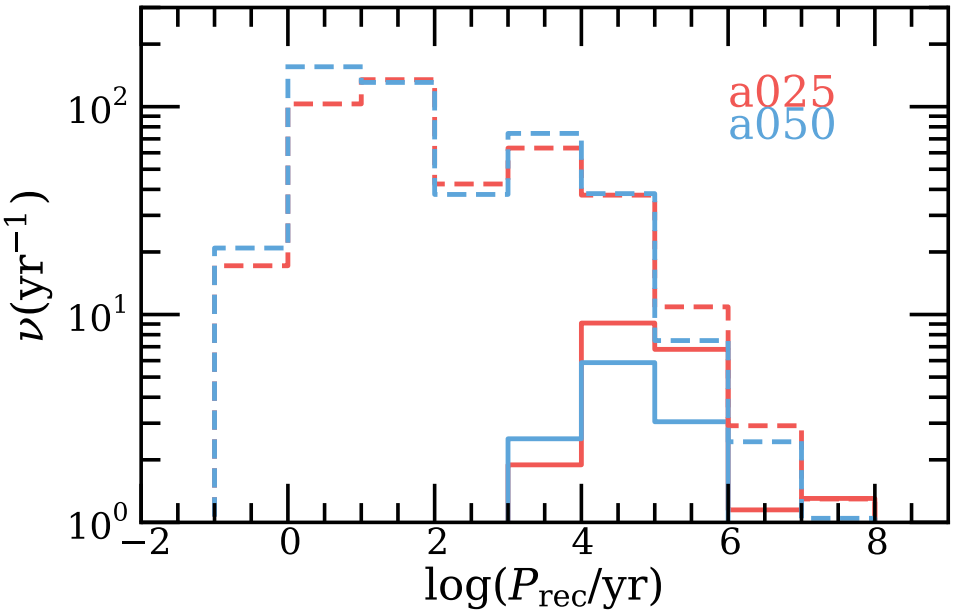

Figure 4.7: Comparison of recurrence periods distribution of current nova population for elliptical-like (solid line) and spiral-like galaxies (dashed line) in a025 model (red line) and a050 model (blue line).

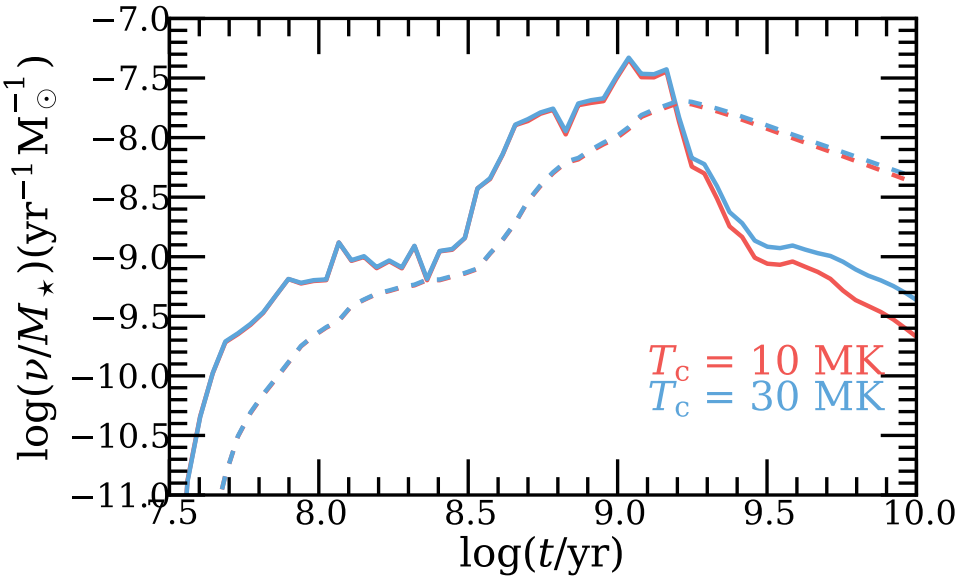

Figure 4.8: Mass-normalized nova rates as a function of stellar age for elliptical-like galaxies (solid line) and spiral-like galaxies (dashed line) in a025 model assuming WD temperatures $T_c = 1 \times 10^7$ K (red colour), $T_c = 3 \times 10^7$ K (blue colour).

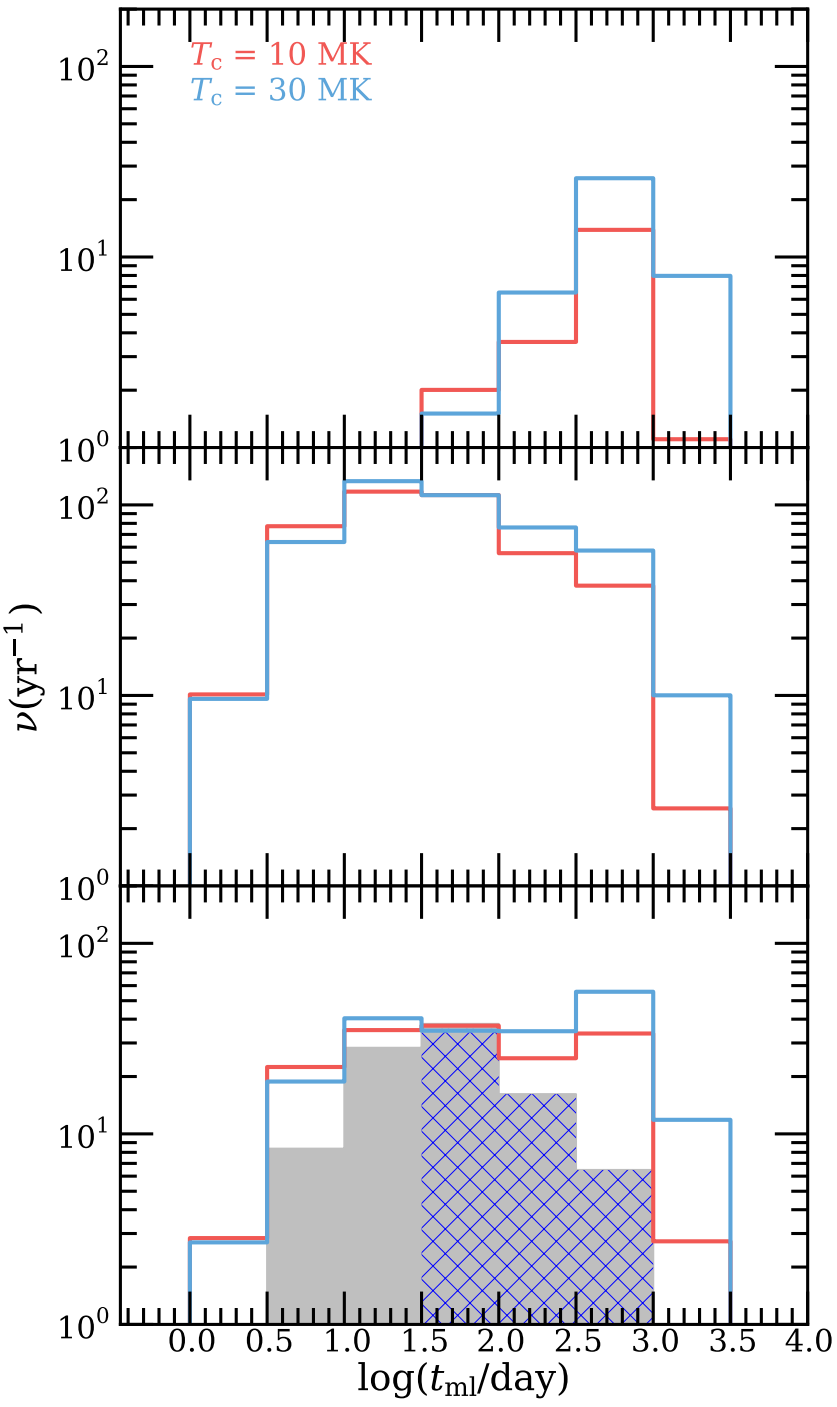

Figure 4.9: Mass loss time distribution of current nova population for elliptical-like galaxies (upper panel), spiral-like galaxies (middle panel) and M31-like galaxies (lower panel) in a025 model assuming WD temperatures $T_c = 1 \times 10^7$ K (red colour), $T_c = 3 \times 10^7$ K (blue colour). The gray histogram shows the observational nova data from Arp (1956) and Darnley et al. (2006) taking the incompleteness into consideration (Soraisam & Gilfanov, 2015; Soraisam et al., 2016). The shaded histogram shows the observational nova data of Darnley et al. (2006) only.

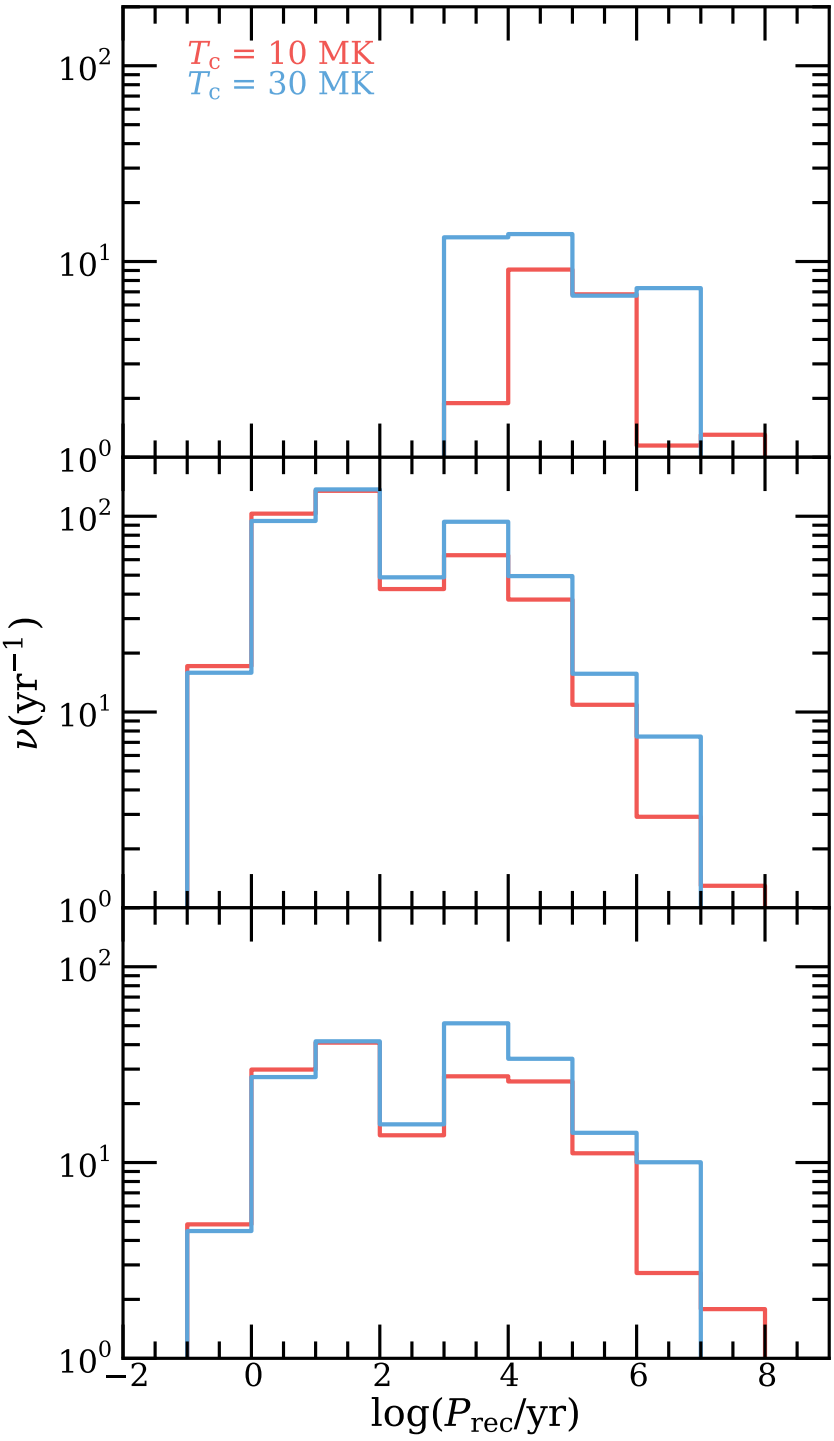

Figure 4.10: Recurrence period distribution of current nova population for elliptical-like galaxies (upper panel), spiral-like galaxies (middle panel) and M31-like galaxies (lower panel) in a025 model assuming WD temperatures $T_c = 1 \times 10^7$ K (red colour), $T_c = 3 \times 10^7$ K (blue colour).

becomes larger at old ages. This is due to the fact that the difference in ignition mass at different temperatures is larger for low WD masses than for massive WD (Yaron et al., 2005).

In Fig. 4.9, we show the distribution of mass loss time at 10 Gyr in different types of galaxies for a025 model assuming different WD temperatures. Compared with model with WD temperature $T_{\rm c} = 1.0 \times 10^7$ K, there is an enhancement of novae with long mass loss times ($t_{\rm ml} > 100$ days) for all galaxies types in the model with a higher WD temperature. In Fig. 4.10, we show the distribution of recurrence period of novae. There is an enhancement of novae with long recurrence period for the model with a high WD temperature. The trend seen in Figs. 4.9 and 4.10 is explained by the fact that, at $\dot{M}_{\rm acc} \leq 10^{-8}\,M_{\odot}\,{\rm yr}^{-1}$ at which most of novae occur, $P_{\rm rec}$ drops with increase of $T_{\rm c}$, while $t_{\rm ml}$ increases with increase of $T_{\rm c}$ (Yaron et al., 2005).

4.5.3 Influence of metallicity

Saglia et al. (2010) found that in the inner few arcsecs of the bulge of M31, the metallicity is $\sim 3\,Z_{\odot}$. Except for this region, the metallicity is solar. In addition, the metallicity of the disc is less than solar. In our computation, we assume that the metallicity of the stellar population is solar. The influence of metallicity on our results is rather complicated. First, it will influence the binary evolution. For example, Meng, Chen & Han (2008) found that, for $Z \geq 2Z_{\odot}$, the final WD mass will increase as metallicity increases, while for metallicity $Z < 2Z_{\odot}$, it will decrease as metallicity increases. Additionally, Piersanti et al. (2000) computed the evolution of accreting WDs for H-rich material with different metallicities and they found that the accretion rate for stable burning WD will be lower for lower metallicity and the width of the stable burning regime will be reduced. On the other hand, metallicity will influence the nova properties. For example, Starrfield et al. (2000) have studied the effects of metallicity on nova outburst and found that the ignition mass is higher for lower metallicity. Although metallicity is important in our calculation, it is difficult for us to quantitatively assess its influence on our results, and further studies are needed in this regard.

4.5.4 Novae with donors at differing evolutionary states

We classify novae according to the donor type at the onset of mass transfer. In Fig. 4.11, we show the recurrence period distribution of the "current" nova population with different donor types in elliptical-like galaxies and spiral-like galaxies. The contribution to the total nova rate from WD binaries with non-MS donors is comparable to that of WD binaries with MS donors. This conclusion is also true for our model of a M31-like galaxy. In Fig. 4.12, we show the orbital period distribution of the current nova population in elliptical-like and spiral-like galaxies. It is found that the secondaries of those novae with non-MS donors are mainly located in the hydrogen-shell burning stage. Those WD binaries with evolved secondaries have relatively higher mass transfer rates. In addition, the WD will accumulate mass during the thermal timescale mass transfer. For higher mass transfer rates and large

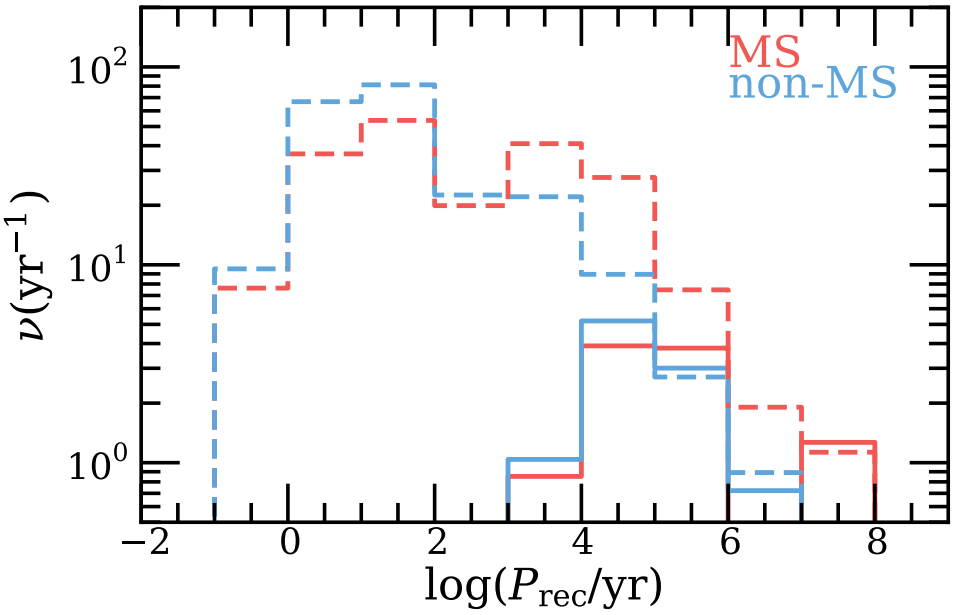

Figure 4.11: Distribution of recurrence period for current nova population with different types of donors in elliptical-like (solid line) and spiral-like galaxies (dashed line). The red and blue lines shows the novae with MS donors and non-MS donors (i.e. HGs and RGs), respectively. The donor type is defined according to the donor type at the onset of mass transfer.

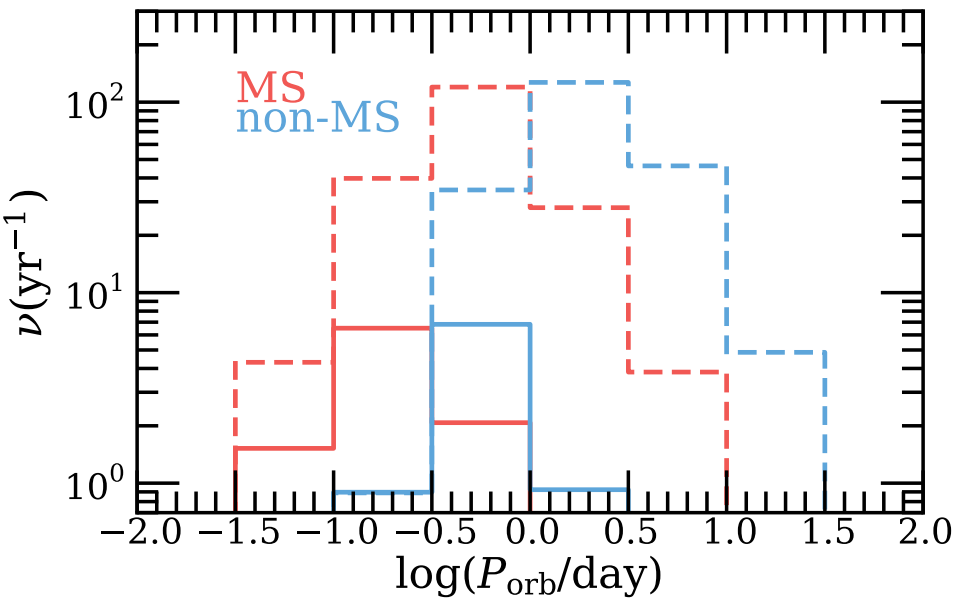

Figure 4.12: Distribution of orbital periods for current nova population with different types of donor in elliptical-like (solid line) and spiral-like galaxies (dashed line). The red and blue lines shows the novae with MS donors and non-MS donors (i.e. HGs and RGs), respectively. The donor type is defined according to the donor type at the onset of mass transfer.

WD masses, the ignition mass will be smaller. Therefore, there will be more frequent outbursts for these binaries.

Williams et al. (2014) found 11 nova progenitor systems with evolved secondaries in a survey with 38 confirmed nova progenitor systems. This leads to a fraction of $\sim 30\%$ of the nova progenitor systems which harbour evolved secondaries. Given the nova progenitor systems with evolved secondaries have relatively higher mass transfer rates compared with nova progenitor systems with MS donors, nova progenitor systems with evolved secondaries should have more frequent outbursts. Therefore, the contribution of novae with evolved donors to the total nova rate should be larger than the fraction of corresponding binary systems, 30%. Recently, Williams et al. (2016) conducted a more accurate statistical analysis of their preceding results and came to the conclusion that $\sim 30^{+13}_{-10}\%$ of nova eruptions in M31 Galaxy are RG-novae.

4.5.5 Correlation between mass-specific nova rate and morphological type of galaxy

Observations give contradicting results regarding the dependence of the mass-specific nova rate on the Hubble type of the galaxy. Some observational studies (e.g. Ciardullo et al., 1990; Shafter, Ciardullo & Pritchet, 2000; Ferrarese, Côté & Jordán, 2003; Williams & Shafter, 2004) claimed that there is no strong dependence of mass-specific nova rate on the Hubble types of galaxies: the majority of galaxies have around $2 \pm 1 \times 10^{-10} {L_{\odot,K}}^{-1}\,\mathrm{yr}^{-1}$. However, there are several galaxies which may have a higher mass-specific nova rate, e.g. the SMC, LMC, M33 and others (Della Valle et al., 1994; Della Valle, 2002; Neill & Shara, 2005; Alis & Saygac, 2014; Mróz et al., 2016; Shara et al., 2016). The mass-specific nova rate of elliptical-like galaxies at 10 Gyr in our calculation is around $(1-2) \times 10^{-10}\,{\mathrm{M}_\odot}^{-1}\,\mathrm{yr}^{-1}$. This is consistent with Williams & Shafter (2004), since the total stellar mass-to-light ratio $M_\star/L_\mathrm{K} \sim 1.0$, slightly depending on the colour of the galaxy (Bell & de Jong, 2001). However, for spiral-like galaxies, we obtained a mass-specific nova rate 10-20 times larger. It would seem then that our results are inconsistent with measurements of Williams & Shafter (2004). However, one crucial point to understand this discrepancy is the incompleteness of nova surveys. For example, the nova rate of M31 in the analysis of Williams & Shafter (2004) is significantly lower than the nova rates of Darnley et al. (2006). As we discussed above, a more reliable value should be $\approx 97\,\mathrm{yr}^{-1}$, giving a luminosity-specific nova rate $\sim 7.0 \times 10^{-10}\,{L_{\odot,K}}^{-1}\,\mathrm{yr}^{-1}$, which is a factor of $3-4$ larger than the value in Williams & Shafter (2004). In our model for M31, we find a mass-specific nova rate of $\approx (7-14) \times 10^{-10}\,{\mathrm{M}_\odot}^{-1}\,\mathrm{yr}^{-1}$, which is consistent with the above number. In our model of spiral-like galaxies, we assume the SFR to be constant, which is almost certainly oversimplified in the general case. As shown in Figs. 4.1 and 4.2, if there was an initial spike of SFR, certain fraction of total mass of "realistic" spirals sits in old population which does not contribute much to the current nova rate. This will lead to a smaller value of luminosity-specific nova rate (cf. table 4.1).

4.5.6 Novae with short recurrence periods

In M31-like galaxies, the predicted rate of novae with recurrence period $P_{\rm rec} < 1\,{\rm yr}$ is around $4\,{\rm yr}^{-1}$ (see Fig. 4.6). The typical WD mass of these novae is $1.30 - 1.40\,{\rm M}_{\odot}$ and their typical accretion rate is $10^{-7} - 10^{-6}\,{\rm M}_{\odot}\,{\rm yr}^{-1}$. Recently, Tang et al. (2014) discovered a nova with recurrence period of around 1 yr, and Henze et al. (2015) found that the recurrence period of this nova is more likely to be 6 months. Based on the recurrence period and the X-ray emission, Tang et al. (2014) constrained the WD mass of the nova to be $> 1.30\,{\rm M}_{\odot}$ and its accretion rate to be $> 1.7 \times 10^{-7}\,{\rm M}_{\odot}\,{\rm yr}^{-1}$. Presently, this is the only nova with a recurrence period less than 1 yr detected in M31 giving a nova rate $\sim$2 yr^{-1}. We predict a rate of around 4 yr^{-1}. Given the uncertainties of observations and simulations, our results for short recurrence periods are consistent with observations.

4.5.7 Novae with ONe WDs

In our calculation, we do not distinguish ONe WDs from CO WDs. Evidently, some massive WDs should be ONe WDs. José & Hernanz (1998) found that ONe WDs have higher ignition masses (about a factor of 2), compared with CO WDs. This is due to the lower ^{12}C abundance in the envelope which will reduce the reaction rate of the CNO cycle and less energy will be released at the same temperature. Therefore, the ONe WDs should have longer recurrence periods. However, the difference of $t_{\rm ml}$ and $M_{\rm V}$ between ONe WD and CO WD with same mass has not been investigated. Assuming that the ignition mass of novae for ONe WD is the same as for CO WD, we compute the nova rate of ONe WDs based on the WD type identification in BSE code. We find that, for the current nova population in elliptical-like and spiral-like galaxies, the contribution of ONe WDs to the total nova rate is rather small (less than 10%).

4.5.8 Novae in Globular Clusters

Motivated by observations that the mass-specific number of low mass X-ray binaries is enhanced in globular clusters (GCs) (e.g. Clark, 1975), it is also expected that a significant population of WD binaries could be formed through dynamical process in GCs (e.g. Bailyn, 1991). Observations from the Chandra X-Ray Observatory and the Hubble Space Telescope have revealed dozens of cataclysmic variables in GCs (e.g. Grindlay et al., 2001; Heinke et al., 2005; Pooley et al., 2002). Consequently, we will expect the nova rate to be enhanced in GCs. So far, there are five novae found in GCs: one in M80 (Dieball et al., 2010), one in a GC of M87 (Shara et al., 2004), two in the GCs of M31 (Shafter & Quimby, 2007; Henze et al., 2013), and one in a GC of M84 (Curtin et al., 2015). Based on the two novae discovered in the GCs of M31 (Henze et al., 2013), the estimated nova rate in the M31 GC system is $0.05\,{\rm yr}^{-1}\,{\rm GC}^{-1}$. Curtin et al. (2015) found two novae in the GCs of M87 and M84 and estimated that novae are likely enhanced by at least an order of magnitude in GCs compared with the field. This evidence indicates that dynamical interactions in GCs may be an important factor in the calculation of the nova rate in a galaxy. Obviously, in

our calculation, we do not take GCs into consideration.

4.6 Conclusions

With a hybrid binary population synthesis method, we have modelled the nova population for a starburst (i.e. elliptical-like galaxies) and a constant SFR model (i.e. spiral-like galaxies). In addition, we have also provided a composite model as an analog of M31 (i.e. M31-like galaxies). We have computed the nova rates and the nova properties, such as their distributions of mass loss time, maximum magnitude, for different stellar populations. We compare these results with observational data of M31. Our main results are summarized as follows.

1) We computed the nova rates as a function of stellar age in elliptical-like and spiral-like galaxies (see Fig. 4.1). In elliptical-like galaxies, the mass normalized nova rate peaks around 1 Gyr and declines by ~ 2 orders of magnitude at 10 Gyr. In spiral-like galaxies, it peaks around 2 Gyr and declines by a factor of ~ 4 at 10 Gyr. The mass-specific nova rate for elliptical-like galaxies at 10 Gyr in our calculation is $\sim (1-2)\times10^{-10}\,\mathrm{M_\odot}^{-1}\,\mathrm{yr}^{-1}$, which is consistent with observations. However, the mass-specific nova rate for spiral-like galaxies at 10 Gyr is $\sim (20-40)\times10^{-10}\,\mathrm{M_\odot}^{-1}\,\mathrm{yr}^{-1}$, which is larger than seen in some observations. The mismatch may be due to both the incompleteness of past surveys and the assumption of a constant SFR in our model. Moreover, our predictions go in the direction suggested by several papers which found high luminosity-specific nova rates in late-type systems like LMC and M33 (e.g. Della Valle et al., 1994; Della Valle, 2002; Alis & Saygac, 2014).

2) The current nova population is dominated by novae with low mass WDs in elliptical-like galaxies and by novae with massive WDs in spiral-like galaxies.

3) In elliptical-like galaxies, the majority of current novae have long mass loss times, are relatively faint, and have long recurrence periods. In spiral-like galaxies, the majority of the current nova population have short mass loss times, are relatively bright, and have short recurrence periods.

4) Given the uncertainties in both our calculation and observations, the predicted nova rate and the distribution of nova mass loss times in our M31-like galaxy are in good agreement with observational data for M31. The observed distribution may be subject to incompleteness at $t_{\rm ml} < 10$ day and $t_{\rm ml} > 300$ day. In addition, it is possible that we underestimate the number of very bright novae in our calculations. This may be due to the lack of low temperature WDs or the assumption of a unique spectral type for novae at the maximum luminosity in our work.

Acknowledgements

We would like thank the referee for useful comments, which helped to improve the paper. HLC would like to thank Monika Soraisam and Hans Ritter for helpful discussion about the calculation of novae. We are grateful to the MESA council for the MESA instrument papers

and website. HLC acknowledges the computing time granted by the Yunnan Observatories and provided on the facilities at the Yunnan Observatories Supercomputing Platform.

Bibliography

Alis S., Saygac A. T., 2014, in Astronomical Society of the Pacific Conference Series, Vol. 490, Stellar Novae: Past and Future Decades, Woudt P. A., Ribeiro V. A. R. M., eds., p. 95

Arp H. C., 1956, AJ, 61, 15

Bailyn C. D., 1991, in Astronomical Society of the Pacific Conference Series, Vol. 13, The Formation and Evolution of Star Clusters, Janes K., ed., pp. 307–323

Barmby P. et al., 2007, ApJL, 655, L61

Bell E. F., de Jong R. S., 2001, ApJ, 550, 212

Bode M. F., Evans A., 2008, Classical Novae

Capaccioli M., Della Valle M., Rosino L., D'Onofrio M., 1989, AJ, 97, 1622

Chen H.-L., Woods T. E., Yungelson L. R., Gilfanov M., Han Z., 2014, MNRAS, 445, 1912

Chen H.-L., Woods T. E., Yungelson L. R., Gilfanov M., Han Z., 2015, MNRAS, 453, 3024

Chen X., Han Z., 2008, MNRAS, 387, 1416

Ciardullo R., Ford H. C., Neill J. D., Jacoby G. H., Shafter A. W., 1987, ApJ, 318, 520

Ciardullo R., Tamblyn P., Jacoby G. H., Ford H. C., Williams R. E., 1990, AJ, 99, 1079

Clark G. W., 1975, ApJL, 199, L143

Coelho E. A., Shafter A. W., Misselt K. A., 2008, ApJ, 686, 1261

Curtin C., Shafter A. W., Pritchet C. J., Neill J. D., Kundu A., Maccarone T. J., 2015, ApJ, 811, 34

Darnley M. J. et al., 2014, in Astronomical Society of the Pacific Conference Series, Vol. 490, Stell Novae: Past and Future Decades, Woudt P. A., Ribeiro V. A. R. M., eds., p. 49

Darnley M. J. et al., 2006, MNRAS, 369, 257

Davis P. J., Kolb U., Knigge C., 2012, MNRAS, 419, 287

Davis P. J., Kolb U., Willems B., 2010, MNRAS, 403, 179

de Kool M., 1990, ApJ, 358, 189

Della Valle M., 2002, in American Institute of Physics Conference Series, Vol. 637, Classical Nova Explosions, Hernanz M., José J., eds., pp. 443–456

Della Valle M., Bianchini A., Livio M., Orio M., 1992, A&A, 266, 232

Della Valle M., Livio M., 1998, ApJ, 506, 818

Della Valle M., Rosino L., Bianchini A., Livio M., 1994, A&A, 287, 403

Dieball A., Long K. S., Knigge C., Thomson G. S., Zurek D. R., 2010, ApJ, 710, 332

Duerbeck H. W., 1990, in Lecture Notes in Physics, Berlin Springer Verlag, Vol. 369, IAU Colloq. 122: Physics of Classical Novae, Cassatella A., Viotti R., eds., p. 34

Ferrarese L., Côté P., Jordán A., 2003, ApJ, 599, 1302

Franck J. R., Shafter A. W., Hornoch K., Misselt K. A., 2012, ApJ, 760, 13

Gehrz R. D., Truran J. W., Williams R. E., Starrfield S., 1998, PASP, 110, 3

Giannone P., Weigert A., 1967, ZAp, 67, 41

Grindlay J. E., Heinke C., Edmonds P. D., Murray S. S., 2001, Science, 292, 2290

Hachisu I., Kato M., 2001, ApJ, 558, 323

Hachisu I., Kato M., Nomoto K., 1996, ApJL, 470, L97

Hachisu I., Kato M., Nomoto K., 1999, ApJ, 522, 487

Han Z., Podsiadlowski P., Maxted P. F. L., Marsh T. R., Ivanova N., 2002, MNRAS, 336, 449

Heinke C. O., Grindlay J. E., Edmonds P. D., Cohn H. N., Lugger P. M., Camilo F., Bogdanov S., Freire P. C., 2005, ApJ, 625, 796

Henze M., Darnley M. J., Kabashima F., Nishiyama K., Itagaki K., Gao X., 2015, A&A, 582, L8

Henze M. et al., 2013, A&A, 549, A120

Hernanz M., Jose J., Coc A., Isern J., 1996, ApJL, 465, L27

Hillman Y., Prialnik D., Kovetz A., Shara M. M., 2015, ArXiv e-prints

Hjellming M. S., Webbink R. F., 1987, ApJ, 318, 794

Hurley J. R., Tout C. A., Pols O. R., 2002, MNRAS, 329, 897

Idan I., Shaviv N. J., Shaviv G., 2013, MNRAS, 433, 2884

Ivanova N. et al., 2013, Astron. Astrophys. Rev., 21, 59

Izzo L. et al., 2015, ApJL, 808, L14

Johnson H. L., 1966, ARA&A, 4, 193

José J., Hernanz M., 1998, ApJ, 494, 680

Kato M., Hachisu I., 2004, ApJL, 613, L129

Kouwenhoven M. B. N., Brown A. G. A., Goodwin S. P., Portegies Zwart S. F., Kaper L., 2009, A&A, 493, 979

Kraft R. P., 1964, ApJ, 139, 457

Kraicheva Z. T., Popova E. I., Tutukov A. V., Yungelson L. R., 1979, SvA, 23, 290

Kraus A. L., Hillenbrand L. A., 2009, ApJ, 703, 1511

Kroupa P., 2001, MNRAS, 322, 231

Kudryashov A. D., Chugaĭ N. N., Tutukov A. V., 2000, Astronomy Reports, 44, 170

Livio M., Govarie A., Ritter H., 1991, A&A, 246, 84

Loveridge A. J., van der Sluys M. V., Kalogera V., 2011, ApJ, 743, 49

Matteucci F., Renda A., Pipino A., Della Valle M., 2003, A&A, 405, 23

Meng X., Chen X., Han Z., 2008, A&A, 487, 625

Mestel L., 1952a, MNRAS, 112, 583

Mestel L., 1952b, MNRAS, 112, 598

Mróz P. et al., 2016, ApJS, 222, 9

Munari U., 2014, in Astronomical Society of the Pacific Conference Series, Vol. 490, Stell Novae: Past and Future Decades, Woudt P. A., Ribeiro V. A. R. M., eds., p. 183

Neill J. D., Shara M. M., 2005, AJ, 129, 1873

Nelemans G., Siess L., Repetto S., Toonen S., Phinney E. S., 2016, ApJ, 817, 69

Nelson L. A., MacCannell K. A., Dubeau E., 2004, ApJ, 602, 938

Olsen K. A. G., Blum R. D., Stephens A. W., Davidge T. J., Massey P., Strom S. E., Rigaut F., 2006, AJ, 132, 271

Paczynski B., Zytkow A. N., 1978, ApJ, 222, 604

Passy J.-C., Herwig F., Paxton B., 2012, ApJ, 760, 90

Patterson J., 1984, ApJS, 54, 443

Pavlovskii K., Ivanova N., 2015, MNRAS, 449, 4415

Paxton B., Bildsten L., Dotter A., Herwig F., Lesaffre P., Timmes F., 2011, ApJS, 192, 3

Paxton B. et al., 2013, ApJS, 208, 4

Piersanti L., Cassisi S., Iben, Jr. I., Tornambé A., 2000, ApJ, 535, 932

Piersanti L., Tornambé A., Yungelson L. R., 2014, MNRAS, 445, 3239

Politano M., 1996, ApJ, 465, 338

Politano M., Livio M., Truran J. W., Webbink R. F., 1990, in Lecture Notes in Physics, Berlin Springer Verlag, Vol. 369, IAU Colloq. 122: Physics of Classical Novae, Cassatella A., Viotti R., eds., p. 386

Pooley D. et al., 2002, ApJ, 569, 405

Prialnik D., Kovetz A., 1995, ApJ, 445, 789

Prialnik D., Shara M. M., Shaviv G., 1978, A&A, 62, 339

Prialnik D., Shara M. M., Shaviv G., 1979, A&A, 72, 192

Ricker P. M., Taam R. E., 2012, ApJ, 746, 74

Robertson B., Yoshida N., Springel V., Hernquist L., 2004, ApJ, 606, 32

Rosino L., 1964, Annales d'Astrophysique, 27, 498

Rosino L., 1973, A&AS, 9, 347

Rosino L., Capaccioli M., D'Onofrio M., Della Valle M., 1989, AJ, 97, 83

Saglia R. P. et al., 2010, A&A, 509, A61

Sana H. et al., 2012, Science, 337, 444

Schreiber M. R., Zorotovic M., Wijnen T. P. G., 2016, MNRAS, 455, L16

Schwartzman E., Kovetz A., Prialnik D., 1994, MNRAS, 269, 323

Shafter A. W., Ciardullo R., Pritchet C. J., 2000, ApJ, 530, 193

Shafter A. W. et al., 2015, ApJS, 216, 34

Shafter A. W., Irby B. K., 2001, ApJ, 563, 749

Shafter A. W., Quimby R. M., 2007, ApJL, 671, L121

Shafter A. W., Rau A., Quimby R. M., Kasliwal M. M., Bode M. F., Darnley M. J., Misselt K. A., 2009, ApJ, 690, 1148

Shara M. M., Doyle T., Lauer T. R., Zurek D., Neill J. D., Madrid J. P., Welch D. L., Baltz E. A., 2016, ArXiv e-prints

Shara M. M., Yaron O., Prialnik D., Kovetz A., Zurek D., 2010, ApJ, 725, 831

Shara M. M., Zurek D. R., Baltz E. A., Lauer T. R., Silk J., 2004, ApJL, 605, L117

Sion E. M., Acierno M. J., Tomczyk S., 1979, ApJ, 230, 832

Soraisam M. D., Gilfanov M., 2015, A&A, 583, A140

Soraisam M. D., Gilfanov M., Wolf W. M., Bildsten L., 2016, MNRAS, 455, 668

Starrfield S., Schwarz G., Truran J. W., Sparks W. M., 2000, in American Institute of Physics Conference Series, Vol. 522, American Institute of Physics Conference Series, Holt S. S., Zhang W. W., eds., pp. 379–382

Starrfield S., Sparks W. M., Shaviv G., 1988, ApJL, 325, L35

Starrfield S., Truran J. W., Sparks W. M., 1978, ApJ, 226, 186

Starrfield S., Truran J. W., Sparks W. M., Kutter G. S., 1972, ApJ, 176, 169

Tajitsu A., Sadakane K., Naito H., Arai A., Aoki W., 2015, Nature, 518, 381

Tajitsu A., Sadakane K., Naito H., Arai A., Kawakita H., Aoki W., 2016, ArXiv e-prints

Tang S. et al., 2014, ApJ, 786, 61

Townsley D. M., Bildsten L., 2004, ApJ, 600, 390

Truran J. W., Livio M., 1986, ApJ, 308, 721

Tutukov A. V., Ergma E. V., 1979, Soviet Astronomy Letters, 5, 284

Tutukov A. V., Yungel'Son L. R., 1972, Astrophysics, 8, 227

van Haaften L. M., Nelemans G., Voss R., Toonen S., Portegies Zwart S. F., Yungelson L. R., van der Sluys M. V., 2013, A&A, 552, A69

Webbink R. F., 1984, ApJ, 277, 355

Webbink R. F., 1988, The Formation and Evolution of Symbiotic Stars, Mikolajewska J., Friedjung M., Kenyon S. J., Viotti R., eds., p. 311

Williams S. C., Darnley M. J., Bode M. F., Keen A., Shafter A. W., 2014, ApJS, 213, 10

Williams S. C., Darnley M. J., Bode M. F., Shafter A. W., 2016, ApJ, 817, 143

Williams S. J., Shafter A. W., 2004, ApJ, 612, 867

Wolf W. M., Bildsten L., Brooks J., Paxton B., 2013, ApJ, 777, 136

Woods T. E., Ivanova N., 2011, ApJL, 739, L48

Yaron O., Prialnik D., Shara M. M., Kovetz A., 2005, ApJ, 623, 398

Yungelson L., Livio M., Truran J. W., Tutukov A., Fedorova A., 1996, ApJ, 466, 890

Yungelson L., Livio M., Tutukov A., 1997, ApJ, 481, 127

Zorotovic M., Schreiber M. R., Gänsicke B. T., Nebot Gómez-Morán A., 2010, A&A, 520, A86

Chapter 5

Conclusions

In this thesis, we adopted a hybrid binary population synthesis approach employing the population synthesis code BSE with the detailed stellar evolution code MESA to model the formation and evolution of accreting white dwarf populations. We investigate the evolution of the number of rapidly accreting white dwarfs, stably nuclear-burning white dwarfs and type Ia supernovae rate. We also study the X-ray and UV emission of accreting white dwarf and the influence of their radiation on the line emission from warm interstellar medium. In addition, we explore the properties of nova population in galaxies of different Hubble types. We summarize our main results below.

First, we study the population of accreting white dwarfs with two different binary population approaches, i.e. 'rapid' and 'hybrid' approach. With these two approaches, we study the evolution of the number of different kinds of accreting white dwarfs. We compare the results computed with these two approaches.

We show that the 'hybrid' approach have a better treatment of mass transfer compared with the 'rapid' approach, which is important in the binary population synthesis calculations. We also computed the number of rapidly accreting white dwarfs and stably nuclear-burning white dwarfs in different types of galaxies. In addition, we calculated the delay time distribution of type Ia supernovae and type Ia supernova rate in Galaxy. We found that our computed delay time distribution of type Ia supernova in single degenerate scenario is not consistent with observations and the type Ia supernova rate of Galaxy in our calculation is much smaller than observation, in agreement with previous results.

We then proceed with the study of accreting white dwarfs. Based on the results of previous part and using simple assumptions regarding the emission of accreting white dwarfs, we study the number of observed supersoft X-ray sources, soft X-ray luminosity of accreting white dwarfs, and their H and He II ionizing luminosity for galaxies with different star formation history.

We found that the results of binary population synthesis with commonly adopted assumptions is not consistent with observations for stellar population with ages of $\sim 4-8$ Gyr. We propose that this controversy can be solved by the modification of criteria of dynamically unstable mass transfer for giant stars. In addition, we have computed the evolution of the number of supersoft X-ray sources for galaxy with different star formation history.

We then produce model populations of novae using a hybrid binary population synthesis approach for galaxies with different star formation histories. We explore the properties of nova population in different Hubble types of galaxies. Then we compare these results with observations.

We show the evolution of nova rate as a function of stellar ages. We also present the distribution of white dwarf mass, recurrence period, maximum magnitude and the mass loss time for nova population in galaxies of different Hubble types. We found that our results of M31-like galaxy are in agreement with observational data for Andromeda.

Acknowledgements

I would like to thank Rashid Sunyaev and Marat Gilfanov for supporting me to work at the High Energy group.

I would also like to express my deepest appreciation to my supervisor Marat Gilfanov. This thesis would never have been possible without him. He spent a lot of time to discuss with me and teach me how to do good scientific work, which will be still useful for me in the future. I deeply appreciate his invaluable guidance and patience to me.

I am grateful to Lev Yungelson for a lot of helpful discussion on binary evolution, population synthesis and answering my all sorts of questions. I also thank him for his patience to me. I also thank Tyrone Woods, Zhenwen Han for their help and collaboration.

I would like to thank Jens Stuecker for his help in writing a good abstract in German.

I also thank the many other people I meet here. Without them my life here would become difficult. I am grateful to the administration staff at MPA, particularly Gabi, Sonja, Maria, Cornelia, and Stella. I would also like to thank Xiaoling, Li Yangfang, Li Dong, Qingbo, Jia Shi, Shao Shi, Luo Yu for their help and friendship.

I also would like to thank my parents and brothers for their love and support.